

Dendritic cell-specific function of deubiquitinating enzyme OTUD7b in experimental cerebral malaria

Thesis

for the degree of

doctor rerum naturalium

(Dr. rer. nat.)

approved by the Faculty of Natural Sciences of
Otto von Guericke University Magdeburg

by M.Sc. Kunjan Harit

born on 18.09.1994 in Anand, India

Examiner:

Prof. Dr. Dunja Bruder

Prof. Dr. Bernd Lepenies

Submitted on: 13.09.2023

Defended on: 02.02.2024

TABLE OF CONTENTS	II
LIST OF ABBREVIATIONS	V
LIST OF FIGURES	VII
LIST OF TABLES	IX
ABSTRACT	X
ZUSAMMENFASSUNG	XI
1. INTRODUCTION	
1.1 Malaria	1
1.1.1 Life cycle of <i>Plasmodium</i>	1
1.1.2 Cerebral Malaria	3
1.1.3 CM and ECM	4
1.1.4 Role of immune response in the disease pathogenesis	5
1.2 TNF	8
1.2.1 TNF Signaling	9
1.2.2 Checkpoints in TNF signaling	11
1.2.3 Role of ubiquitination and deubiquitination in TNF signaling	12
1.3 OTU domain-containing protein 7b (OTUD7b)	13
2. AIMS OF THE STUDY	
2.1 Study the DC-specific function of OTUD7b in experimental cerebral malaria	21
2.2 Understand the molecular mechanisms by which OTUD7b regulates DC function	21
3. MATERIALS AND METHODS	
3.1 Materials	22
3.1.1 Chemicals for animal experiments	22
3.1.2 Materials for cell culture	22
3.1.3 Materials for transfection	24
3.1.4 Reagents for molecular biology	24
3.1.5 Reagents for protein analysis	25
3.1.6 Reagents for flow cytometric analysis	27
3.1.7 Kits used in this study	28
3.1.8 List of instruments	29
3.1.9 Software	30
3.1.10 Animals	30
3.2 Methods	30
Mice experiments	
3.2.1 Genotyping of mice	30

3.2.2 Parasite infection	30
3.2.3 Assessment of neurological symptoms	31
3.2.4 Assessment of parasitemia	31
3.2.5 Assessment of blood-brain barrier integrity	32
3.2.6 Leukocyte isolation from spleen and brain	32
3.2.7 Flow cytometry	32
3.2.8 Measurement of cell death by flow cytometry	33
3.2.9 Adoptive transfer of dendritic cells	33
3.2.10 Magnetic sorting for splenic leukocytes	33
Cell culture	
3.2.11 Bone marrow derived dendritic cell (BMDC)/ Bone marrow derived macrophage (BMDM) culture	34
3.2.12 HEK293T cell line	34
3.2.13 Human monocyte derived dendritic cells	34
Cell viability assays	
3.2.14 LDH assay	35
3.2.15 MTT assay	35
Stimulation of BMDC	
3.2.16 Enrichment of <i>Plasmodium</i> infected erythrocytes and stimulation of BMDC	35
3.2.17 Cytokine stimulation of BMDC	35
Protein analysis	
3.2.18 Western Blotting	36
3.2.19 Co-immunoprecipitation	36
Gene expression analysis	
3.2.20 qRT-PCR	37
Inhibitor experiments	
3.2.21 <i>In vitro</i> cell death inhibition	38
3.2.22 <i>In vivo</i> Z-VAD-FMK and Nec-1s treatment	38
Transfection	
3.2.23 Nucleofection of BMDCs	38
3.2.24 Site directed mutagenesis	39
3.2.25 Transfection of HEK293T cells	39
3.2.26 Nucleofection of human monocyte derived dendritic cells	39
4. RESULTS	
4.1 Generation and characterization of CD11c-Cre Otud7b ^{fl/fl} conditional knockout mice	41
4.2. DC-specific OTUD7b-deficiency confers protection against ECM	42

4.3 Reduced number of DCs and CD8 ⁺ T cells in CD11c-Cre Otud7b ^{fl/fl} mice after <i>PbA</i> infection	44
4.4 Increased death of DC in CD11c-Cre Otud7b ^{fl/fl} mice after <i>PbA</i> infection	49
4.5 Inhibition of DC death induces ECM in CD11c-Cre Otud7b ^{fl/fl} mice	53
4.6 OTUD7b prevents proteasomal degradation of TRAF2	55
4.7 OTUD7b regulates DC apoptosis by cleaving K48-linked ubiquitin chains from TRAF2	57
4.8 UBA domain of OTUD7b is required for TRAF2 binding	58
4.9 OTUD7b fosters the activation of NF- κ B, MAP kinase signaling pathways via the stabilization of TRAF2	59
4.10 TRAF2-deficiency sensitizes OTUD7b ^{+/+} BMDCs to TNF-mediated apoptosis	60
4.11 Increased TNF mediated apoptosis of OTUD7b deficient human moDCs	64
4.12 OTUD7b regulates TRAIL and CD95L (FasL)- induced apoptosis of DCs	64
5. Discussion:	
4.1 DC-specific function of OTUD7b during ECM	66
4.2 Mechanistic role of OTUD7b in TNFR1 signaling	67
6. Conclusion	70
7. References	71
Declaration of honour	77

LIST OF ABBREVIATION

7-AAD	7-amino actinomycin D
ACT	Artemisinin-based combination therapy
BBB	Blood-brain barrier
BMDC	Bone marrow derived dendritic cell
BMDM	Bone marrow derived macrophage
CM	Cerebral malaria
CCL	Chemokine (C-C motif) receptor ligand
CCR	Chemokine (C-C motif) receptor
cIAP-1/2	Cellular inhibitor of apoptosis protein-1/2
CXCL	Chemokine (C-X-C motif) ligand
DAMP	Danger associated molecular patterns
DC	Dendritic cells
DMEM	Dulbecco's modified eagle's medium
DMSO	Dimethyl sulfoxide
dNTPs	Deoxyribonucleotide triphosphates
DPBS	Dulbecco's phosphate buffered saline
DTT	Dithiothreitol
DUB	Deubiquitinating enzyme
ECM	Experimental cerebral malaria
EPCR	Endothelial protein C receptor
FADD	Fas associated death domain protein
Flt3L	fms-like tyrosine kinase 3 ligand
GAP-50	Glideosome associated protein-50
GM-CSF	Granulocyte-macrophage colony stimulating factor
ICAM-1	Intracellular adhesion molecule-1
IFN- γ	Interferon γ
IL-1 α	Interleukin-1 α
IL-1 β	Interleukin-1 β
iRBC	Infected red blood cell
K11	Lysine 11-linked ubiquitination
K48	Lysine 48-linked ubiquitination
K63	Lysine 63-linked ubiquitination
LDH	Lactate Dehydrogenase
LPS	Lipopolysaccharide
LT- α	Lymphotoxin α
LUBAC	Linear ubiquitin chain assembly complex

M-CSF	Macrophage colony stimulating factor
MAPK	Mitogen activated protein kinase
MLKL	Mixed lineage kinase domain-like pseudokinase
MoDC	Monocyte derived dendritic cells
MTT	3-(4,5-dimethylthiazol-2-yl)-2,5-diphenyl tetrazolium bromide
Nec-1s	Necrostatin-1s
NF- κ B	Nuclear factor kappa light chain enhancer of activated B cells
OTUD7b	Ovarian tumor domain containing protein 7b
PAMP	Pathogen associated molecular patterns
<i>PbA</i>	<i>Plasmodium berghei</i> ANKA
PBMC	Peripheral blood mononuclear cell
PCR	Polymerase chain reaction
PfEMP1	<i>P. falciparum</i> erythrocyte membrane protein-1
<i>PyXL</i>	<i>Plasmodium yoelii</i>
qRT-PCR	quantitative reverse transcription PCR
RBC	Red blood cell
RIPA buffer	Radioimmunoprecipitation assay buffer
RIPK-1	Receptor interacting serine/threonine protein kinase-1
RMCBS	Rapid murine coma behavioral scale
TAB-1/2	TAK-1 binding protein-1/2
TACE	TNF α converting enzyme
TAK-1	Transforming growth factor β -activated kinase-1
TCR	T cell receptor
TNF	Tumor necrosis factor
TNFR	TNF receptor
TRADD	TNFR associated death domain protein
TRAF-2/5	TNFR associated factor-2/5
TRAIL	TNF-related apoptosis inducing ligand
Ub	Ubiquitin
VCAM-1	Vascular cell adhesion molecule-1
WHO	World health organisation
zVAD-FMK	Carbobenzoxy-valyl-alanyl-aspartyl-O-methyl-fluoromethylketone

LIST OF FIGURES

Figure 1: Life cycle of *Plasmodium* parasite

Figure 2: Pathogenesis of experimental cerebral malaria

Figure 3: TNFR signaling

Figure 4: Checkpoints in TNFR-I signaling

Figure 5: Mechanism of ubiquitination and types of ubiquitin linkages

Figure 6: Deconjugation and recycling of ubiquitin molecules by deubiquitinases

Figure 7: Regulation of TNFR1 signaling by ubiquitination and deubiquitination

Figure 8: Structure of deubiquitinating enzyme OTUD7b

Figure 9: Strategy for generation of CD11c-Cre Otud7b^{fl/fl} mice

Figure 10: Dendritic cell specific deletion of OTUD7b

Figure 11: OTUD7b is dispensable for the development of immune system

Figure 12: Deletion of Otud7b confers protection against *PbA* induced ECM

Figure 13: Reduced number of dendritic cells in CD11c-Cre Otud7b^{fl/fl} mice upon *PbA* infection

Figure 14: Reduced numbers of conventional dendritic cell subpopulation upon *PbA* infection

Figure 15: Reduced priming of CD8⁺ T cells in spleen of CD11c-Cre Otud7b^{fl/fl} mice upon *PbA* infection

Figure 16: Reduced intracerebral accumulation of CD8⁺ T cells in CD11c-Cre Otud7b^{fl/fl} mice protects against ECM

Figure 17: OTUD7b is dispensable for cell surface expression of MHC-I,II and CD80/86 on dendritic cells

Figure 18: Impaired IL-12 production by OTUD7b deficient DCs upon infection

Figure 19: Deletion of OTUD7b in DCs impairs cytotoxic CD8⁺ T cell response to *PbA* infection

Figure 20: Increased dendritic cell death in absence of OTUD7b upon *PbA* infection

Figure 21: OTUD7b is dispensable for TLR mediated cell death

Figure 22: OTUD7b is a negative regulator of TNF induced dendritic cell apoptosis

Figure 23: OTUD7b inhibits RIPK1-dependent and independent apoptosis upon TNF stimulation

Figure 24: Inhibition of cell death in CD11c-Cre Otud7b^{fl/fl} mice renders them susceptible to ECM

Figure 25: OTUD7b prevents the proteasomal degradation of TRAF2 upon TNF stimulation

Figure 26: OTUD7b removes K48-linked polyubiquitin chains from TRAF2

Figure 27: OTUD7b regulates K63-linked ubiquitination of RIPK1 via TRAF2

Figure 28: UBA domain of OTUD7b is indispensable for binding with TRAF2

Figure 29: Impaired activation of NF- κ B, MAPK signaling pathways in OTUD7b deficient BMDCs.

Figure 30: OTUD7b inhibits proteasomal degradation of TRAF2 upon TNF stimulation

Figure 31: OTUD7b prevents proteasomal degradation of TRAF2 by removing K48-linked polyubiquitin chains

Figure 32: OTUD7b regulates RIPK1 dependent apoptosis via TRAF2 mediated K63-linked ubiquitination of RIPK1

Figure 33: Adoptive transfer of WT BMDCs in CD11c-Cre Otud7b^{fl/fl} mice induces ECM

Figure 34: OTUD7b inhibits TNF mediated apoptosis in human mo-DC by stabilizing TRAF2

Figure 35: OTUD7b negatively regulates TRAIL and Fas-L mediated dendritic cell apoptosis via TRAF2

Figure 36: Schematic summary of OTUD7b mediated regulation of TNF signaling in dendritic cells

LIST OF TABLES

Table 1: Types of ubiquitin chains and cellular functions

Table 2: Interaction partners and signaling pathways regulated by OTUD7b

Table 3: List of reagents used for *in vivo* experiments

Table 4: Cell line

Table 5: List of cell culture reagents

Table 6: List of cell stimulation reagents

Table 7: List of inhibitors used *in vitro* and *in vivo*

Table 8: List of consumables

Table 9: List of guide RNAs sequence

Table 10: Vectors

Table 11: List of reagents for nucleofection

Table 12: List of reagents for molecular biology

Table 13: List of primers

Table 14: TaqMan™ gene assay probes

Table 15: List of reagents for protein analysis

Table 16: List of antibodies for western blotting

Table 17: Reagents for flow cytometry

Table 18: List of antibodies for flow cytometry

Table 19: List of kits

Table 20: Instruments

Table 21: Software for data analysis

Table 22: Composition of erythrocyte lysis buffer

Table 23: Composition of RIPA lysis buffer

Table 24: cDNA synthesis

Table 25: qRT-PCR reaction mix

ABSTRACT

Cerebral malaria caused by the infection with the parasite *Plasmodium falciparum* is a neurological complication of malaria, which can result in severe cognitive deficits and death of infected individual. A hallmark of cerebral malaria is a disturbance of the blood brain barrier and despite anti-malarial treatment, around 25% of the patients suffer from long term neurocognitive deficits. Since cerebral malaria can be studied in humans mainly post mortem, murine experimental cerebral malaria (ECM) induced by infection with *Plasmodium berghei* ANKA is widely employed to understand the mechanisms underlying the human cerebral malaria. Studies in experimental cerebral malaria have shown that dendritic cells (DCs) process and present malarial antigens to CD8⁺ T, which migrate to the brain microvasculature and induce the disruption of the blood brain barrier via perforin and granzyme-B mediated cytotoxicity

Both human and murine cerebral malaria are characterized by high levels of TNF in the blood. TNF is a pleiotropic cytokine which can induce both pro-inflammatory signaling and activation of cell death pathways. These pathways are tightly regulated by the process of ubiquitination and deubiquitination. Here we have investigated the DC-specific role of the deubiquitinating enzyme OTUD7b in ECM. these studies identified that OTUD7b prevents TNF induced apoptosis of DCs resulting in enhanced priming and intracerebral accumulation of pathogenic CD8⁺ T cells. Mechanistically, OTUD7b stabilized the E3 ligase TRAF2 by removing K48-linked polyubiquitin chains and prevented its proteasomal degradation. These increased levels of TRAF2 foster K63-linked polyubiquitination of RIPK1 leading to increased activation of the NF- κ B and MAP kinase pathways and upregulation of anti-apoptotic FLIP and Bcl-xL. In addition, increased K63-linked polyubiquitination of RIPK1 reduced its S166 autophosphorylation, impaired its kinase activity and protected DCs from RIPK1-independent and dependent apoptosis. Mice with DC-specific deletion of OTUD7b showed enhanced apoptosis of DCs, were unable to induce CD8⁺ T cell-mediated brain pathology and were protected from ECM. Taken together, our study identifies OTUD7b as a molecular switch regulating the activation or death of DCs and a novel target to regulate DC-T cell mediated immunopathology.

ZUSAMMENFASSUNG

Die zerebrale Malaria ist eine neurologische Komplikation der Malaria und wird durch eine Infektion mit dem Parasiten *Plasmodium falciparum* verursacht. Sie kann zu schweren kognitiven Beeinträchtigungen und zum Tod des Infizierten führen. Charakteristisch für die zerebrale Malaria ist eine Störung der Blut-Hirn-Schranke. Auch bei erfolgreicher medikamentöser Elimination des Parasiten leiden etwa 25 % der Patienten langfristig an neurokognitiven Defiziten. Die zerebrale Malaria kann beim Menschen nur eingeschränkt und bezüglich der zerebralen Pathogenese vorwiegend post mortem untersucht werden. Um die Mechanismen zu verstehen, die der zerebralen Malaria beim Menschen zugrunde liegen, wird daher häufig die experimentelle zerebrale Malaria (ECM) bei Mäusen eingesetzt, die durch eine Infektion mit *Plasmodium berghei* ANKA ausgelöst wird. Studien zur ECM haben gezeigt, dass Dendritische Zellen (DCs) Plasmodien-Antigene prozessieren und diese CD8+ T-Zellen präsentieren, die in die Mikrogefäße des Gehirns einwandern und durch Perforin- und Granzym B-vermittelte Zytotoxizität eine Störung der Blut-Hirn-Schranke verursachen. Sowohl die humane als auch die murine zerebrale Malaria sind durch hohe Konzentrationen des Zytokins Tumor Nekrose Faktor (TNF) im Blut gekennzeichnet. TNF ist ein pleiotropes Zytokin, das sowohl proinflammatorische Signale als auch die Aktivierung von Zelltod-Signalwegen auslösen kann. Diese Signalwege werden durch posttranslationale Ubiquitinierung und Deubiquitinierung von Signaltransduktionsmolekülen streng reguliert. Wir haben die DC-spezifische Rolle des Deubiquitinierungsenzyms OTUD7b in der ECM untersucht. Diese Studien zeigen, dass OTUD7b die TNF-induzierte Apoptose von DCs verhindert, was zu einer verstärkten Aktivierung, Expansion und intrazerebralen Akkumulation pathogener CD8+ T-Zellen führt. Mechanistisch stabilisiert OTUD7b die E3-Ligase TRAF2, indem es K48-gebundene Polyubiquitin-Ketten abspaltet und so den proteasomalen TRAF2-Abbau verhindert. Diese erhöhten TRAF2-Spiegel fördern die K63-gebundene Polyubiquitinierung von RIPK1, was zu einer verstärkten Aktivierung von NF- κ B- und MAP-Kinase-Signalwegen und einer Hochregulation der anti-apoptischen Moleküle FLIP und Bcl-xL führt. Zusätzlich reduziert die erhöhte K63-gebundene Polyubiquitinierung von RIPK1 seine S166-Autophosphorylierung, beeinträchtigt seine Kinaseaktivität und schützt die DCs vor RIPK1-unabhängiger und -abhängiger Apoptose. Mäuse mit einer DC-spezifischen Deletion von OTUD7b zeigten eine erhöhte Apoptose der DCs. Dadurch wurde eine CD8+ T-Zell-vermittelte zerebrale Immunpathologie verhindert und die Mäuse waren vor der ECM geschützt. Zusammenfassend identifiziert unsere Studie OTUD7b als einen molekularen Schalter, der die Aktivierung und den Zelltod von DCs reguliert und einen neuen Ansatzpunkt für die Regulation von DC / T-Zell-vermittelten Immunpathologien darstellt.

1. INTRODUCTION

1.1 Malaria

Malaria is a life-threatening disease. caused by parasitic protozoa of the genus *Plasmodium*. According to WHO report 2022, 247 million cases were reported worldwide resulting in 619,000 deaths in 2021. Malaria occurs in tropic and sub-tropical countries, predominantly in Africa and South-east Asia. In 2021, African region alone reported 95% of the worldwide malarial cases and 96% of associated deaths amongst which the most affected were children under the age of 5 years. Despite recent advances, malaria still remains to be a big burden in these areas (1).

Malaria is a vector-transmitted disease and spreads through bite of an infected female *Anopheles* mosquito. Human malaria can be caused by five *Plasmodium* species including *Plasmodium (P.) falciparum*, *P. vivax*, *P. ovale*, *P. malariae* and *P. knowlesi* (2). General symptoms of malaria include chills, headache and fever but can rapidly progress to severe anemia or upon infection with *P. falciparum* to cerebral malaria (CM), (3). Around 5 - 20% of *P. falciparum*-infected patients succumb to the disease despite anti-malarial treatment and the majority of surviving patients suffer from long-term neurological impairment (4, 5). Artemisinin-based combination therapy (ACT) is currently the most effective treatment against CM. The only approved vaccine against CM is RTS,S/AS01 vaccine with an efficacy of only 25% (6). Due to the emergence of drug-resistant *Plasmodium* strains and modest efficacy of the vaccine there is an urgent need of the development of alternative therapeutic strategies particularly targeting the host immune response to prevent CM (6, 7).

1.1.1 Life cycle of plasmodium

Plasmodium has a complex life cycle involving 2 hosts. The female *Anopheles* mosquito is the primary host in which the sexual reproduction takes place, and also serves as vector for the parasite transmission. Humans are the secondary hosts in which the asexual reproduction takes place. Infection in human begins with a bite of female *Anopheles* mosquito which injects sporozoites from its salivary glands into host dermis during a blood meal (8). Upon injection, sporozoites migrate to the liver via the bloodstream where they invade the hepatocyte and replicate within a parasitophorous vacuole establishing a clinically silent, exo-erythrocytic phase of infection. The sporozoites undergo schizogony to develop into merozoites. Towards the end of schizogony, merozoites are packed into vesicles known as merozoites and released into blood stream (9). Free merozoites invade the erythrocytes, replicate and develop into ring stage trophozoites which further undergo numerous rounds of asexual replication (erythrocytic schizogony) without cytokinesis to form schizonts (late-stage parasites) (10). Rupture of erythrocyte membrane releases up to 30 merozoites in a duration of 24 – 72h into

the blood stream where they invade new erythrocytes and initiate a new cycle of replication. Blood stage of malaria is the symptomatic stage and is linked to all the disease related morbidity and mortality (11).

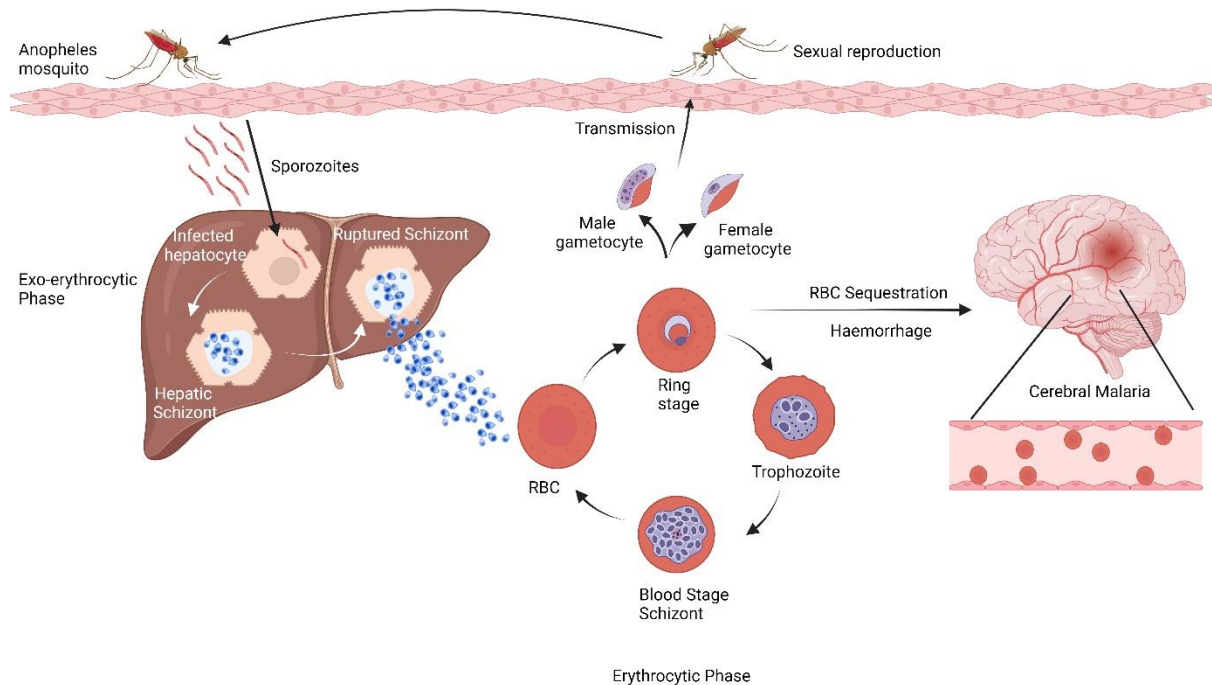


Figure 1: Life cycle of *Plasmodium* parasite

During a blood meal, infected female anopheles mosquito injects sporozoites into the skin of human host. Motile sporozoites migrate to the liver, invade the hepatocytes and undergo pre-erythrocytic schizogony to mature into merozoites. One sporozoite can generate up to 10,000 merozoites. Merozoites are released from hepatocytes into the blood stream where they infect RBCs and undergo another cycle of asexual replication and mature from the ring stage via the trophozoites stage to schizont stage. The mature schizont ruptures releasing merozoites into the blood stream, thereby initiating a fresh cycle of infection. Some asexual parasites develop into gametocytes, which are taken up by the mosquito during a blood meal. The sexual life cycle takes place within the mosquito resulting the in development of sporozoites, which are transmitted to the human host via a mosquito bite initiating a fresh round of infection. During severe cases of malaria, parasite infected RBCs migrate to the brain and sequester within the brain microvasculature leading to edema, hemorrhage and BBB disruption. This condition is known as cerebral malaria. (Modified from (12), figure created using biorender)

During erythrocytic schizogony, a subpopulation of merozoites undergo sexual reproduction and form male and female gametocytes within human host which are subsequently ingested by female *Anopheles* mosquito during its blood meal. Gametocytes differentiate into gametes inside the mosquito midgut and fuse to form a zygote, which multiplies to form ookinets and

subsequently, differentiate into sporozoites to re-initiate the infection and replication cycle (13, 14) (Fig 1).

1.1.2 Cerebral malaria

Cerebral malaria is a neurological complication of human malaria caused by the parasite *Plasmodium falciparum*. CM is the leading cause of deaths, especially among children in sub-Saharan Africa and adults in Asia (15). The severe manifestations of CM are clouding of consciousness, cerebral seizures and coma. Around 25% of the patients surviving CM, suffer from long term neurological sequelae including deficits in cognitive function, behavioral alteration, impairment in motor skills and epilepsy leading to significant disability (16).

A characteristic feature of cerebral malaria is coma. In pediatric cerebral malaria, coma develops suddenly with onset of seizures, papilledema and retinal vessel changes whereas in adult cerebral malaria presents typically as a multi-organ disease including renal failure, pulmonary edema and respiratory distress syndrome (5, 17).

The sequence of events leading to CM pathology is complex and several parameters have been reported to contribute to brain pathology and disruption of the blood brain barrier (BBB). The two main theories that describe the pathogenesis of CM are - the "sequestration theory" and the "cytokine theory". Sequestration is the adherence of infected red blood cells to the brain microvasculature. Mechanical obstruction of vessel caused by binding of infected red blood cells to vascular endothelium results in reduced blood flow and hypoxia which may ultimately lead to coma (18). Sequestration is mediated by *P. falciparum* erythrocyte membrane protein-1 (PfEMP-1), which is anchored on parasite induced knob-like structures on the surface of infected RBCs. PfEMP-1 facilitates the binding of RBCs to various cell surface receptors on the cerebral endothelial cells including intracellular adhesion molecule-1 (ICAM-1), vascular cell adhesion molecule-1 (VCAM-1) and endothelial protein C receptor (EPCR) (19). Binding of PfEMP-1 to receptors on endothelial cell surface activates several downstream signaling pathways leading to rearrangement of tight junction proteins occludin, vinculin and ZO-1 resulting in enhanced BBB permeability (20).

The "Cytokine theory" suggests that heightened pro-inflammatory response, against the parasite results in endothelial dysfunction and disruption of the BBB (21). A direct correlation between increased systemic cytokine levels with severity of disease has been reported and high plasma concentrations of TNF, interferon (IFN)- γ , lymphotoxin (LT)- α , interleukin (IL)-1 α and IL-1 β are observed in CM cases as compared non-severe malaria cases (22).

TNF has been suggested to be a principle cytokine involved in pathogenesis of cerebral malaria (23). TNF levels in serum is a diagnostic marker for disease progression (24). TNF is produced by various immune cells including macrophages, DCs, NK cells and T cells during various stages of the parasite's life cycle (25, 26). Studies in ECM have shown a dual role of TNF in the disease progression. During early stages of infection, TNF fosters clearance of the parasite, at later stages elevated levels of TNF promote disease severity (27). During CM, TNF and IFN- γ induce upregulation of cell adhesion molecule ICAM-1 on the endothelial cells, which contributes to sequestration of RBCs and thereby promotes disease pathology (22, 28). On the contrary, inhibition of TNF by anti-TNF monoclonal antibody did not improve survival of CM patients arguing against a critical role of this cytokine in CM. This could be due to two reasons: (a) anti-TNF antibody stabilizes and retains soluble TNF in circulation thereby aggravates the disease pathology and/or (b) the antibody cannot inhibit cerebral TNF.

IFN- γ produced by NK cells, CD4⁺ T cells and CD8⁺ T cells induce activation of macrophages and contribute to the control of parasite load. In addition, IFN- γ synergizes with TNF and activates endothelial cells to produce cytokines and chemokines (29-31). Furthermore, elevated levels of IL-1 α and IL-1 β are observed in patients with cerebral malaria. Both IL-1 α and IL-1 β induce the expression of chemokines including CCL2, CCL4, CXCL4, CXCL8 and CXCL10 which recruits leukocytes to cerebral microvasculature and further aids in inflammation and BBB disruption (22).

The intracerebral pro-inflammatory response leads to endothelial dysfunction and increased intravascular coagulation. *Plasmodium*-infected RBCs activate both the intrinsic and extrinsic pathway of the coagulation cascade by inducing the expression of tissue factors by the endothelial cells. In addition, iRBCs further enhance coagulation by suppressing the levels of anticoagulative factors, including activated protein C (aPC) and antithrombin. These complex events contribute independently or in tandem to the activation of endothelial cells leading to vascular dysfunction and BBB disruption (19). A detailed understanding of the cellular and molecular process contributing to the disruption of BBB and the subsequent neurological sequelae would aid in the identification of new therapeutic targets.

1.1.3 CM and ECM

Despite several decades of research, precise mechanism and processes that contribute to development of CM remains unknown. The major limitation to study the pathogenesis of cerebral malaria in humans is the restricted availability of physiological data from patients as detailed analysis of the brain pathology can be performed only *post mortem*. Therefore, animal

models including non-human primate models and rodent models have been developed to study the pathogenesis of CM in humans.

Plasmodium berghei ANKA (*PbA*) induced ECM is the most widely used murine model for cerebral malaria as it recapitulates many of the features of human CM. Both CM and ECM display severe brain vasculopathy, resulting from activation of endothelial cells, increased cerebral inflammation, reduced blood flow, development of edema, intracerebral hemorrhages and disruption of the BBB leading to motor and cognitive impairment (3).

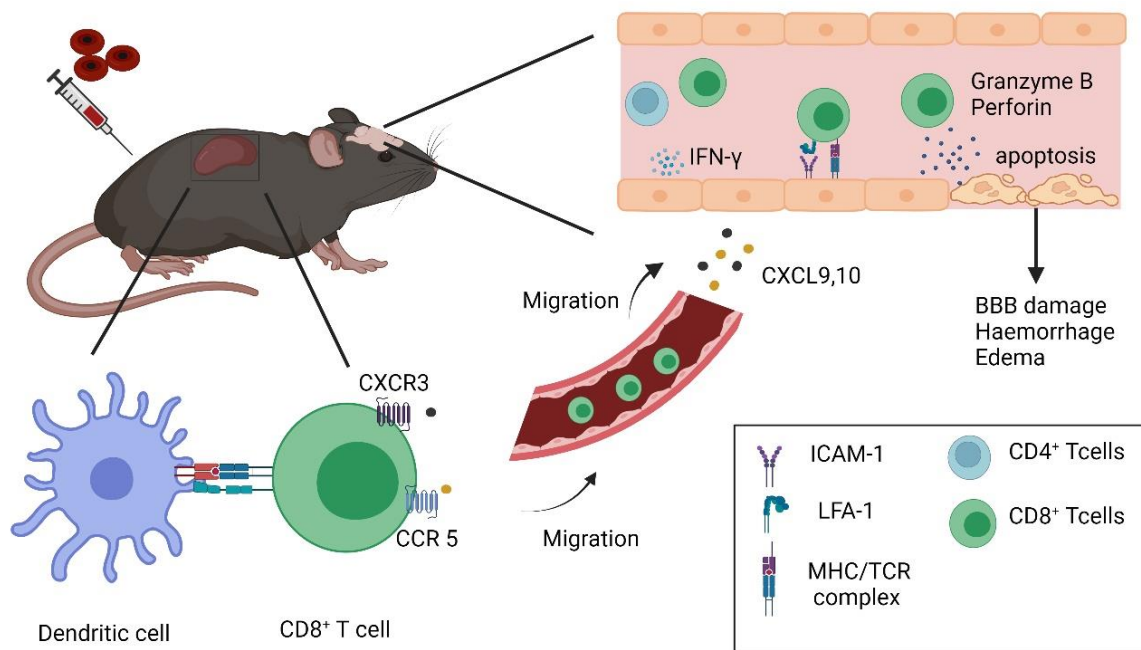


Figure 2: Pathogenesis of experimental cerebral malaria

C57BL/6 mice are intraperitoneally injected with *Plasmodium berghei* ANKA infected RBCs to induce cerebral malaria. Upon phagocytosis, dendritic cells in spleen capture and present *PbA* derived antigens to CD8⁺ T cells. Activated CD8⁺T cells upregulate chemokine receptors CCR5 and CXCR3 and migrate to brain following a CXCL9, 10 gradient. IFN-γ produced by CD4⁺ T cell and CD8⁺ T cells in brain endothelium activates endothelial cells for antigen presentation. Granzyme-B and perforin produced by CD8⁺ T cells causes endothelial cell death resulting in disruption of blood-brain barrier

Despite the above similarities, there are some differences between CM and ECM. Sequestration and accumulation of RBCs is a key pathological feature of CM, whereas in the murine model intracerebral accumulation of pathogenic CD8⁺ T cells and inflammation are essential for driving the brain pathology. Several studies report accumulation of RBCs within brain microvasculature of *PbA* infected mouse but no direct correlation between ECM and RBC sequestration has been reported yet (3). Our group has recently found out that early-

stage accumulation of infected RBCs precedes inflammation during ECM and has a direct effect on edema formation as a result of reduced venous efflux (unpublished data). In addition, recent study shows accumulation of CD8⁺ T cells in brain of patients with cerebral malaria (32, 33). These recent findings emphasize on the similarities between murine and human cerebral malaria.

Infection of mice with *Plasmodium yoelii* (PyXL) also induces accumulation of iRBCs within brain vasculature and development of neuropathological syndromes comparable to human cerebral malaria. However, one of the major drawbacks of this model is hyper-parasitemia, which is not seen in human cerebral malaria cases thus limiting utility of this model (34).

1.1.4 Role of immune response in disease pathogenesis

Upon infection with *PbA*-infected RBCs, parasitized RBCs enter the blood circulation and migrate to the spleen. The spleen is the epicenter of the immune response against *Plasmodium* infection and for parasite control. In the spleen, erythrocyte rupture releases merozoites and parasite-derived antigens into circulation which are taken up by DCs and macrophages (35) (Fig 2).

Dendritic cells

During the blood-stage of infection, DCs are the professional antigen presenting cells responsible for the priming and activation of CD8⁺ T cells. DCs play a central role not only in the initiation of innate and adaptive response against *PbA* but also in pathogenesis of cerebral malaria (36). Activation of DCs through pathogen recognition receptors upon binding to parasite specific PAMPs and DAMPs such as hemozoin, Glycosylphosphatidylinositol (GPI), *Plasmodium* DNA or cytokines such as TNF promotes phagocytosis and upregulation of antigen presenting molecules such as MHC-II, CD80, CD86 and CD40 (36, 37).

DCs also induce an innate-cytokine response following PRR stimulation, which have important modulator functions. IL-12 production by mature DCs is required for optimal priming and activation of T cells (37-39). Conventional CD8 α ⁺ CD11c⁺ DCs have been identified as a major driver of ECM. Antigen cross-presentation and priming of CD8⁺ T cell by CD8 α ⁺ CD11c⁺ DCs is required for development of ECM. Mice lacking CD8 α ⁺ CD11c⁺ DCs or early depletion of conventional CD8 α ⁺ CD11c⁺ DCs confers complete protection against ECM (40, 41).

CD8⁺ T cells:

CD8⁺ T cells play a pivotal role in the pathogenesis of ECM. Pathogen-specific CD8⁺ T cells are primed in spleen by DCs 24 – 48 h after infection. The primed T cells migrate to the brain,

where they receive a second stimulation from the cerebro-vascular endothelial cells which cross-present *PbA* antigen. In response to restimulation, CD8⁺ T cells produce granzyme B and perforin, key molecules that induce the disruption of the BBB (22, 42-44).

Absence of DCs results in impaired cytotoxic T lymphocyte activity due to reduced priming and activation of CD8⁺ T cells and concomitantly reduced accumulation of disease causing CD8⁺T cells in brain microvasculature of *PbA* infected mice. Reduced intracerebral accumulation of CD8⁺ T cells results in reduced cerebral inflammation and protects the mice from ECM (40, 45). Studies using RAG-deficient mice, which lack T cells, or depletion of CD8⁺ T cells after *PbA* infection have shown that CD8⁺ T cells are the major drivers of the disease. Noteworthy that complete protection against ECM could be achieved even when anti-CD8⁺ antibodies were administered only during later stages of infection (46-48). Furthermore, perforin-deficient mice also show complete protection against ECM without BBB damage. Taken together, the development of ECM is dependent on perforin/granzyme-producing CD8⁺ T cells, which mediate endothelial apoptosis and BBB damage (42).

Migration of parasite specific T cells to brain microvasculature upon plasmodium infection is heavily dependent on the chemokine gradient. The chemokine receptors CXCR3 and CCR5 are associated with ECM development as they direct migration of CD8⁺ T cells and NK cells to the brain. IFN- γ promotes cross-presentation of Plasmodium antigens by cerebral endothelial cells, which induces increased production of CXCL9 and CXCL10, ligands for CXCR3 and CCR5. Mice deficient in chemokine receptors CXCR3/CCR5 or their cognate ligands CXCL9/CXCL10 show complete protection against ECM by inhibition of T cell-endothelial cell interaction and the associated inflammatory cascade (22).

CD4⁺T cells

Activation of CD4⁺ T cells by DCs following infection provides protective immunity. CD4⁺T cells contributes to the control of parasite by IFN- γ production, which activates the macrophages, and by maturation of *Plasmodium* specific germinal center B cells which produce protective antibodies. IFN- γ production by Th1 CD4⁺T cells also induces the expression of CXCL9 and CXCL10 within the brain, which further fosters CD8⁺T cell migration and accumulation. On contrary, Foxp3⁺ regulatory T cells (Treg) play a protective role by impairing CD4⁺ and CD8⁺ T cell response and promoting an anti-inflammatory immunosuppressive milieu by production of IL-10 and IL-27 (49).

Role of brain parenchymal cells in CM and ECM pathogenesis

The BBB is composed of microvascular endothelial cells, pericytes and astrocytes, which together with microglia and neurons forms neurovascular unit. Endothelial cell tight junction proteins between adjacent cells contribute to the integrity of BBB. In addition, astrocytes contribute to BBB structure by building glia limitans with their end-feet and induce expression of tight junction proteins by ECs. We and others have shown that astrocytes are activated during infection, and produce leukocyte recruiting chemokines CXCL9 and CXCL10 (50, 51). Pericyte dysfunction during *Plasmodium* infection contributes to loss of BBB integrity by upregulation of chemokines and adhesion molecules on ECs (19).

1.2 TNF

The pleiotropic cytokine TNF has been associated with the cerebral malaria and high levels of circulating TNF have been reported in both CM and ECM. While low levels of TNF are associated with protection against severe malaria high levels of TNF foster ECM. In response to *Plasmodium* infection, TNF is produced by various cell types *in vivo* including macrophages, DCs, T cells and exerts its numerous physiological effects by binding to specific receptors (27). At the cellular level, TNF activates signaling pathways which promote various cellular responses including inflammation, proliferation, differentiation, survival and death (52). TNF is produced as a trimeric type II transmembrane protein that can be cleaved by the metalloproteinase TNF-converting enzyme (TACE). TNF signals via two different TNF receptors, TNFR1 and TNFR2, which differ in their structure, expression and downstream signaling pathways. Soluble TNF preferentially signals through TNFR1, whereas TNFR2 requires membrane bound TNF for its activation. TNFR1 is expressed on all mammalian cell types but expression of TNFR2 is restricted to certain cell types such as immune cells, hepatocytes and endothelial cells (53).

1.2.1 TNF signaling

Signaling via the TNFR1 can induce both cell survival and cell death pathways. Upon binding of TNF to TNFR1, the receptor translocates to the lipid rafts in the plasma membrane and initiates the formation of TNFR signaling complex I, comprising of TNFR1-associated death domain protein (TRADD), which binds to TNFR1 via its C-terminal death domain (DD) and recruits secondary adaptor molecules receptor-interacting serine/threonine-protein kinase 1 (RIPK1), E3 ubiquitin ligases TNF associated factor (TRAF) 2/5, cellular inhibitor of apoptosis (c-IAP) 1/2 and linear ubiquitin chain assembly complex (LUBAC) (Figure 3). The TRAF/c-IAP complexes add K63-linked polyubiquitin chains on RIPK1, generating a docking site for transforming growth factor (TGF)- β -activated kinase 1 (TAK1)/TAK1-binding protein (TAB) 2 complexes. TAK1 further induces canonical NF- κ B activation via the kinase (IKK) complex or

mitogen-activated kinases (MAPK) via the MKK complex. Activation of canonical NF- κ B induces transcription of pro-survival genes such as B cell lymphoma-2 (Bcl-2) and cellular FLICE-inhibitory protein (c-FLIP) and pro-inflammatory genes such as TNF and IL-12 (Fig 3).

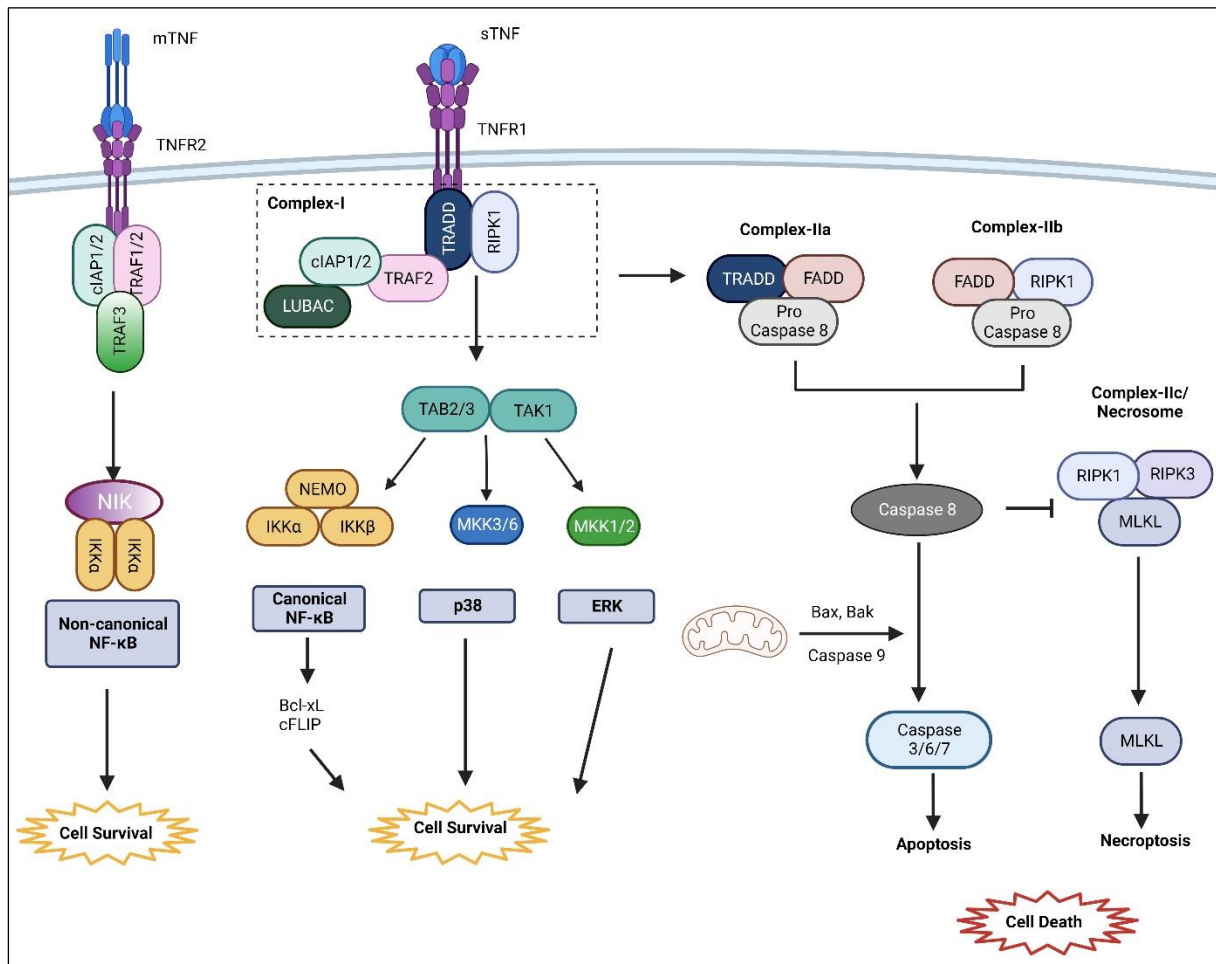


Figure 3: TNFR Signaling

Activation and trimerization of TNF receptor requires ligand-receptor interaction. Post-activation rapid recruitment of TRADD occurs via death domain which further recruits RIPK1, TRAF2, cIAP1 forming membrane bound complex-I followed by assembly of LUBAC complex, TAK/TAB complex and IKK complex and activation of canonical-NF- κ B and MAP kinase signaling pathways. Formation of cytoplasmic complexes inducing TRADD-dependent apoptosis (complex IIa), RIPK1-dependent apoptosis (complex IIb) or necroptosis (complex IIc) depends upon survival signals from membrane bound complex I. Activation of TNFR2 induces formation of membrane proximal complex containing cIAP1/2, TRAF1/2 and TRAF3. K48-linked ubiquitination and degradation of TRAF2 promotes release of NIK and processing of p100 to p52 subunit. (Adapted and modified from (54), Figure created using Biorender)

Ubiquitination of RIPK1 and insufficient pro-survival signals determine the shift between membrane bound complex-I and cytosolic cell death complexes-complex IIa, IIb and IIc.

Complex IIa induces RIPK1 independent apoptosis and involves a DD mediated interaction between TRADD-FADD and initiator caspase, Caspase-8. cFLIP is an inhibitor of caspase-8 and forms heterodimer with caspase-8 to limit its activation. Therefore, formation of complex IIa and activation of RIPK1-independent apoptosis requires inhibition of NF- κ B response and downregulation of pro-survival molecules.

Complex IIb, on the other hand, requires kinase activity of RIPK1 and includes RIPK1, FADD and Caspase-8. As formation of this complex is dependent on kinase activity of RIPK1, this form of cell death is known as RIPK1-dependent apoptosis (RDA). In the absence of c-IAP1 or TRAF2 (54), which act as inhibitors of RDA, complex IIb is formed. In addition to RDA, kinase activity of RIPK1 is also required for the assembly of complex IIc, also called the necrosome. Formation of necrosome requires RIP homotypic interaction motif (RHIM)-dependent interaction between RIPK1 and RIPK3 followed by autophosphorylation and activation of RIPK3 that leads to recruitment and phosphorylation of pseudo-kinase MLKL to the complex. Phosphorylated MLKL translocates from the cytosol to the plasma membrane and forms membrane pores that ultimately lead to osmotic swelling, rupture and cell lysis (54, 55).

In contrast to TNFR1, TNFR2 lacks a death domain and therefore, cannot induce activation of cell death pathways. Stimulation of TNFR2 induces the activation of non-canonical NF- κ B via NF- κ B-inducing kinase (NIK) that mediates phosphorylation and K48-linked ubiquitination of NF- κ B precursor protein p100. p100 is further processed to NF- κ B subunit p52 in a proteasome dependent manner to form active dimers that transcribe numerous target genes fostering cell survival (54).

1.2.2 Checkpoints of TNF signaling

Although TNF signaling can induce activation of signaling cascades with opposite outcomes, i.e. cell survival and cell death, the activation of TNFR1 leads to pro-survival NF- κ B signaling and suppression of cell death pathways in most cell types. Decision to activate cell death signaling is tightly regulated by two distinct checkpoints: (i) an early ubiquitin-dependent TNF checkpoint and (ii) a late transcription-dependent checkpoint.

Ubiquitin-dependent checkpoint: RIPK1 is a key effector protein involved in TNF signaling which can induce or inhibit formation of cell death complex via its kinase activity or scaffolding function respectively (56, 57). While kinase activity of RIPK1 is indispensable for cell death, the role of RIPK1 in activation of NF- κ B is strictly cell type-specific. Ubiquitination of RIPK1 upon TNF stimulation by the TRAF2/c-IAP1 complex has a dual function: (i) K63 ubiquitination

of RIPK1 by TRAF2/c-IAP1 complex facilitates recruitment of LUBAC which mediates M1 ubiquitination of RIPK1. These ubiquitin linkages tethers RIPK1 to membrane bound complex I and prevents migration of RIPK1 to cytosol and formation of complex II (ii) K63 linked ubiquitination of RIPK1 suppresses its activation by autophosphorylation at S166 residue and thus prevents its kinase activity. In addition, direct phosphorylation of RIPK1 by TAK1, IKK and MK2, also inhibit its kinase function (58) (Fig 4).

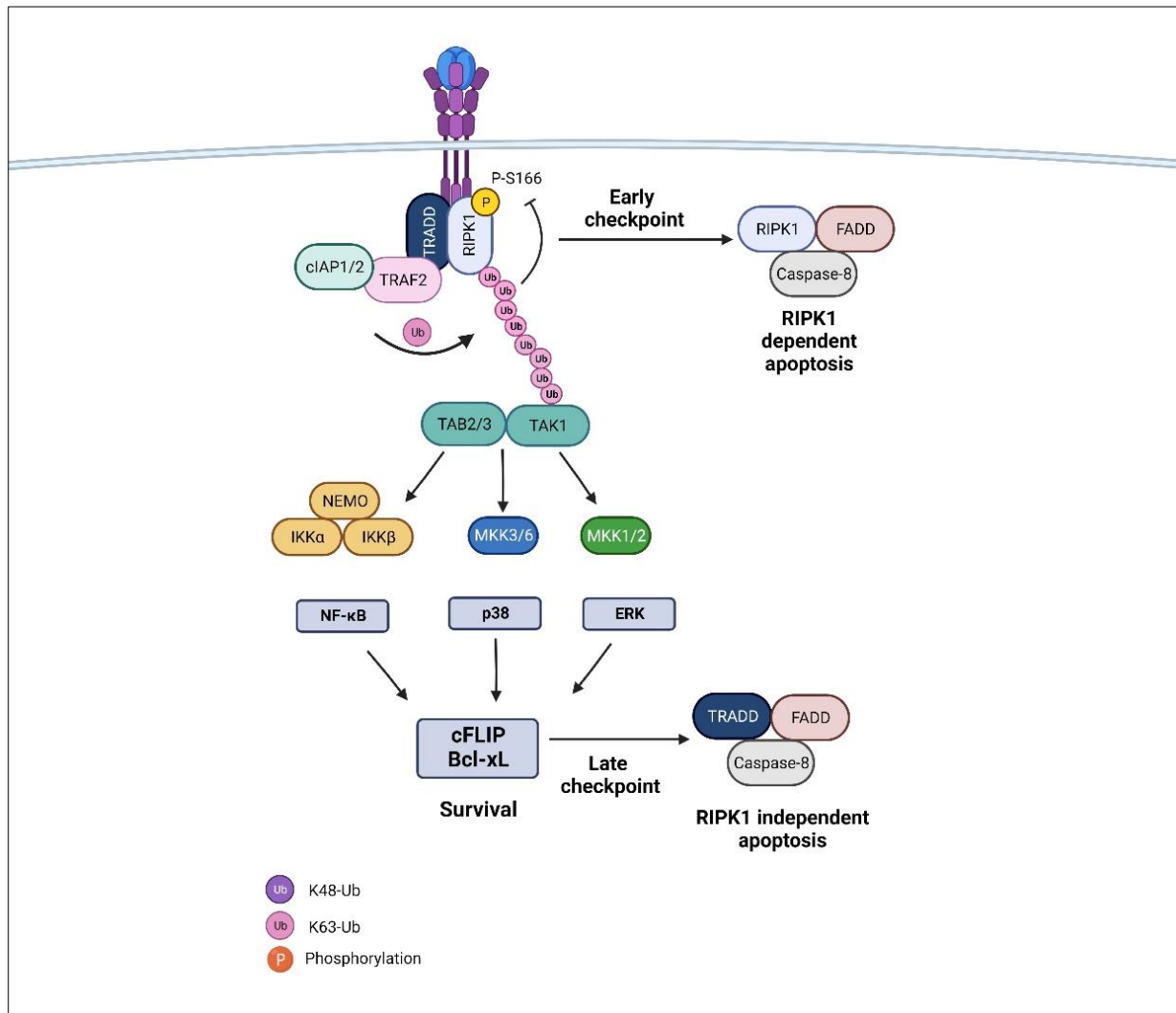


Figure 4: Checkpoints in TNFR-I signaling

Upon engagement TNFR1, RIPK1 in membrane bound complex translocates to cytoplasm initiating cell death cascades. Formation of cytosolic complexes and activation of cell death is tightly regulated by two checkpoints: ubiquitin dependent (K63 ubiquitination of RIPK1) and transcription dependent production of anti-apoptotic molecules cFLIP and Bcl-xL.(Adapted and modified from (58), figure created using Biorender).

Transcription-dependent checkpoint: Activation of NF- κ B pathway and production of pro-survival/anti-apoptotic molecules such as cFLIP, and Bcl-xL inhibit RIPK1-independent apoptosis. cFLIP is a caspase-8 homolog and competitive inhibitor of caspase-8. Caspase-8/cFLIP heterodimer renders caspase-8 inactive by inhibiting its autocatalysis and activation (55, 58) (Fig 4).

1.2.3 Role of ubiquitination and deubiquitination during TNF signaling

Ubiquitination is a process by which the small regulatory protein ubiquitin consisting of 76 amino acids is covalently attached to substrate molecules. Ubiquitination is a multi-step post translational modification which regulates diverse cellular processes. The process of ubiquitination begins with covalent ligation of a single ubiquitin moiety to a lysine residue of protein substrate. Substrates can be modified by a single ubiquitin molecule (monoubiquitination) or several monomers (multi-monoubiquitination). Additionally, ubiquitin can polymerize via isopeptide bonds to form homotypic or heterotypic mixed or branched chain linkages via its seven lysine residues or N-terminal amino group on target substrates (59, 60). Ubiquitination of a protein is a three-step enzymatic reaction which requires ubiquitin activating E1 enzyme, ubiquitin conjugation E2 enzyme and ubiquitin ligating E3 enzymes. The substrate specificity is primarily determined by E3 ligases. Till date, there are 2 E1s, around 40 E2s and over 600 identified E3 ligases (61). Activation of enzymatic cascade begins with hydrolysis of adenosine triphosphate (ATP) by E1 enzyme and formation of a thioester bond between cysteine residue in active site of E1 enzyme and C-terminal glycine residue of ubiquitin, thus activating the COOH-terminus of ubiquitin moiety. Upon activation, ubiquitin is transferred to an E2 enzyme by trans-thiolation reaction and ultimately is transferred via an E3 ligase which binds to both E2-Ub complex and substrate to epsilon-amino group of a lysine residue of the substrate. E3 ligases can either mediate a direct transfer of ubiquitin moiety from E2 enzyme to target by functioning as a scaffolding protein (RING E3 ligases) or in a 2-step reaction by catalyzing transfer of ubiquitin moiety from E2 enzyme to cysteine residue in active site of E3 and thereafter to lysine residue of substrate (HECT E3s, RBR E3s). After this nucleation step, chain elongation requires modification and conjugation of consecutive ubiquitin molecules at either one of seven lysine residues (K6, K11, K27, K29, K33, K48, K63) or through N-terminal amino group of ubiquitin (M1, linear) (62-64) (Fig 5).

Table 1: Types of ubiquitin chains and cellular functions

Type of ubiquitin linkage	Cellular function (65)
M1	Cell signaling, DNA repair, autophagy
K6	DNA damage, mitophagy, cell cycle
K11	Cell cycle, proteasomal degradation
K27	Cell signaling, proteasomal degradation
K29	Proteasomal degradation, cell signaling
K33	Protein trafficking, Protein interaction
K48	Proteasomal degradation
K63	Cell signaling, DNA repair, trafficking, translation

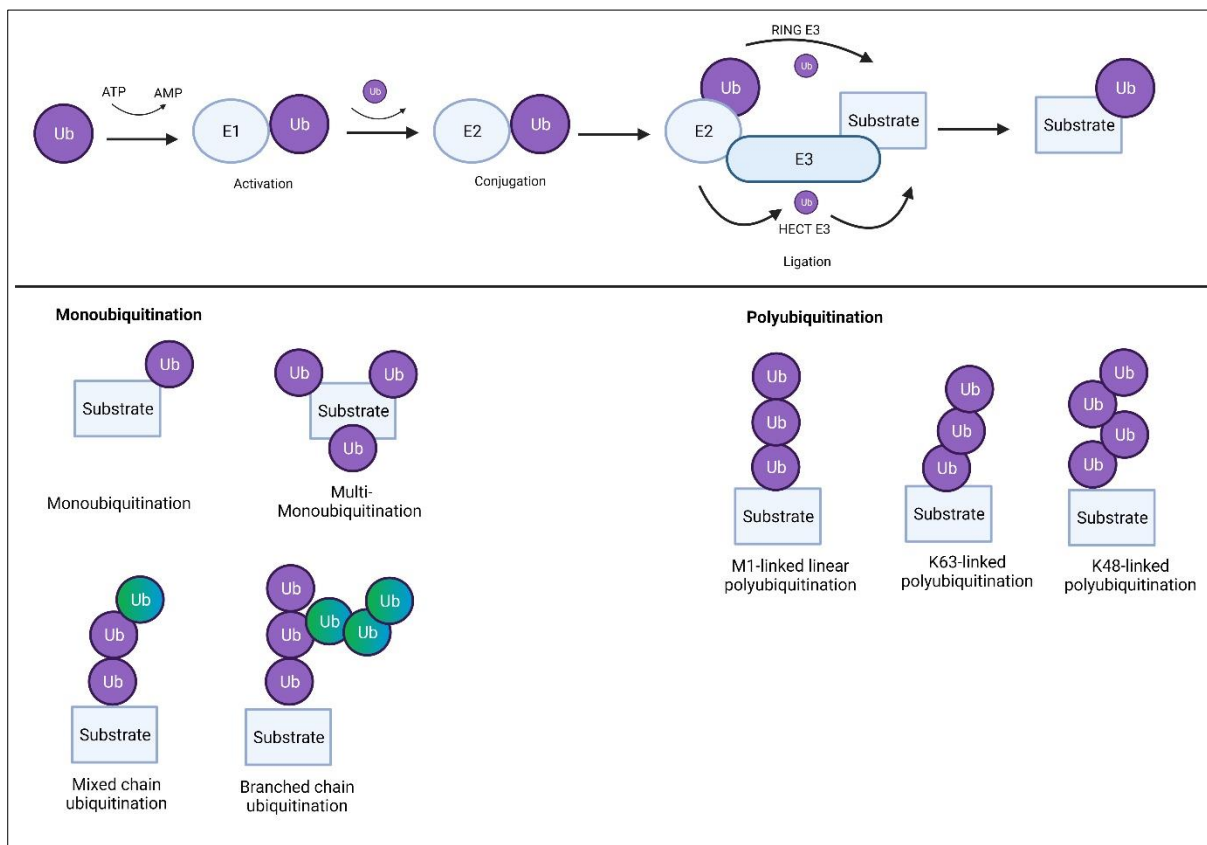


Figure 5: Mechanism of ubiquitination and types of ubiquitin linkages

Binding of ubiquitin to a target molecule is a sequential reaction that requires E1, E2 and E3 enzymes. Ubiquitin linkages can consist of single ubiquitin residue (monoubiquitination, multi-monoubiquitination) or ubiquitin moieties linked together via isopeptide bonds can form chains of ubiquitin, which could be linear, mixed or branched chains. (Figure adapted and modified from (60), figure created using Biorender).

Regulation of TNF signaling by ubiquitination

Post-translational modification by ubiquitin plays a major role in regulating the diverse outcomes of TNF signaling. While initially K48-linked ubiquitination was regarded as the major regulator of TNFR1 signaling, recent studies have shown the importance of other ubiquitin linkages including M1, K11 and K63 in shaping these signaling events. Upon stimulation, the E3 ligases TRAF2/5 and cIAP1/2 are required for K63-linked polyubiquitination of RIPK1 at residue K376 (66, 67) and autoubiquitination of cIAP1 serves as a docking site for LUBAC consisting of adapter proteins SHANK-associated RH-domain interactor (SHARPIN), heme-oxidized IRP2 ubiquitin ligase 1 (HOIL1) and E3 enzyme HOIL1-interacting protein (HOIP) which mediate M1 linked polyubiquitination of RIPK1, TNFR1, TRADD and NEMO (68, 69). K63- and M1-linked ubiquitin modification of RIPK1 facilitates binding and recruitment of the downstream signaling TAB2/3 complex containing TAK1 and IKK-NEMO leading to the subsequent activation of NF- κ B and MAPK pathways (69). In addition to K63 linked polyubiquitination, cIAP1/2 also adds K11- and K48-linked polyubiquitin chains on RIPK1 and together, these modifications repress autoactivation of RIPK1 kinase activity and mark RIPK1 for proteasomal degradation and thereby prevents the formation of death signaling complexes (66, 70).

Binding of TAK1 complex to RIPK1 activates TAK1 kinase which is required for the subsequent activation of IKK kinase (71). In the NF- κ B signaling cascade, heterodimers of NF- κ B transcription factors p50 and Rel τ are maintained in an inactive state by I κ B proteins under steady state. Phosphorylation of NF- κ B inhibitor I κ B by IKK- β kinase is required for K48-linked polyubiquitination and proteasomal degradation of I κ B, and translocation of NF- κ B transcription factor to the nucleus and induction of gene expression. Of note, activation of IKK kinase requires phosphorylation by TAK1 (72, 73). Furthermore, processing of precursor protein p105 to p50 subunit is mediated by K48-linked polyubiquitin chains (74). Along with phosphorylation and activation of IKK kinase 2 and NF- κ B pathway, TAK1 also activates the MAP kinase signaling pathways but precise mechanism remains poorly defined (75).

RIPK1 serves as a switch between pro-survival and pro-cell death signaling. Inhibition of RIPK1 ubiquitination in TRAF2 or cIAP1 deficient cells promotes formation of complex II, increases autophosphorylation of RIPK1 at S166, i.e. increases the kinase activity of RIPK1 and thereby enhances susceptibility to cell death (76). Linear ubiquitination of RIPK1 by LUBAC is also shown to restrict kinase activity of RIPK1 independent of its role in NF- κ B activation (66). In addition to RIPK1, TRAF2 is also required for K48-linked polyubiquitination of p18 subunit of Caspase-8 and forms an additional checkpoint in control of cell death signaling. K48 linked ubiquitination and subsequent degradation of Caspase-8 restrains

activity of caspase-8 subunits p40 and p18 and thereby activation of caspase-3; mediator of apoptotic cell death (77). RIPK1 also promotes stability of TRAF2 as RIPK1-deficient liver parenchymal cells show proteasomal degradation of TRAF2 in a kinase independent manner resulting in hyperactivation of caspase-8 (56).

The dynamic modifications of components of TNFR1 signaling by ubiquitin is required for proper activation of this signaling pathway as well as to achieve a balance between pro-survival, inflammatory response and cell death responses. Fine-tuning of ubiquitination is accomplished by E3-ubiquitin ligases and De-UBiquitinating (DUB) enzymes that can remove ubiquitination from target protein and counteract ubiquitin-ligase function.

De-ubiquitination

Removal of ubiquitin moieties from target protein requires the activity of DUBs. Therefore, DUBs critically regulate several cellular processes. Furthermore, DUBs are also required for the formation of active ubiquitin from ubiquitin pro-proteins in ribosomal subunits or from linear polyubiquitin chains. They also release trapped ubiquitin residues from cellular nucleophiles with thiol-ester intermediates and lastly, DUBs recycle monoubiquitin residues from polyubiquitin chains (78) (Fig 6).

DUBs contain ubiquitin binding domain, protein-protein interaction domains and catalytic domains. They can be subdivided into two classes based on their catalytic site in cysteine proteases and zinc-dependent metallo-proteases. Based on their structural similarity and mechanism of action they can be further subdivided into seven subfamilies, amongst which six are cysteine proteases. This subfamily includes the ubiquitin-specific protease superfamily (USPs), the ovarian tumor protease superfamily (OTUs), ubiquitin C-terminal hydrolase superfamily (UCHs), Machado-Josephin superfamily (MJD), MINDY family, recently discovered ZUFSP family and metallo-protease JAB1/MPN/MOV34 (JAMMs) domain superfamily. DUBs function by hydrolyzing the iso-peptide bond between ubiquitin molecules and target substrates. Some DUBs also display non-catalytic activity where they prevent the transfer of ubiquitin molecule to target protein either by actively binding to E2 enzyme and restricting the generation of E2-ubiquitin thioesters or by restraining transfer of ubiquitin from E3s to substrate (78).

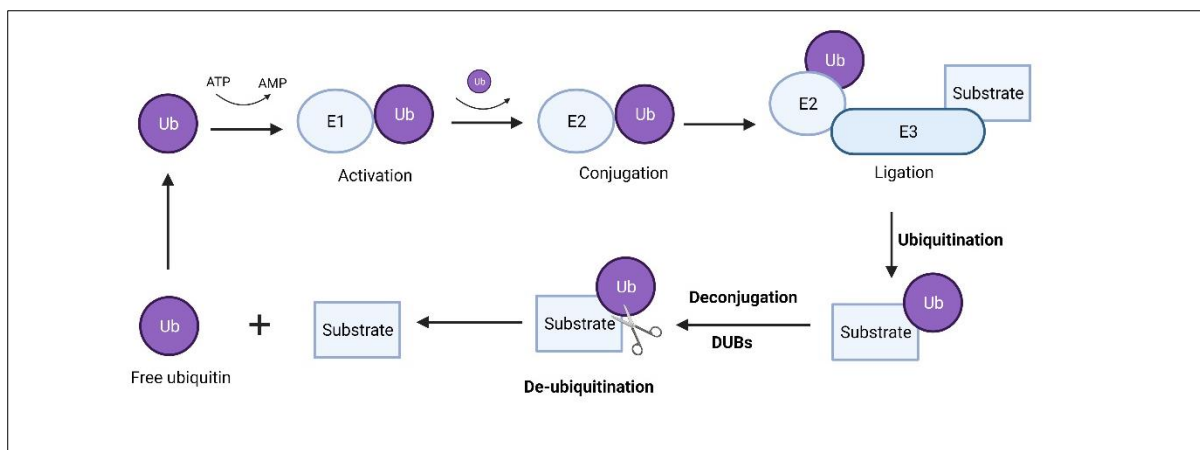


Figure 6: Deconjugation and recycling of ubiquitin molecules by deubiquitinases

DUBs serve several roles in ubiquitin system: Removal of ubiquitin linkages from target proteins, recycling of ubiquitin moieties, reversing ubiquitin mediated post-translational modification on proteins.

Role of DUBs in TNF signaling

DUBs play a pivotal role in the regulation of TNF signaling, In complex I, the DUBs Cyldromatosis (CYLD), TNF- α -induced protein 3 (A20) and OTU Deubiquitinase 7B (OTUD7b) cleave K63-linked ubiquitin chains from RIPK1 (79-81). CYLD destabilizes complex I and facilitates translocation to cytoplasmic complex II by removing M1-and K63-linked ubiquitin chains from RIPK1, TRADD and TNFR1 and loss of CYLD impairs formation of complex II and thereby inhibits cell death. CYLD also interacts with NEMO and TRAF2 and negatively regulates NF- κ B activation (81-83). A20 also suppresses NF- κ B activation and performs a remarkable dual function of de-ubiquitination and ubiquitin ligation. Induction of A20 is NF- κ B dependent. A20 binds to ubiquitinated RIPK1 and removes K63-linked polyubiquitination chains from RIPK1. Furthermore, it conjugates K48-linked polyubiquitin chains on RIPK1 targeting it for proteasomal degradation. Thus, A20 forms an inhibitory feedback loop to prevent hyper activation of NF- κ B and RIPK1 dependent apoptosis (80). It also stabilizes M1-linked ubiquitination in complex I, which is required to inhibit RIPK1 dependent and independent apoptosis (84). This protective effect of A20 is antagonized by the DUB activity of CYLD. OTU deubiquitinase with linear linkage specificity (OTULIN) is another DUB known to catalytically remove M1-linked ubiquitin chains from RIPK1 (85). Studies using OTUD7b (OTU-domain containing protein 7B)-deficient epithelial cells have shown an increased K63-linked ubiquitination of RIPK1 upon TNFR1 stimulation and thereby enhanced NF- κ B activation whereas no regulation of canonical NF- κ B was observed in mouse embryonic fibroblasts (MEFs), bone-marrow-derived macrophages (BMDM) or B cells. Since requirement of K63-linked ubiquitination of RIPK1 for NF- κ B activation is broadly cell-type specific, the role of OTUD7b in regulation of TNFR1 signaling remains to be examined (79, 86). In addition, the function of OTUD7b in the regulation of TNF-induced cell death remains

largely unexplored. In this project, we have studied role OTUD7b in the regulation of NF- κ B and MAP Kinase activation as well as the induction of cell death upon TNFR1 stimulation in primary mouse and human DCs. Furthermore, we also studied whether OTUD7b is involved in cell death induced by other members of TNFR superfamily (Fig 7).

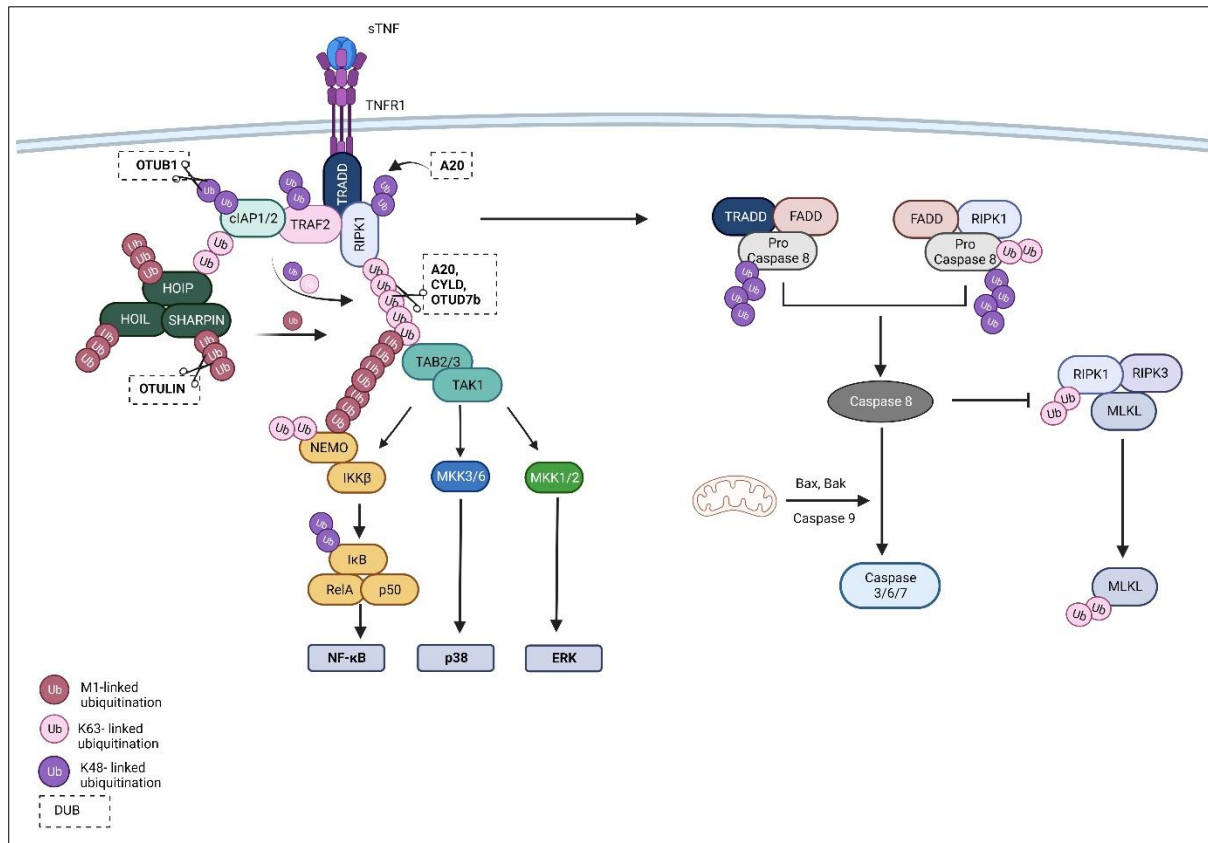


Figure 7: Regulation of TNFR1 signaling by ubiquitination and deubiquitination

Outcome of TNFR1 signaling is tightly regulated by E3 ligase-mediated ubiquitination of proteins present in complex-I/II and by DUBs which cleave ubiquitin linkages. (Figure adapted and modified from (87), figure created using Biorender).

1.3 OTU domain-containing protein 7b (OTUD7b)

OTUD7b belongs to the OTU family of DUBs and shares sequence similarities with A20. The *Otud7b* gene is located on chromosome 1 in the human genome and chromosome 3 in mouse genome. OTUD7b is ubiquitously expressed in all tissues. It removes K11-, K48- and K63-linked ubiquitin from target molecules (88) (Table 2). Structurally, OTUD7b comprises of three domains: the ubiquitin-association domain (UBA), the catalytic OTU domain and Zinc finger domain (ZnF) (89) (Figure 8). UBA domain is a 40aa domain that is responsible for recognition of ubiquitinated substrate by binding to ubiquitin residues on target substrate. In the absence of bound ubiquitin, OTUD7b remains in a closed conformation. Binding of ubiquitin through the UBA domain results in conformational changes in the OTU domain and exposes the catalytic

C194 residue that hydrolyses the ubiquitin moiety (90). The OTU domain of OTUD7b is 182 aa long and also harbors a TRAF binding domain (89). Given that OTUD7b is a cysteine protease, it has two catalytic active residues: cysteine residue positioned at 194aa and histidine residue positioned at 358aa. Mutagenesis experiments have shown that loss of either one of the residues or combined loss results in loss of deubiquitinating activity. The Zinc-finger domain serves as a protein binding domain. OTUD7b shares sequence homology with the ZnF domain of A20 (91) (Fig 8).

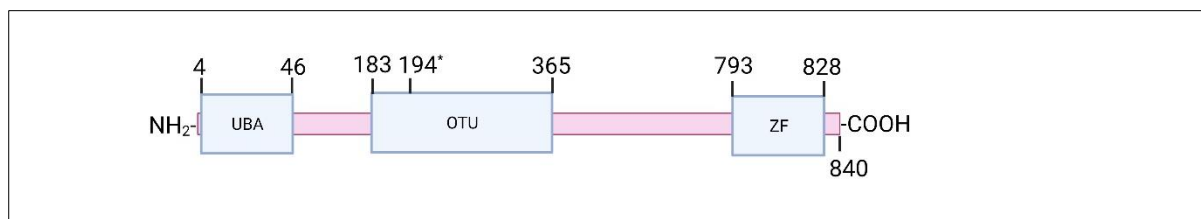


Figure 8: Structure of deubiquitinating enzyme OTUD7b

OTUD7b comprises of ubiquitin binding domain (UBA), A20-like OTU domain and zinc finger domain (ZF) with catalytic active residue at C194 within OTU domain of enzyme. (Figure adapted from (86), figure created using Biorender).

Table 2: Interaction partners and signaling pathways regulated by OTUD7b

Target	Ub-linkage	Cellular processes
TRAF3	K48	Non-canonical NF-κB pathway (86)
ZAP70	Poly-Ub	T-cell activation (92)
EGFR	FLAG-tagged Ub	EGFR trafficking (93)
TRAF6	K63	Inflammatory response to hypoxia (94)
PARK7	Inhibition of deubiquitinase activity	Canonical NF-κB pathway (95)
GβL	K63	mTORC2 formation (96)
APC/C complex	K11	Cell cycle (97)
LSD-1	K63	Cell cycle (98)
IRF3-SQSTM1/p62	K63	Autophagy (99)
PIK3C3	K48	Autophagy (100)
RIPK1	K63	Canonical NF-κB signaling (79)

OTUD7b has several interaction partners and regulates several cellular processes summarized in Table 2. However, very few studies have addressed role of OTUD7b in

infections. During *L. monocytogenes* infection, conventional OTUD7b-deficient mice harbored higher bacterial load in liver and displayed impaired CD4⁺ and CD8⁺ T-cell response against the pathogens compared to wildtype mice (92). On the contrary, OTUD7b-deficient mice showed B-cell hyperresponsiveness and better pathogen control of the intestinal bacterial pathogen *Citrobacter rodentium* (86). OTUD7b has also been shown to impair anti-viral response during vesicular stomatitis virus infection by fostering autophagic degradation of IRF3 in macrophages (99). However, the role of OTUD7b in parasitic diseases has yet not been studied.

2. Aims of this study:

Since DCs play an important role in initiating host defense against *Plasmodium* infection and the function of OTUD7b in parasitic infections is unknown, we studied the DC-specific function of OTUD7b in ECM employing a novel conditional knockout mouse strain with selective deletion of *Otud7b* in DCs.

The overall aims of this project are:

1) Study the DC-specific function of OTUD7b in experimental cerebral malaria

The role OTUD7b has been previously studied during bacterial (*Listeria monocytogenes*, *Citrobacter rodentium*) and viral (Vesicular stomatitis virus) infection. Here we studied the impact of OTUD7b in DCs on survival and parasite control using *Otud7b^{fl/fl}* and CD11c-Cre *Otud7b^{fl/fl}* mice. In addition, we investigated whether OTUD7b-deficiency of DCs influences the activation, survival and cytokine production of DCs and the induction of a CD8⁺ T cells response during *PbA* infection.

2) Understand the molecular mechanisms by which OTUD7b regulates DC function

Using primary BMDCs and human monocyte-derived DCs we analyzed the regulation of TNF-mediated inflammatory and cell death signaling by OTUD7b and the molecular mechanism how OTUD7b influences the outcome of TNF signaling.

MATERIAL AND METHODS

3.1 Materials:

3.1.1 Chemicals for animal experiments

Table 3: List of reagents used for invivo experiments

Reagent	Company
Isoflurane (Forene ®)	Abbott, Germany
Heparin 5000U/mL	Biochrom AG, Germany
Glycerol	Calbiochem, Germany
Evans blue solution	Sigma Aldrich, Germany
Giemsa stain	Carl Roth, Germany

3.1.2 Material for cell culture

Table 4: Cell line

Cell line	Company
HEK 293T	ATCC

Table 5: List of cell culture reagents

Reagent	Company
Dulbecco's modified eagle medium (DMEM)	Gibco by Thermo Fischer Scientific, USA
RPMI 1640 medium	Gibco by Thermo Fischer Scientific, USA
Dulbecco's Phosphate-Buffered Saline (DPBS)	Gibco by Thermo Fischer Scientific, USA
10% Fetal Calf Serum (FCS)	PAA Laboratories GmbH, Austria
Penicillin/Streptomycin	Gibco by Thermo Fischer Scientific, USA
Sodium Pyruvate	Gibco by Thermo Fischer Scientific, USA
L-Glutamine	Gibco by Thermo Fischer Scientific, USA
Non-Essential Amino Acids	Gibco by Thermo Fischer Scientific, USA
2-mercaptoethanol	Gibco by Thermo Fischer Scientific, USA
Murine Granulocyte macrophage colony-stimulating factor (GM-CSF)	Peprtech, Germany
Murine fms-like tyrosine kinase 3 ligand (Flt3L)	Peprtech, Germany
Murine Macrophage Colony-Stimulating Factor (MCSF)	Peprtech, Germany

Human Granulocyte macrophage colony-stimulating factor (GM-CSF)	Peprotech, Germany
Human IL-4	Peprotech, Germany
LPS, <i>E.coli</i>	Sigma Aldrich, Germany
Trypsin-EDTA	Gibco by Thermo Fischer Scientific, USA

Table 6: List of cell stimulation reagents

Reagent	Company
Recombinant murine IL-6	Peprotech, Germany
Recombinant murine IL-10	Peprotech, Germany
Recombinant murine IFN- γ	Peprotech, Germany
Recombinant murine TNF	Peprotech, Germany
Recombinant human TNF	Peprotech, Germany
Recombinant murine TRAIL	Peprotech, Germany
Purified anti-mouse CD95 antibody	BD Bioscience

Table 7: List of inhibitors used *in vitro* and *in vivo*

Inhibitor	Target	Company
MG132	Proteasome inhibitor	Sigma Aldrich, Germany
Necrostatin-1s (Nec-1s)	RIPK1	BioVision Inc., USA
Z-VAD-FMK (zVAD)	Pan-caspase	Enzo Life Sciences, USA

Table 8: List of consumables

Description	Company
Cell strainer (40 μ m, 100 μ m)	Falcon, USA
Cell culture plates (10 cm, 6 well, 12 well, 96 well)	Greiner Bio-One, Germany
Cell culture flasks (T-25, T-75, T-175)	Greiner Bio-One, Germany
Cuvettes	Sarstedt AG& Co., Germany
Eppendorf tubes	Eppendorf, Germany
Filter paper 583 gel dryer	Bio-Rad, USA
5mL polystyrene round-bottom tube	Falcon, USA
Polyvinylidene fluoride (PVDF) membrane	Roche Diagnostics, Germany
Serological pipette	Greiner Bio-One, Germany
Lightcycler plates 480 plate 96 white	Roche diagnostics, Germany

3.1.3 Materials for transfection

Table 9: List of guide RNAs sequence

Target Gene	Design ID	Sequence
Traf 2 (mouse)	Mm.Cas9.TRAF2.1.AA	CGGACCAGGCCTTTACATGC
Traf 2 (mouse)	Mm.Cas9.TRAF2.1.AB	ACCCTGTAGCCACGTGGACC
Traf 2 (mouse)	Mm.Cas9.TRAF2.1.AC	CTCTGCAGATTCCACACCGT
Otud7b (human)	Hs.Cas9.OTUD7b.1.AA	CAGCTACGTCAAGTCCATGC
Otud7b (human)	Hs.Cas9.OTUD7b.1.AB	TCAGATTTTGTCCGTTCCAC
Otud7b (human)	Hs.Cas9.OTUD7b.1.AC	ATGATCGGGACTTGATGCTG

Table 10: Vectors

Expression plasmid	Company
pCMV6-GFP-OTUD7b	Origene, USA

Table 11: List of reagents used for nucleofection

Reagent	Company
P4 primary cell 4D-nucleofector X kit	Lonza, switzerland
P3 primary cell 4D-nucleofector X kit	Lonza, switzerland
Cas9 Nuclease V3	Integrated DNA technology, USA
CRISPR-Cas9 traacrRNA	Integrated DNA technology, USA
Cas9 Electroporation Enhancer	Integrated DNA technology, USA
Lipofectamine 3000	Thermo Fischer Scientific, USA
Opti-MEM Medium	Thermo Fischer Scientific, USA

3.1.4 Reagents for molecular biology

Table 12: List of reagents for molecular biology techniques

Reagent	Company
Dithiothreitol (DTT)	Qiagen, Germany
Deoxyribonucleotide triphosphates (dNTPs)	Thermo Fischer Scientific, USA
First Strand Buffer (5x)	Thermo Fischer Scientific, USA
HotStar Taq DNA Polymerase	Qiagen, Germany
Oligo(dT) ₁₂₋₁₈ Primer	Thermo Fischer Scientific, USA
Polymerase chain reaction (PCR) Buffer (10x)	Qiagen, Germany
SuperScript II Reverse Transcriptase	Thermo Fischer Scientific, USA

Table 13: List of primers

Primer	Sequence (5'-3')
CD11c Cre Sense	5'-ACT TGCCAGCTGTCTGCCA-3'
CD11c Cre Anti-Sense	5'-GCGAACATCTTCAGGTTCTG-3'
Otud7b Sense	5'-CAGAATAAAGAGGTGGGTGAGC-3'
Otud7b Anti-Sense	5'-ACTCACATTGCAGTGATCATGC-3'

All primers were purchased from Eurofins MWG, Germany.

Table 14: TaqMan™ gene assay probes

TaqMan Assay probe	Gene	Assay ID	Amplicon length
Bcl-xL	<i>Bcl2l1</i>	Mm00437783_m1	65
c-FLIP	<i>Cflar</i>	Mm01255576_m1	83
HPRT	<i>Hprt</i>	Mm01545399_m1	81
Ifn-γ	<i>Ifng</i>	Mm00801778_m1	101
IL-6	<i>Il6</i>	Mm00446190_m1	78
TNF	<i>Tnf</i>	Mm00443258_m1	81
IL-12	<i>Il12</i>	Mm99999067_m1	63
IL-10	<i>Il10</i>	Mm00439616_m1	85

All TaqMan™ were purchased from Thermo Fischer Scientific, Germany.

3.1.5 Reagents for protein analysis

Table 15: List of reagents for protein analysis

Reagent	Company
GammaBind G Sepharose Beads	GE Healthcare, Sweden
PageRuler Prestained Protein Ladder (10 -180 kDa)	Thermo Fischer Scientific, USA
Phenylmethanesulfonylfluoride (PMSF)	Cell Signaling Technology, USA
Protease Inhibitor Cocktail (25x)	Sigma Aldrich, Germany
Protein Assay Dye Reagent Concentrate	Bio-Rad, USA
Radioimmunoprecipitation assay (RIPA) buffer (10x)	Cell Signaling Technology, USA

Table 16: List of antibodies for western blotting

Primary Antibody	Specification	Catalogue number	Company
α -OTUD7b	Rabbit Polyclonal	16605-1-AP	Proteintech, USA
α -GAPDH	Rabbit Monoclonal	2118	Cell Signaling Technologies, USA
α -Caspase 3	Rabbit Polyclonal	9662	Cell Signaling Technologies, USA
α -Cleaved Caspase 3	Rabbit Monoclonal	9664	Cell Signaling Technologies, USA
α -phospho-p65	Ser536 Rabbit Polyclonal	3031	Cell Signaling Technologies, USA
α - I κ B α	Rabbit Monoclonal	4812	Cell Signaling Technologies, USA
α -p65	Rabbit Monoclonal	8242	Cell Signaling Technologies, USA
α -phospho-p38	Thr180/Tyr182, Rabbit Monoclonal	9215	Cell Signaling Technologies, USA
α -p38	Rabbit Polyclonal	9212	Cell Signaling Technologies, USA
α - phospho-p44/42	Thr202/Tyr204, Rabbit Polyclonal	9101	Cell Signaling Technologies, USA
α -p44/42 MAPK	Rabbit Polyclonal	9102	Cell Signaling Technologies, USA
α -TRAF2	Rabbit Polyclonal	4724	Cell Signaling Technologies, USA
α -RIPK1	Rabbit Monoclonal	3493	Cell Signaling Technologies, USA
α -Caspase 8	Rabbit Monoclonal	4790	Cell Signaling Technologies, USA
α -Cleaved Caspase 8	Asp 387 (mouse specific), Rabbit Polyclonal	9429	Cell Signaling Technologies, USA
α -phospho-MLKL	S345, Rabbit Monoclonal	ab196436	Abcam, United Kingdom
α -cIAP1	Rabbit Polyclonal	ab154525	Abcam, United Kingdom
α -FADD	Rabbit Monoclonal	ab124812	Abcam, United Kingdom

α -ubiquitin Lys48-specific	Rabbit Monoclonal	05-1307	Merck Millipore, USA
α -ubiquitin Lys63-specific	Rabbit Monoclonal	05-1308	Merck Millipore, USA
α -MLKL	Rat Monoclonal	MABC604	Merck Millipore, USA
α -tGFP	Mouse Monoclonal	TA150041	Origene, USA

Secondary Antibody	Company
Rabbit Anti-Mouse IgG/HRP (polyclonal)	Dako, Denmark
Swine Anti-Rabbit IgG/HRP (polyclonal)	Dako, Denmark
Goat Anti-Rat IgG/HRP (polyclonal)	Abcam, United Kingdom
Mouse Anti-Rabbit IgG, light chain specific	Jackson ImmunoResearch Europe Ltd., UK
Goat Anti-Rabbit IgG, light chain specific	Jackson ImmunoResearch Europe Ltd., UK

3.1.6 Reagents for flow cytometric analysis

Table 17: Reagents for flow cytometry

Description	Company
RPMI 1640 media	Gibco by Thermo Fischer Scientific, USA
GAP-50 peptide (SLLNAKYL)	JPT Peptide Technologies, Germany
PE-conjugated H2-Db SLLNAKYL pentamer	ProlImmune, United Kingdom
GolgiPlug	BD Biosciences, USA
Percoll	GE Healthcare, Sweden
α -CD16/32	Thermo Fischer Scientific, USA
Fixable Viability Dye eFluor 780	eBioscience by Affymetrix, USA

Table 18: List of antibodies for flow cytometry

Fluorochrome	Antibody	Clone	Company
FITC	α -CD3	17A2	BioLegend, USA
BV421	α -CD8	536.7	BioLegend, USA
PerCP	α -CD45	30-F11	BioLegend, USA
PE	α -CD11c	N418	eBioscience by Affymetrix, USA
FITC	α -CD8	CC63	eBioscience by Affymetrix, USA

PeCy7	α -CD11b	M1/70	BioLegend, USA
APC	α -PDCA1	927	BioLegend, USA
FITC	α -CD86	GL-1	BioLegend, USA
PE	α -CD80	16-10A1	BioLegend, USA
PE	α -MHC I	M1/42	BioLegend, USA
FITC	α -MHC II	39-10-8	BioLegend, USA
PE	α -IL 12	C17.8	eBioscience by Affymetrix, USA
PE	α -IFN γ	B27	eBioscience by Affymetrix, USA
PE	α -GranzymeB	16-10A1	eBioscience by Affymetrix, USA
APC	α -Annexin V	-	BioLegend, USA
PerCP	7AAD	-	eBioscience by Affymetrix, USA

3.1.7 Kits used in this study

Table 19: List of kits

Description	Company
EasySep™ Mouse CD11c positive selection kit	STEMCELL Technologies, Germany
EasySep™ Mouse CD11b positive selection kit	STEMCELL Technologies, Germany
EasySep™ Mouse CD3 negative selection kit	STEMCELL Technologies, Germany
EasySep™ Mouse NK1.1 positive selection kit	STEMCELL Technologies, Germany
EasySep™ Mouse CD19 positive selection kit	STEMCELL Technologies, Germany
RNeasy Mini kit	Qiagen, Germany
Pierce ECL plus western blotting substrate	Thermo Fischer Scientific, USA
Intracellular fixation and permeabilization buffer set	eBioscience by Affymetrix, USA
KAPA mouse genotyping kit	KAPA Biosystems, USA
KAPA PROBE FAST qPCR master mix (2x) kit	KAPA Biosystems, USA

CyQUANT LDH Cytotoxicity Assay	Thermo Fischer Scientific, USA
QIA shredder kit	Qiagen, Germany
Q5 site directed mutagenesis kit	NEB, USA
Cell Proliferation Kit (MTT)	Sigma-Aldrich, Germany
MojoSort Human CD14 Nanobeads	BioLegend, USA
Annexin V Apoptosis Detection Kit	BioLegend, USA

3.1.8 List of instruments

Table 20: Instruments

Instrument	Company
Biometra standard power pack P25	AnalytikJena, Germany
Bio-Rad mini protein system	Bio-Rad, USA
Intas Chemo Cam Luminescent Image Analysis system	INTAS Science Imaging Instruments, Germany
Trans-Blot Turbo Transfer System	Bio-Rad, USA
Agagel Midi-wide	Biometra Analytik, Germany
Lightcycler 480 II	Roche Diagnostics, Germany
Professional gel documentation system	PHASE, Germany
Neubauer counting chamber (improved)	LO laboroptik, UK
Incubator Heraeus Cytosperm 2	Heraeus, Germany
Cytek NL-3000	Cytek Bioscience, USA
Biotek microplate reader	BioTek, USA
Bio Photometer	Eppendorf, Germany
Centrifuge ROTANTA 460R	Hettich, USA
Centrifuge Mikro 22R	Hettich, USA
EasySep Magnet	STEMCELL Technologies, Germany
Laminar flow hood	Heraeus, Germany
Microscope Olympus-CX41	Olympus, Germany
Thermomixer	Eppendorf, Germany
Vortex Genius 3	IKA, Germany

3.1.9 Softwares

Table 21: Software for data analysis

Software	Description	Company
FlowJo® software	Analysis of Flow Cytometry data	FlowJo LLC, USA
GraphPad Prism 9	Statistical analysis	GraphPad Software, USA
LabImage	Analysis of Western Blot data	Intas Science Imaging Instruments GmbH, Germany

3.1.10 Animals

C57BL/6 Otud7b^{fl/fl} were crossed with C57BL/6 CD11c-Cre mice to generate novel conditional CD11c-Cre Otud7b^{fl/fl} transgenic mice which lack the expression of OTUD7b specifically in dendritic cells. C57BL/6 Otud7b^{fl/fl} mice were used as controls in all experiments. Animals were maintained and bred under pathogen free conditions throughout. Age and sex matched animals were used for all experiments. Experiments were performed in compliance with German Animal Welfare Act in a protocol approved by local authorities (Landesverwaltungsamt Sachsen-Anhalt) under license number- 33.12-42502-04-20/3500.

3.2 Methods-

In vivo experiments

3.2.1 Mice Genotyping

Mice strains were genotyped by polymerase chain reaction (PCR) from genomic DNA extracted from tail biopsy sample of four-week-old mice using KAPA mouse genotyping kit. DNA extraction and subsequent PCR was performed according to manufacturer's instruction using primers listed in Table 13. PCR products were separated on 1.5% agarose gel in TAE (Tris base, Acetic acid and EDTA) buffer.

3.2.2 Parasite infection

Rodent parasite *Plasmodium berghei* strain ANKA (*PbA*) infected erythrocytes were used to induce cerebral malaria in susceptible C57BL/6 mice. Parasite stocks were prepared *in vivo* by passage of infected erythrocytes in C57BL/6 mice and stabilates were harvested in Alsever's solution with 10% glycerol and stored in liquid nitrogen. Mice were injected intra-peritoneal (i.p.) with a dose adjusted to 1×10^6 RBCs/100 μ l for each stabilate and disease symptoms appeared at day 7 p.i.

3.2.3 Assessment of neurological symptoms

PbA infected mice were assessed daily for 10 parameters of Rapid Murine Coma and Behavior Scale (RMCBS) with a score range of 0-2 for each parameter (0 = lowest function, 2 = highest function) (101).

Label	Score	Description
Coordination		
• Gait	(0-2)	(none-ataxia-normal)
• Balance	(0-2)	(no body extension-extends front feet on wall-entire body lift)
Exploratory Behavior		
• Motor Performance	(0-2)	(none-explores 2-3 corners in 90 secs-explores 4 corners in 15 secs)
Strength and Tone		
• Body Position	(0-2)	(on side- hunched- full extension)
• Limb Strength	(0-2)	(no grasp- weak pull back- strong pull back)
Reflexes and Self-Preservation		
• Touch Escape	(0-2)	(none-unilateral-instant and bilateral)
• Pinna Reflex	(0-2)	(none-unilateral-instant and bilateral)
• Toe Pinch	(0-2)	(none-unilateral-instant and bilateral)
• Aggression	(0-2)	(none-bite attempt with tail cut-bite attempt prior to tail cut, in 5 seconds)
Hygiene-Related Behavior		
• Grooming	(0-2)	(ruffled-dusty/piloreraction-normal/clean with sheen)

3.2.4 Assessment of parasitemia

Parasitemia was monitored daily by microscopic examination of Giemsa-stained thin blood smears prepared from tail blood. Blood films were fixed in absolute methanol and stained with 10% Giemsa in phosphate buffer saline (PBS). Parasite load was calculated as percentage of infected RBCs per 10 microscopic light fields.

3.2.5 Assessment of Blood-Brain Barrier integrity

Blood-brain barrier permeability was assessed by Evans blue dye extravasation in brain tissue. Mice received 100µl of 2% Evans blue solution in PBS. After 1h, mice were anesthetized with isoflurane and perfused transcardially. Perfused brains were collected and photographed.

3.2.6 Leukocyte isolation from spleen and brain

For isolation of leukocytes, mice were perfused intracardially with 0.9% NaCl and organs were isolated. Mechanical dissociation of organ was performed using 70µm cell strainer and 100µm cell strainer for spleen and brain respectively. Erythrocytes were lysed using ammonium chloride RBC lysis buffer and washed with Hank's Balanced Salt Solution (HBSS) + 3% FCS at 1200 rpm for 6 minutes. For spleen samples, cell pellet was resuspended in PBS and cell numbers were determined.

Table 22: Composition of erythrocyte lysis buffer (pH 7.2-7.4)

NH ₄ Cl	8.29 g
KHCO ₃	1 g
Na ₂ EDTA	37.2 mg
Distilled water	Volume makeup to 1L

To purify leukocytes from brain, an additional percoll density gradient centrifugation was performed using discontinuous 80%-40% percoll gradients. Single cell suspension was resuspended in 15mL of 80% percoll and 15mL of 40% percoll was slowly pipetted onto the top ensuring formation of a two-layered gradient. Tubes were centrifuged at 1200 x g at 25° C for 20 minutes with no brakes for gradual deceleration. Afterwards, top layer was discarded and the interface layer which contained leukocytes was collected. Cells were washed once with HBSS supplemented with 3% FCS at 1200 rpm for 6 minutes and number of viable cells were determined using trypan blue staining.

3.2.7 Flow cytometry

Leukocytes isolated from spleen and brain were stained for flow cytometric analysis. For staining extracellular surface antigens, an aliquot of 1x10⁶ cells was transferred to 5 mL polystyrene round bottom tube and washed once with FACS buffer (DPBS supplemented with 3% FCS). To block non-specific antibody binding, cells were incubated for 10 mins at 4°C in dark with 1:50 dilution of CD16/32 in FACS buffer. To discriminate between live and dead cell population, cells were stained with Fixable Viability Dye eFluor 506 in 1:100 dilution for 30

minutes at 4° C, protected from light. Cell surface marker staining was performed with a 1:100 dilution of specific flurochrome-conjugate antibodies mentioned in table 18 for 30mins at 4°C in dark. Plasmodium specific CD8⁺ T cells were detected by staining with PE-conjugated H-2Db SLLNAKYL pentamer in conjugation with anti-CD8 antibody. Cells were then washed once with FACS buffer at 1200 rpm for 6 minutes at 4°C and resuspended in PBS for acquisition.

For analysis of intracellular cytokines, cells were stimulated *ex vivo* with *PbA* epitope glideosome-associated protein 50 (GAP-50) or Phorbol 12 myrisate 13-acetate at a concentration of 10µg/mL in RPMI 1640 media supplemented with 10% FCS for 4h at 37°C with 1µg/mL of GolgiPlug for the enrichment of protein concentration in Golgi complex by inhibition of protein transport. After stimulation, cells were washed with PBS at 1200 rpm for 6 minutes, followed by FcR blocking with CD16/32 and extracellular antigen staining as described above. Thereafter, cells were washed twice with PBS and resuspended in 1x intracellular staining perm wash buffer. Intracellular stains were added at a dilution of 1:100 in 1x perm wash buffer with appropriate IgG negative control and incubated at 4°C in dark for 30 minutes. Afterwards, cells were washed twice with 1x perm wash buffer and pellet was resuspended in PBS for acquisition.

3.2.8 Measurement of cell death by flow cytometry

Annexin V/ 7AAD staining kit was used for *ex-vivo* analysis of cell death. Splenocytes were washed twice and resuspended in Annexin V binding buffer and stained with FITC labelled Annexin V and 7-amino actinomycin D (7-AAD) in combination with anti-CD11c for 15 minutes at room temperature in dark. Cells were then analyzed by flow cytometry.

3.2.9 Adoptive cell transfer

Control and TRAF2 deficient BMDC were resuspended in PBS at a concentration of 1x10⁶ cells/100 µl and 100µl of cell suspension was injected intravenously in CD11c-Cre Otud7b^{fl/fl} mice prior to infection with *PbA*.

3.2.10 Magnetic sorting for splenic leukocytes

Isolation of different cell types-dendritic cell, macrophage, T cell, B cell and NK cell, from spleen of Otud7b^{fl/fl} and CD11c-Cre Otud7b^{fl/fl} were isolated using specific kits from STEMCELL Technologies as mentioned in table 19. Spleen harvested from Otud7b^{fl/fl} and CD11c-Cre Otud7b^{fl/fl} were minced in PBS containing 2% FCS and single cell suspension was obtained by passing through 70µm strainer. Afterwards, cell pellet was incubated with rat serum to block non-specific binding followed by labelling and magnetic cell separation with specific antibody according to manufacturer's instructions. Isolated population was

resuspended in RIPA buffer for isolation of protein and level of OTUD7b was analyzed by western blotting.

Cell Culture

3.2.11 Bone Marrow-derived Dendritic Cell (BMDC)/ Bone Marrow-derived Macrophage (BMDM) culture-

C57BL/6 *Otud7b^{fl/fl}* and *CD11c-Cre Otud7b^{fl/fl}* were anesthetized with isoflurane and femur and tibia were removed under sterile conditions. Both ends of bone were cut off and bone marrow cells were flushed using Dulbecco's Modified Eagle Medium (DMEM). The cell suspension was centrifuged at 1200 r.p.m. for 6 minutes and cell pellet was resuspended with ammonium chloride RBC lysis buffer. Following RBC lysis, cell suspension was washed twice with DMEM medium and cultured in 10 cm plates with DMEM supplemented with 10% FCS, 1% penicillin/streptomycin, 1% non-essential amino acids, 1% glutamine, 50 μ M 2-mercaptoethanol. Mouse bone marrow cells were supplemented with 200ng/mL of murine fms-like tyrosine kinase 3 ligand (Flt3L) or 35ng of Granulocyte Macrophage Colony-Stimulating Factor (GM-CSF) for differentiation into Bone Marrow-derived Dendritic Cells (BMDC) and with 35ng/mL of Macrophage Colony-Stimulating Factor (MCSF) for differentiation into Bone Marrow-derived Macrophages (BMDM). Medium was changed every 3 days and cells were harvested at day 6 (BMDM) or day 9 (BMDC) to obtain immature cells. For maturation, dendritic cells were incubated with 100ng of Lipopolysaccharide (LPS) from *E.coli* for 24h. Purity of culture was determined by flow cytometry using anti-CD11c antibody for BMDC cultures and anti-CD11b antibody and anti-F4/80 antibody for BMDM cultures.

3.2.12 HEK293T cell line

HEK293T cells were cultured in DMEM media supplemented with 10% FCS and 1% solution of penicillin and streptomycin. Cells were passaged to a ratio of 1:10 every 2-3 days, when 80% confluent. Routine tests were performed to check for mycoplasma contamination in cell culture.

3.2.13 Human monocyte derived dendritic cells

Peripheral Blood Mononuclear Cells (PBMC) were isolated from buffy coat using Ficoll-Paque density gradient centrifugation. Middle layer containing mononuclear cells present between serum and sorbitol was collected in fresh falcon tubes, washed with MACS buffer and counted. CD14⁺ monocytes were positively selected from total mononuclear fraction by Magnetic-activated cell sorting (MACS) using Human CD14 nanobeads according to manufacturer's protocol. After isolation, CD14⁺ monocytes were resuspended in RPMI 1640 supplemented with 10% FCS and differentiated to immature dendritic cells using a cocktail of 50ng human

GM-CSF and 50ng human IL-4 for 5 days followed by incubation with 100ng LPS for 48h for maturation.

***In vitro* cell culture assay**

3.2.14 LDH Assay

Lactate Dehydrogenase (LDH) cytotoxicity assay was performed using CyQUANT LDH assay kit. Supernatant from untreated and treated BMDC cultured in 96 well plate was collected and quantification of extracellular LDH release was performed according to manufacturer's instruction.

3.2.15 MTT Assay

Mature BMDC were cultured in a 96-well plate at a density of 4×10^4 cells/well and stimulated accordingly. MTT assay performed using Cell proliferation kit from Abcam according to manufacturer's instructions. Formazan crystals were dissolved in DMSO and concentration was determined at 570nm.

***In vitro* Dendritic cell stimulation**

3.2.16 Enrichment of Plasmodium infected erythrocytes and dendritic cell stimulation

Separation and concentration of mature stage parasites was performed by magnetic separation by exploiting the paramagnetic properties of hemozoin, a byproduct of hemoglobin digestion by parasite.

PbA infected RBCs were isolated by MACS separation using LS columns. Peripheral blood was collected from *PbA* infected mice by cardiac puncture and parasitemia was determined before enrichment was carried out. LS column was placed into a QuadroMACS separator and rinsed with RPMI1640. Afterwards, column was filled with *PbA* infected blood and flow through was discarded. Column was then washed with RPMI1640 until eluent was free of RBCs. After wash steps, column was removed from the separator and hemozoin containing *PbA* infected RBCs were collected by flushing the column with RPMI1640. Collected fraction was centrifuged and supernatant was discarded. A thin layer giemsa stain was performed to check for the purity of eluent ($\approx 90\%$). Dendritic cells were incubated with *PbA*-iRBCs or uninfected RBCs at a ratio of 1:3 for 6h and 24h. Thereafter, cells were harvested for protein isolation.

3.2.17 Cytokine stimulation of BMDC

Matured BMDC were incubated in serum free media for 12h prior to addition of cytokines. Following day, cells were maintained in complete media supplement with GM-CSF and stimulated with 50 ng of mentioned cytokines. MG132 was used for proteasome inhibition.

Cell Lysate and Sample Preparation-

For protein extraction cells were washed twice with ice cold PBS and lysed with radio immunoprecipitation assay (RIPA) lysis buffer supplement with protease inhibitor and phosphatase inhibitors. Cell lysate were incubated with RIPA lysis buffer for 30 minutes at 4°C. The suspension was centrifuged at 14000 rpm for 10 minutes and supernatant was carefully transferred in a fresh eppendorf tube. BCA assay was used for determination of total protein concentration in cell lysates. To denature the protein, samples were mixed with 1x lane marker reducing sample buffer and boiled at 99°C for 5 minutes.

Table 23: Composition of RIPA lysis buffer

RIPA (10x)	1x
Protease Inhibitor cocktail (25x)	1x
PhosSTOP (10x)	1x
PMSF	1mM

For analysis of phosphorylated proteins, cells were serum starved for 12h to reduce basal level phosphorylation. Proteasomal inhibitor MG132 was added to detect K48 linked polyubiquitin chains.

Protein analysis

3.2.18 Western Blotting

Equal amounts of denatured protein samples were separated by SDS-polyacrylamide gel electrophoresis (SDS-PAGE) and percentage of gel was selected according to molecular weight of protein of interest. Subsequently, separated proteins were transferred to a polyvinylidene difluoride (PVDF) membrane using semi-dry electroblotting. To block non-specific binding of antibodies, membrane was blocked 5% BSA, 5% milk or 1% BSA+1% milk respectively, for 1h at room temperature. The transferred proteins were then probed with target protein specific primary antibody overnight at 4°C (table 16). Thereafter, membrane was washed thrice with TBST buffer and incubated with HRP tagged secondary antibody at room temperature (table 16). ECL Plus chemiluminescent blotting substrate was used for detection of signal and imaged on Chemo Cam Luminescent Image Analysis system. For quantification of protein expression, LabImage Platform software was used.

3.2.19 Co-Immunoprecipitation

Protein samples isolated from control and treated cells were pre-cleared to reduce non-specific binding. Lysates were incubated with GammaBind G Sepharose Beads for 1h at 4°C with continuous mixing. Thereafter, samples were centrifuged at 10,000 rpm, supernatant was

collected and equal amount of protein was incubated with antibody against target protein overnight at 4°C with continuous shaking. Following day, the immune complex was captured by incubating with Sepharose G beads at 4°C and collected by centrifugation at 10,000 rpm. Bead complex was three time with ice cold buffer and proteins were eluted in 2x lane marker reducing sample buffer. Proteins were then analyzed by western blot as discussed above.

Gene expression analysis

3.2.20 qRT-PCR

Total RNA was isolated from spleen or matured BMDCs. Samples were lysed and homogenized in RLT buffer with 1% β -mercaptoethanol and RNA isolation was performed using RNeasy Mini Kit according to manufacturer's instructions. Concentration and purity of isolated RNA was quantified using NanoDrop Spectrophotometer and 1 μ g of total RNA was used for synthesis of first strand complimentary DNA (cDNA) using Superscript Reverse Transcriptase Kit.

Table 24: cDNA synthesis

Total RNA	1 μ g
RNase free water	Volume makeup to 50 μ l

1. Annealing

Oligo (dT) ₁₂₋₁₈ Primer	2 μ l
dNTPs	5 μ l

5 mins at 65°C, afterwards cool on ice

2. First strand cDNA synthesis

First strand buffer (5x)	16 μ l
DTT	8 μ l
SuperScript II Reverse Transcriptase	1.5 μ l
RNase free water	4.5 μ l

50 mins at 42°C

3. Inactivation

10 mins at 70°C

To evaluate the cDNA, conventional PCR for the housekeeping gene HPRT was performed. Quantitative PCR was performed with TaqMan probe based assay using TaqMan probes as listed in table 14 and KAPA PROBE FAST qPCR Master Mix (2x) kit on a LightCycler 480 II according to manufacturer's manual. Gene expression of target gene was normalized to gene expression of HPRT reference gene. Double delta Ct analysis was performed to calculate fold change in gene expression and all data are expressed as the increase in the level of mRNA expression in infected mice over uninfected controls (102).

Table 25: qRT-PCR reaction mix

KAPA PROBE FAST qPCR Master Mix (2x)	10µl
TaqMan gene expression assay probes	0.5µl
cDNA	2µl (1µg/µl)
PCR grade water	Upto 20µl

Inhibitor Experiments

3.2.21 *In vitro* cell death inhibition-

Inhibitor of apoptosis (Z-VAD-FMK) and necroptosis (Necrostatin-1s) were used independently or in combination to determine the mode of cell death in mature TNF stimulated BMDCs. The inhibitor was added 90 minutes prior to TNF stimulation and cells were harvested at indicated timepoints for western blot analysis.

3.2.22 *In vivo* Z-VAD-FMK and Nec-1s treatment

Mice were injected intravenously (i.v.) with 6mg/kg Z-VAD-FMK (zVAD) or 4mg/kg Necrostatin-1s (Nec-1s) 90 minutes prior to *PbA* infection. Treatment with zVAD and Nec-1s was continued upto day 7 p.i. and thereafter mice were sacrificed and organs were collected for Flow cytometry analysis.

Transfection

3.2.23 Nucleofection of BMDCs

Knockdown of TRAF2 in BMDCs was performed on day6 of BMDC culture using P4 Primary cell 4D-nucleofector kit and cells were transfected with program DK-100 in Lonza 4D-nucleofector. Three Cas9-gRNA vectors were used for efficient knockdown (table 9) and

transfected cells were maintained in culture for three more days with GM-CSF. Knockdown efficiency was determined by western blot.

3.2.24 Site directed mutagenesis

OTUD7b cloned in pCMV6-AC-GFP mammalian expression vector was purchased from Origene. Truncated constructs pCMV6-GFP-OTUD7b- Δ N, pCMV6-GFP-OTUD7b- Δ C lacking N-terminal ubiquitin associated domain (UBA) and C-terminal zinc finger domain (ZF) respectively and catalytic inactive pCMV6-GFP-OTUD7b-C194S mutant harboring a point mutation in conserved C194 residue were generated using Q5 Site Directed Mutagenesis Kit from NEB and back-to-back orientation plasmids. Verification of constructs was done by plasmid DNA sequencing (Eurofins Genomics).

Table 26: Primers for OTUD7b plasmid

Primer	Sequence (5'-3')	Amplicon length
OTUD7b Sense	5'-TTTGAACAGTTGCGTCAAGTCC-3'	22
OTUD7b Anti-sense	5'-ATTCCTTCTGCCACTCATC-3'	19

Primer used for mutagenesis

Mutagenesis	Position(s)	Primer Sequence
N-terminal UBA domain	1-45	S: 5'-CAAGTCCATGCTGGGAACCTATCC-3' AS: 5'-CATGGCGATCGCGGCGGC-3'
Active site	194	S: 5'-GATGGGAACTCCCTCCTGCAT-3' AS: 5'-CCCAGTAGTTGCTAAAGG-3'
C-terminal ZF domain	799-840	S: 5'-ACGCGTACGCGGCCGCTC-3' AS: 5'-TTTGGTCTGGGTTGGGGGAAGTCC-3'

3.2.25 Transfection of HEK293T cells-

HEK293T cells were transiently transfected with pCMV6-GFP-OTUD7b plasmid or pCMV6-GFP-OTUD7b- Δ N, pCMV6-GFP-OTUD7b-C194S and pCMV6-GFP-OTUD7b- Δ C mutant constructs using Lipofectamine 3000 reagent according to manufacturer's protocol. Transfection efficiency was monitored by western blotting.

3.2.26 Nucleofection of Human Monocyte derived Dendritic cells-

OTUD7b knockdown in CD14⁺ monocyte was performed using P3 primary cell 4D-nucleofector X kit and 4D-nucleofector from Lonza. For CRISPR mediated knockdown, a

combination of three different CRISPR-Cas9 guide RNAs were used as mentioned in table 9 for each nucleofection reaction. Nucleofected cells were cultured for 5 days in complete RPMI media supplemented with hGM-CSF and hIL-4 as described earlier in section 2.2.12. At day 5, knockdown efficiency was analyzed by western blotting and cells were used for further experiments.

4. RESULTS

4.1 Generation and characterization of CD11c-Cre Otud7b^{fl/fl} conditional knockout mice

To study the DC-specific function of OTUD7b, we generated a conditional knockout mouse which in OTUD7b is specifically deleted in DCs. Embryonic stem cells from C57BL/6 N mice were transfected with the targeting vector in which exon 7 of the Otud7b gene was flanked by loxP sites (Figure 9). The positive clones were selected by lac Z expression and neomycin resistance. The FRT-flanked NeoR and Lac Z cassettes were subsequently removed by crossing to FLP-deleter strain, to generate Otud7b^{fl/fl} mice. To delete OTUD7b in DCs, Otud7b^{fl/fl} mice were further crossed to CD11c-Cre mice to generate CD11c-Cre Otud7b^{fl/fl} mice (Figure 9).

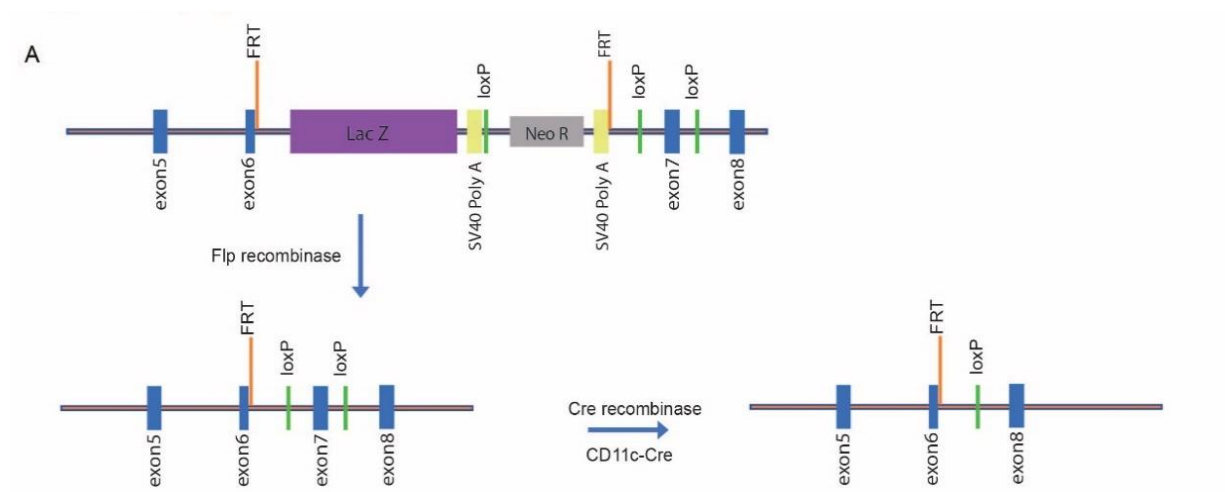


Figure 9: Strategy for generation of CD11c-Cre Otud7b^{fl/fl} mice

Targeting strategy for generating CD11c-Cre Otud7b^{fl/fl} mice with LoxP sequences flanking exon 7 of Otud7b gene

To check whether OTUD7b was specifically deleted in DCs *in vivo*, CD11c⁺ DCs, CD11b⁺ macrophages, NK1.1⁺ NK cells, CD3⁺ T cells and CD19⁺ B cells were isolated from spleen by MACS and the expression of OTUD7b was analyzed by western blot (Figure 10). Furthermore, BMDCs were differentiated *in vitro* in the presence of GM-CSF or Flt3 ligand and BMDMs were differentiated using M-CSF, and the expression of OTUD7b was detected by western blotting. As shown in (Figure 10), OTUD7b was specifically deleted in DC of CD11c-Cre Otud7b^{fl/fl} mice but not in the other cell types.

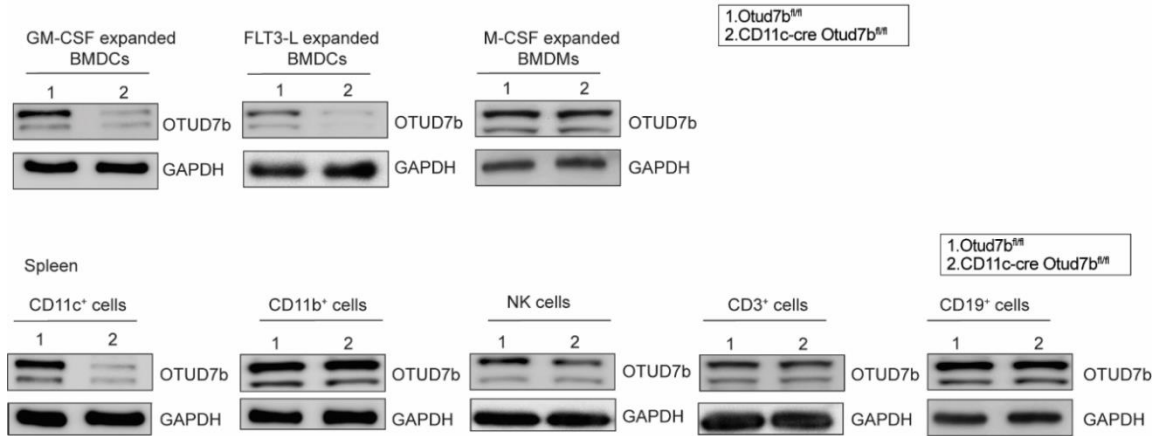


Figure 10: Dendritic cell specific deletion of OTUD7b

(A) OTUD7b expression was analyzed by western blotting in GM-CSF expanded and FLT3-L expanded BMDCs and M-CSF expanded BMDMs. (B) Magnetic cell separation and cell isolation from splenocytes was performed using anti-CD11c⁺, CD11b⁺, NK1.1⁺, CD3⁺ and CD19⁺ antibodies. OTUD7b expression was analyzed by western blotting.

The CD11c-Cre *Otud7b^{fl/fl}* mice were born in a normal mendelian ratio and developed normally with no phenotypical abnormalities. Importantly, flow cytometric analysis showed similar immune cell composition in spleens both *Otud7b^{fl/fl}* and CD11c-Cre *Otud7b^{fl/fl}* mice indicating that OTUD7b is dispensable for the development of the immune system. (Figure 11).

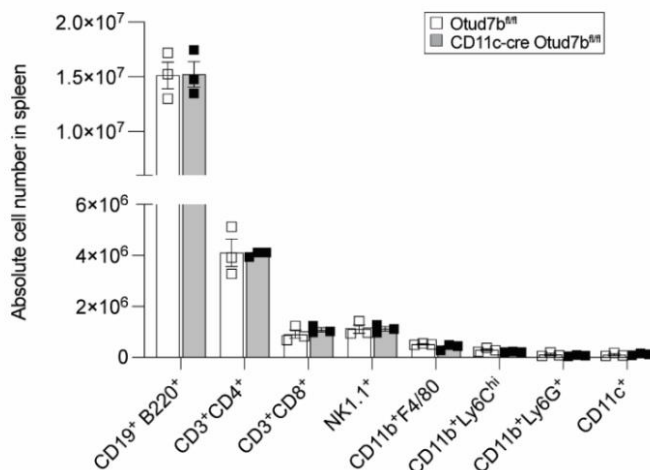


Figure 11: OTUD7b deficiency is dispensable for immune system development

Absolute number of leukocytes in spleen of 52-weeks old *Otud7b^{fl/fl}* and CD11c-Cre *Otud7b^{fl/fl}* mice were determined by flow cytometry (n=3, per group)

4.2 DC-specific OTUD7b-deficiency confers protection against ECM

To study whether OTUD7b in DCs regulates the outcome of ECM, *Otud7b^{fl/fl}* and CD11c-Cre *Otud7b^{fl/fl}* mice were infected with 1×10^6 *PbA*-infected RBCs i.p. and the progression of the disease was monitored daily according to 10 parameters of the RMCBS score (101). While all

the *Otud7b^{fl/fl}* mice showed clinical symptoms of ECM such as ataxia, loss of grip strength, and progressive paralysis within 7 days post infection with an average RMCBS score of 12 at day 7 post infection, all of the *CD11c-Cre Otud7b^{fl/fl}* mice remained healthy with no neurological signs of the disease and a RMCBS score of (Figure 12A).

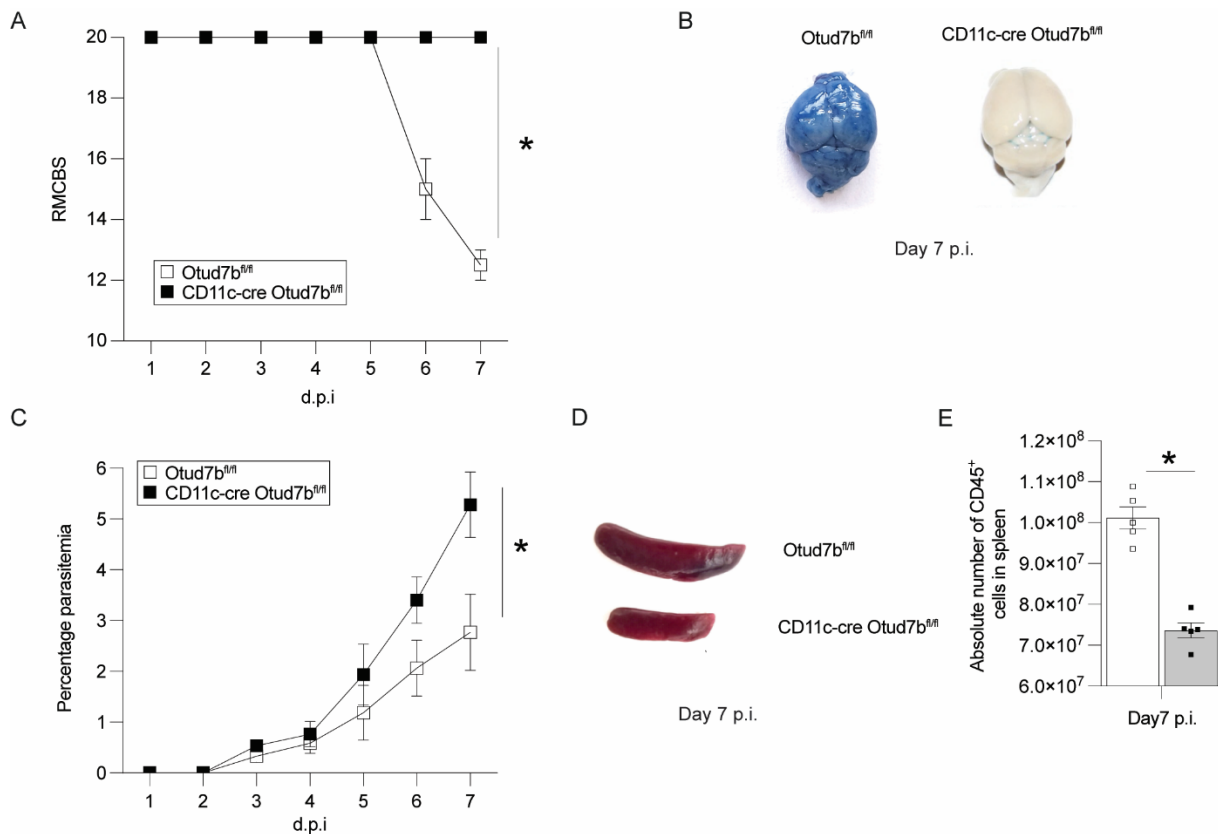


Figure 12: Deletion of *Otud7b* confers protection against *PbA*-induced ECM

Otud7b^{fl/fl} and *CD11c-Cre Otud7b^{fl/fl}* mice were infected i.p. with 1×10^6 *PbA* infected RBCs in 100 μ L (n=10, per experimental group). (A) Mice were assessed daily up to d7 p.i. for neurological signs according to the 10 parameters of the RMCBS score (Student t-test, *p<0.05) (B) At d7 p.i., mice were injected i.v. with 1% Evans blue dye for 1hr and perfused with 0.9% saline. Representative image of one of the three independent experiments (C) Giemsa-stained peripheral blood smears were prepared daily to monitor parasitemia (data represented as mean value + SEM) (*p<0.05) (D) Photos of spleens of *Otud7b^{fl/fl}* and *CD11c-Cre Otud7b^{fl/fl}* mice at d7 p.i.. Representative images of one of three independent experiments are shown. (E) Absolute numbers of CD45⁺ cells in the spleen of *PbA*-infected mice were determined by flow cytometric analysis (data represented as mean value + SEM) (*p<0.05).

Evans blue permeability assay showed extensive BBB damage in *Otud7b^{fl/fl}* mice at day 7 p.i., whereas *CD11c-Cre Otud7b^{fl/fl}* mice showed an intact BBB with no vascular leakage of the dye. This illustrates that OTUD7b in DCs is required for BBB damage and development of ECM. (Figure 12B). To evaluate whether the protection of the *CD11c-Cre Otud7b^{fl/fl}* mice from ECM was due to better pathogen control, the parasite load in the peripheral blood was

enumerated daily in Giemsa-stained thin blood smears. Of note, the parasite load was significantly higher in CD11c-Cre Otud7b^{fl/fl} mice compared to Otud7b^{fl/fl} mice (Figure 12C), indicating that the protection of the CD11c-Cre Otud7b^{fl/fl} mice from ECM was not due an enhanced pathogen control. Interestingly, the spleens of the CD11c-Cre Otud7b^{fl/fl} mice were much smaller compared to the spleens of the Otud7b^{fl/fl} mice at day 7 p.i. (Figure 12D) and contained reduced numbers of CD45⁺ leukocytes (Figure 12E), suggesting that DC-specific OTUD7b may be essential for an effective immune response for the control of the parasite and induction of immunopathology.

4.3 Reduced number of DCs and CD8⁺ T cells in CD11c-Cre Otud7b^{fl/fl} mice upon *PbA* infection

Since the CD11c-Cre Otud7b^{fl/fl} mice harbored higher parasite loads and reduced numbers of CD45⁺ leukocytes, we hypothesized that DC-specific OTUD7b is critical for the induction of the anti-parasitic immune response. Therefore, we first enumerated the DC numbers in response to *PbA* infection. While number of DCs in uninfected naïve control mice were comparable among CD11c-Cre Otud7b^{fl/fl} and Otud7b^{fl/fl} mice groups, the relative and absolute number of CD11c⁺ DCs were reduced in spleens of CD11c-Cre Otud7b^{fl/fl} mice at days 2 and 7 post infection (Figure 13 B,C).

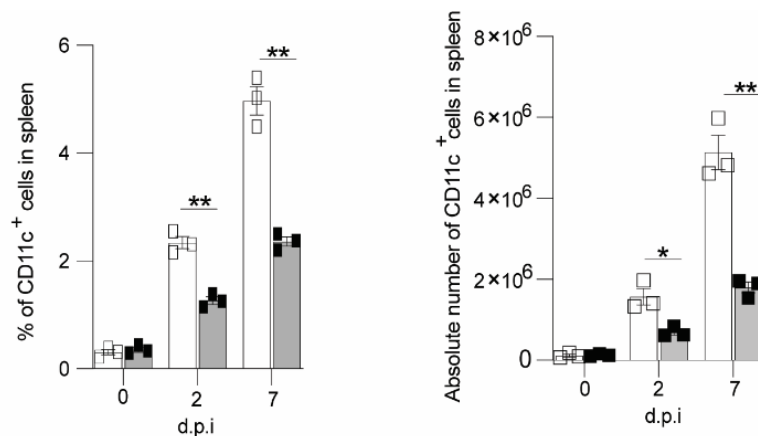


Figure 13: Reduced number of DCs in CD11c-Cre Otud7b^{fl/fl} mice upon *PbA* infection

Otud7b^{fl/fl} and CD11c-Cre Otud7b^{fl/fl} mice were infected with 1x10⁶ *PbA* infected RBCs. At d0, d2 and d7 p.i spleens were harvested and DCs was analyzed by flow cytometry (n=3). (A) relative cell number (right) and absolute cell number (left) of CD11c⁺ DCs.

Flow cytometric analysis revealed that in particular, the conventional DC subsets cDC-1 (CD11c⁺ CD8α⁺) and cDC-2 (CD11c⁺ CD11b⁺) were reduced in spleens of CD11c-Cre Otud7b^{fl/fl} mice at day 2 and day 7 p.i. (Figure 14 A, B, C). while the numbers of PDCA-1⁺ plasmacytoid DCs did not differ between the two mice groups.

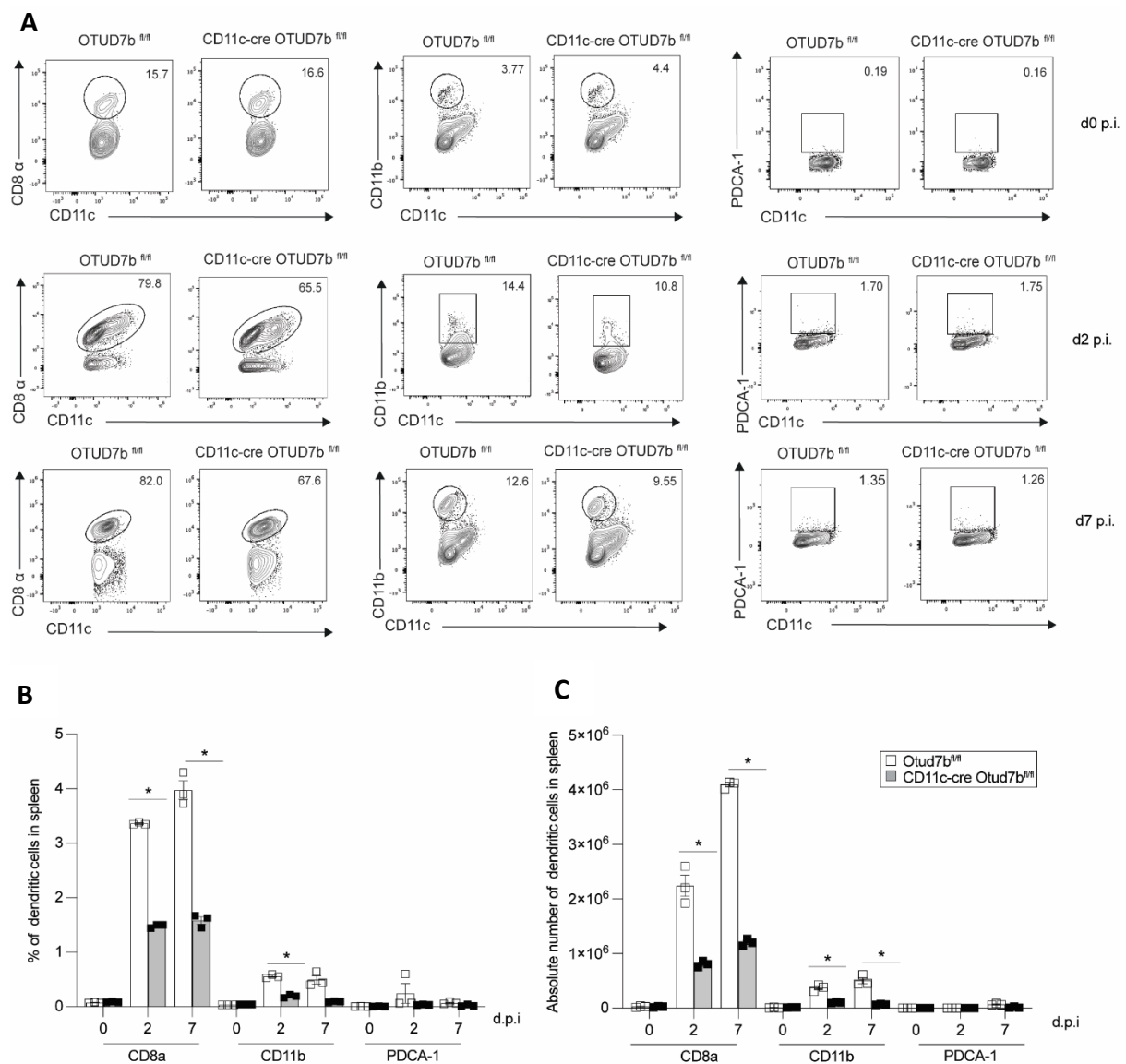


Figure 14: Reduced population of conventional DCs upon *PbA* infection

DC subpopulation were analyzed by flow cytometry in spleens of *PbA*-infected *Otud7b^{fl/fl}* and *CD11c-Cre Otud7b^{fl/fl}* mice. (A) Dot plots, (B) relative cell numbers and (C) absolute cell numbers of $CD11c^+$ $CD8\alpha^+$ cDCs, $CD11c^+$ $CD11b^+$ cDCs and $CD11c^+$ $PDCA-1^+$ pDCs are shown. Data represent the mean value \pm SEM. A-D Student's t-test * $p < 0.05$

Since cDC1 are essential for priming and presenting antigen to disease ECM causing $CD8^+$ T cells (36, 41, 103), we evaluated whether the reduction of cDC1 in *CD11c-Cre Otud7b^{fl/fl}* mice influenced the priming of $CD8^+$ T cells by enumerating the number of $CD8^+$ T cells in spleen at days 2 and 7 p.i. In concurrence to reduced DC numbers, the relative and absolute numbers of total $CD8^+$ T cells and $CD8^+$ T cells specific for the *PbA* GAP50 protein were also significantly reduced in the spleens of *CD11c-Cre Otud7b^{fl/fl}* mice at day 7 p.i. (Figure 15A-C)

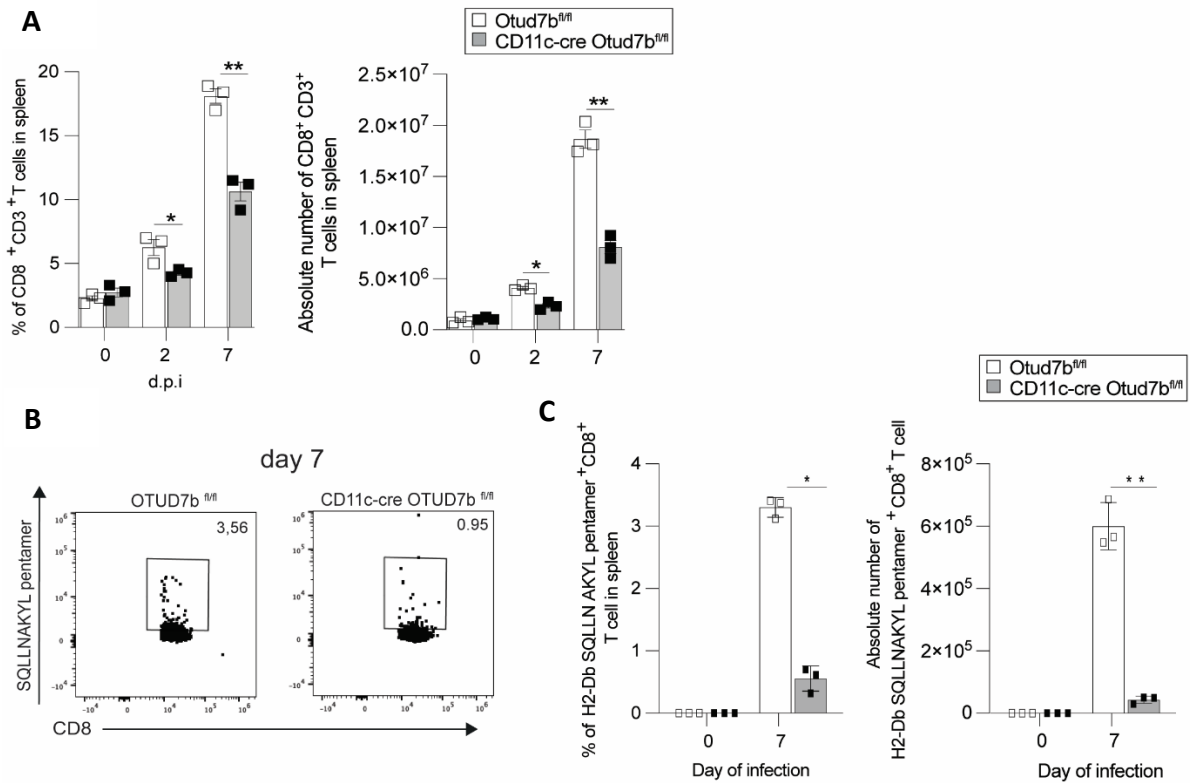


Figure 15: Reduced priming of CD8⁺ T cells in spleen of CD11c-Cre Otud7b^{fl/fl} mice upon *PbA* infection

Otud7b^{fl/fl} and CD11c-Cre Otud7b^{fl/fl} mice were i.p. infected with 1x10⁶ *PbA* parasitized RBCs. Spleens were harvested at d0, d2 and d7 p.i. and CD8⁺ T cells were analyzed by flow cytometry. (A) Relative and absolute numbers of CD3⁺ CD8⁺ T cells in the spleen of uninfected (d0) and infected (d2, d7) mice. (B) Representative dot plots of H2-D^b SQLLNAKYL pentamer⁺ CD8⁺ in spleens of infected mice at d7 p.i. (C) Relative and absolute numbers of CD3⁺CD8⁺ and H2-Db SQLLNAKYL pentamer⁺ CD8⁺ T cells in spleen at d7 p.i. Data represented as mean value ± SEM. A, C student's t-test *p<0.05, **p>0.01.

Moreover, the number of disease-causing parasite-specific CD8⁺ T cells as determined by GAP-50 peptide (SQLLNAKYL) pentamer staining, were also decreased in the the spleen of CD11c-Cre Otud7b^{fl/fl} mice (Figure 15 B,C). Concomitantly, a reduced accumulation of SQLLNAKYL⁺ CD8⁺ T cells was seen in the brains of CD11c-Cre Otud7b^{fl/fl} mice at d7 p.i (Figure 16 C,D).

The impaired peripheral induction of a CD8⁺ T cell response due to reduced DC numbers in spleen led to lesser intracerebral accumulation of total CD8⁺ T cells (Figure 16 A,B) and *PbA* GAP50-specific CD8⁺ T cells in brains (Figure 16 C,D) of CD11c-Cre Otud7b^{fl/fl} mice as determined by FACS. Noteworthy, expression of MHC-I, MHC-II and the co-stimulatory molecules CD80/86 did not differ between the two genotypes upon infection (Figure 17 A-D).

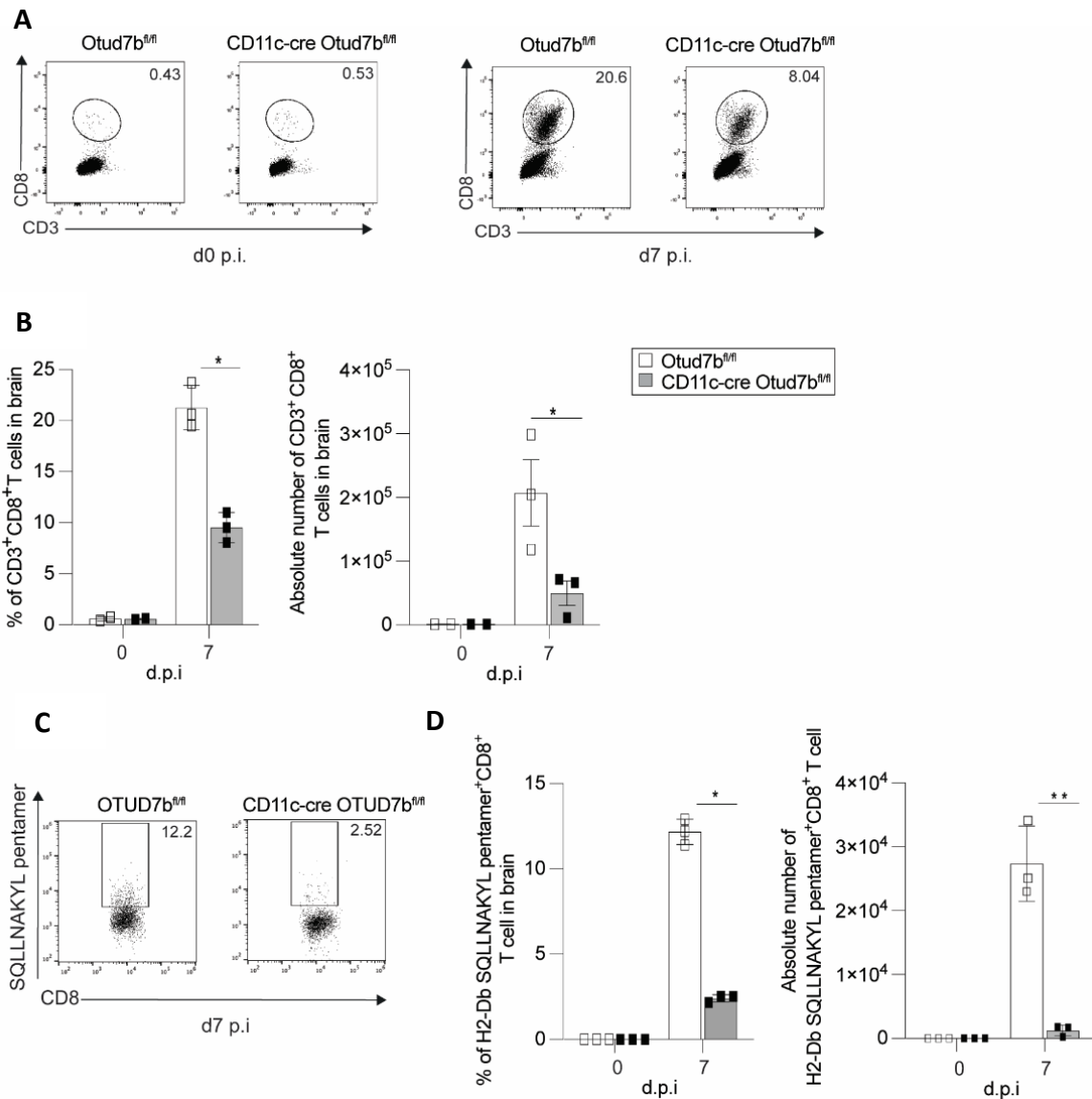


Figure 16: Reduced intracerebral accumulation of CD8⁺ T cells in CD11c-Cre Otud7b^{fl/fl} mice protects against ECM

The number H2-D^b SQQLLNAKYL pentamer⁺ CD8⁺ and total CD8⁺ T cells were determined in the brains of *PbA*-infected Otud7b^{fl/fl} and CD11c-Cre Otud7b^{fl/fl} mice by flow cytometry.

(A, C) Representative dot plots of CD3⁺CD8⁺ T cells and H2-D^b SQQLLNAKYL pentamer⁺ CD8⁺ T cells from the brain of uninfected and *PbA*-infected mice at d7 p.i., respectively (B, D) Relative (left) and absolute (right) cell numbers of CD3⁺ CD8⁺ and H2-D^b SQQLLNAKYL pentamer⁺ CD8⁺ in brains of uninfected and infected mice. Data represented as mean value \pm SEM. B-D student's t-test * $p < 0.05$, ** $p > 0.01$

In summary, these data indicate that the impaired pathogen control and better survival of CD11c-Cre Otud7b^{fl/fl} mice is due to reduced number of DCs which results in diminished priming and activation of CD8⁺ T cells, low accumulation of CD8⁺T cells in brain vasculature and, finally, prevention of BBB breakage.

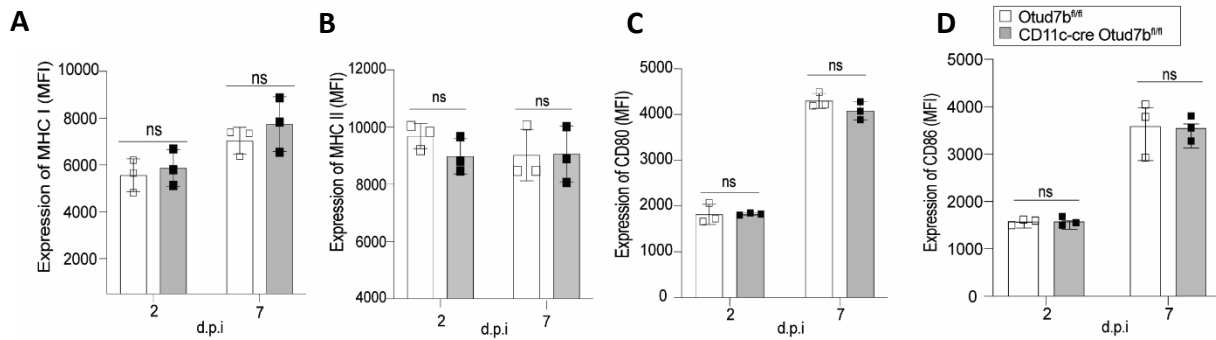


Figure 17: OTUD7b is dispensable for cell surface expression of MHC-I, II and CD80/86 on DCs
Otud7b^{fl/fl} and *CD11c-Cre Otud7b^{fl/fl}* mice were infected with 1×10^6 *PbA*-infected RBCs. Spleens were harvested at d2 and d7 p.i. and cell surface markers were analyzed by flow cytometry. MFI of (A) MHC-I (B) MHC-II (C) CD80 and (D) CD86 at d2 and d7p.i. Data are represented as mean value \pm SEM. A-D student's t-test, n.s.=not significant

Since IL-12 production by DCs is known to augment the activation of CD8⁺ T cells, we analyzed IL-12 production of OTUD7b-sufficient and -deficient DCs after *PbA* infection. Flow cytometric analysis showed reduced relative and absolute numbers of IL-12-producing CD11c⁺ DCs in spleen of *CD11c-Cre Otud7b^{fl/fl}* mice as early as day 2 p.i. (Figure 18 A-B), indicating that deficiency of OTUD7b in DC alters both DC numbers and IL-12 production, which both might result in reduced priming of CD8⁺T cells.

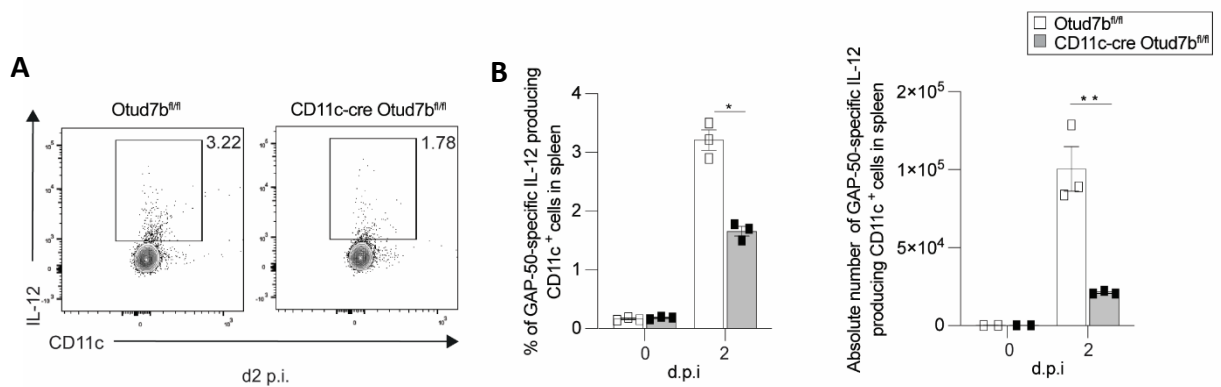


Figure 18: Impaired IL-12 production in OTUD7b deficient DCs upon infection

Otud7b^{fl/fl} and *CD11c-Cre Otud7b^{fl/fl}* mice were infected with 1×10^6 infected RBCs. Mice were harvested at indicated time points after infection and IL-12 production by CD11c⁺ population was determined by flow cytometry. (A) Representative dot plots (B) Relative cell number (left) and absolute cell number (right) of IL-12 producing CD11c⁺ cells at d2p.i. . Data represented as mean value + SEM. (B) n=3 per experimental group, Student's t-test *p<0.05, **p<0.01

In concurrence, production of IFN- γ and Granzyme B by splenic CD8⁺ T cells was also significantly reduced in *CD11c-Cre Otud7b^{fl/fl}* mice (Figure 19 A-D) upon re-stimulation with GAP50 peptide.

Taken together, these findings show that during *PbA* infection, OTUD7b in DCs is essential for maintaining DC numbers and IL-12 production by DCs during *PbA* infection, which leads to effective priming and intracerebral accumulation of disease causing CD8⁺ T cells resulting in BBB disruption and ECM.

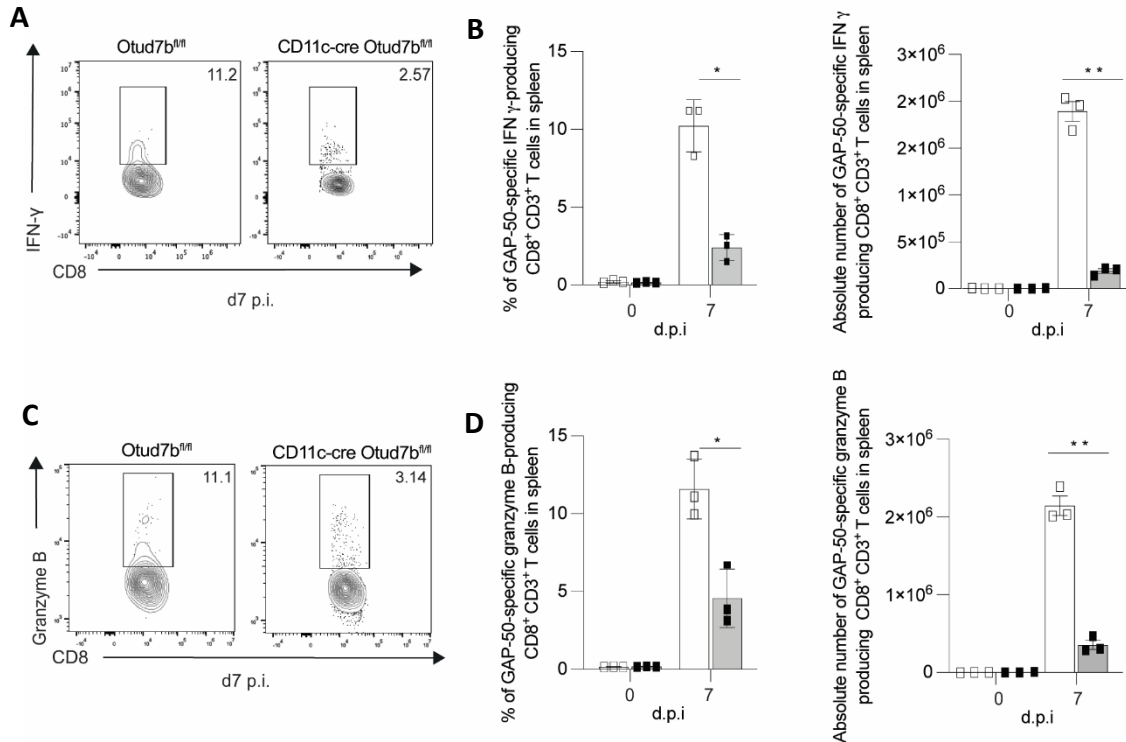


Figure 19: Deletion of OTUD7b in DCs impairs cytotoxic CD8⁺ T cell response to *PbA* infection
 Otud7b^{fl/fl} and CD11c-Cre Otud7b^{fl/fl} mice were infected with 1×10^6 infected RBCs. At the indicated time points after infection, spleens were analyzed for production of IFN- γ and Granzyme B by flow cytometry. (A, B) Representative dot plots (A) and relative cell number (B, left) and absolute cell number (B, right) of IFN- γ producing CD8⁺ T cells at d7 p.i. (C, D) Representative dot plot (C) and relative cell number (D, left) and absolute cell number (D, right) of Granzyme-B producing CD8⁺ T cells at d7 p.i. Data represent the mean value \pm SEM. (A-C) n=3 per experimental group, Student's t-test *p<0.05, **p<0.01

4.4 Increased death of DC in CD11c-Cre Otud7b^{fl/fl} mice after *PbA* infection

To further investigate whether the reduced number of DCs in CD11c-Cre Otud7b^{fl/fl} mice was a result of increased cell death of DCs post *PbA* infection, we performed an *ex-vivo* Annexin-V/7AAD staining of CD11c⁺ DC population in spleen by flow cytometry at d2 p.i and d7 p.i. No spontaneous death of DCs was observed in uninfected OTUD7b-deficient and -competent mice which both showed equally low Annexin-V/7AAD positive DC populations. Upon infection, the number of Annexin-V/7AAD⁺ DCs increased in both mouse strains (Figure 20 A,B) but importantly, numbers of annexin V/7-AAD⁺ DCs were significantly increased in

CD11c-Cre Otud7b^{fl/fl} mice starting as early as day 2 p.i indicating that OTUD7b inhibited cell death of DCs (Figure 20 A,B).

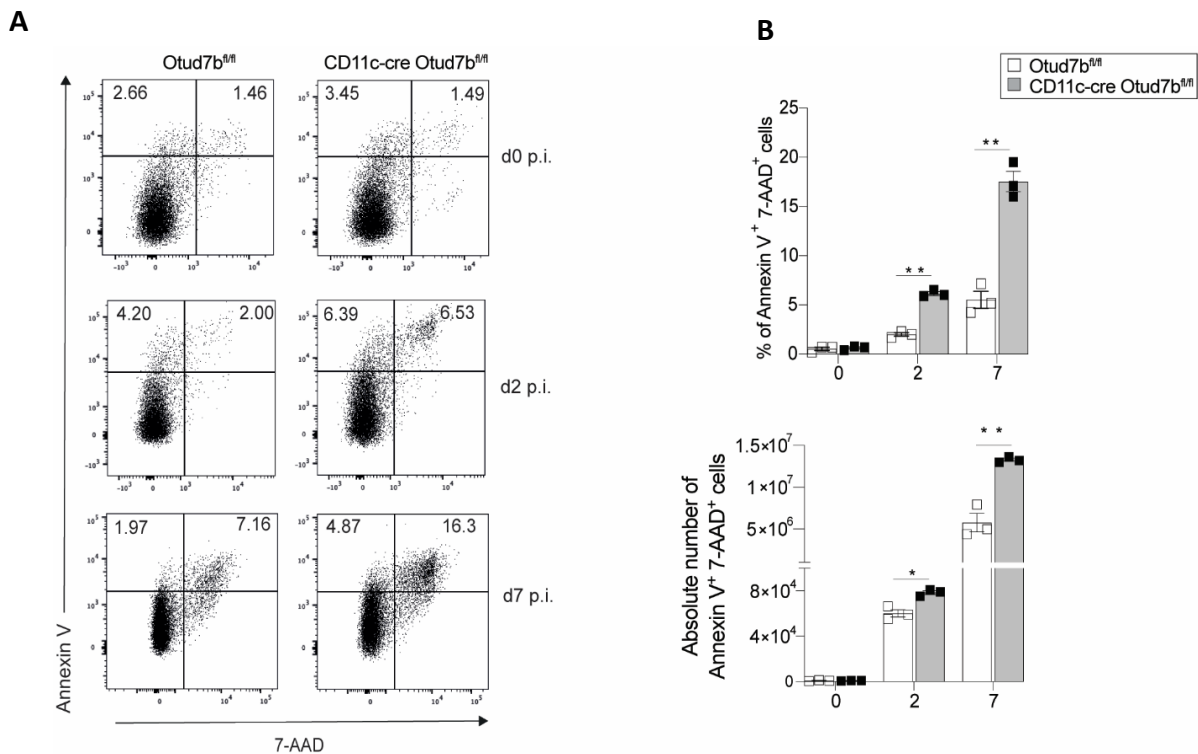


Figure 20: OTUD7b inhibits cell death of DCs in *PbA*-infected mice

Otud7b^{fl/fl} and CD11c-Cre Otud7b^{fl/fl} mice were infected with 1×10^6 infected RBCs. At d2 and d7 p.i. Spleens were harvested and ex-vivo Annexin V and 7AAD staining was performed. (A, B) Representative dot plots (A) and relative (B, upper panel) and absolute (B, lower panel) cell numbers of Annexin V⁺ 7AAD⁺ cell populations. All bars represent the mean value \pm SEM. (B) Student's t test * $p < 0.05$, ** $p < 0.01$

Increased DC death in absence of OTUD7b could be caused by a direct cytopathic effect of the parasite or by cytokines produced during infection. To evaluate parasite-induced DC death, we first incubated BMDCs with *PbA*-infected RBCs at a ratio of 1:3 (DC : iRBC) for 6h and 24h, respectively, and analyzed induction of cell death by WB. Uninfected RBCs were used as controls. iRBC stimulation induced apoptosis to similar extent in both OTUD7b-sufficient and -deficient BMDCs at 6 and 24h post stimulation. Furthermore, we did not observe phosphorylation of MLKL, which is an indicative for necroptosis (Figure 21A). These data indicate that the increased cell death of OTUD7b-deficient DCs was not due to the cytopathic effect of *Plasmodium*.

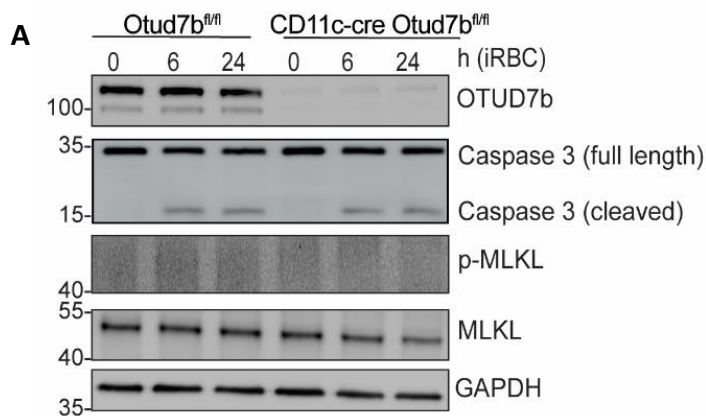


Figure 21: OTUD7b does not regulate iRBC-induced cell death

BMDCs cultured from Otud7b^{fl/fl} and CD11c-Cre Otud7b^{fl/fl} mice were stimulated with *PbA*-infected RBCs at a ratio of 1:3 (BMDC:iRBC) for the indicated time points. Proteins were harvested and activation of apoptosis and necroptosis pathways was analyzed by western blotting. GAPDH was used as loading control. Representative blots of one of three independent experiments are shown.

Since death of DCs can also be induced by cytokines upregulated during *PbA* infection, we analyzed the impact of DC-specific OTUD7b on the level of cytokine mRNA expression in the spleen of infected Otud7b^{fl/fl} and CD11c-Cre Otud7b^{fl/fl} mice at day 2 p.i. A similar increase in the mRNA levels of TNF, IFN- γ , IL-6 and IL-10 was observed upon infection in both mouse strains illustrating that in contrast to IL-12, expression of these cytokines was not regulated by DC-specific OTUD7b at day 2 p.i. (Figure 22A). The levels of IL-12 mRNA were significantly reduced in CD11c-Cre Otud7b^{fl/fl} mice, which is in agreement with our previous data (Figure 18A, B).

To directly assess the role of these upregulated cytokines in DC death, we stimulated BMDCs with equal amounts of IL-6, IFN- γ , IL-10, TNF, respectively, and determined their effect on cell death. Stimulation with IL-6, IFN- γ and IL-10 did not induce cleavage of the effector caspase-3. However, TNF stimulation induced apoptosis in OTUD7b- deficient BMDCs as indicated by increase in levels of cleaved caspase 3, while the induction of apoptosis in OTUD7b- sufficient BMDCs was comparably weak (Figure 22B, C). Of note, TNFR1 expression was similar in both genotypes (Figure 22D). In line with the WB data, TNF-stimulation of OTUD7b-deficient BMDCs resulted in enhanced release of LDH in cell culture supernatant and showed reduced cell viability as detected by MTT assay, compared to OTUD7b sufficient BMDCs (Figure 23 B,C), further showing enhanced sensitivity of OTUD7b-deficient BMDCs towards TNF mediated cell death. Taken together, our data suggests that deletion of OTUD7b protects DCs from TNF- induced apoptosis.

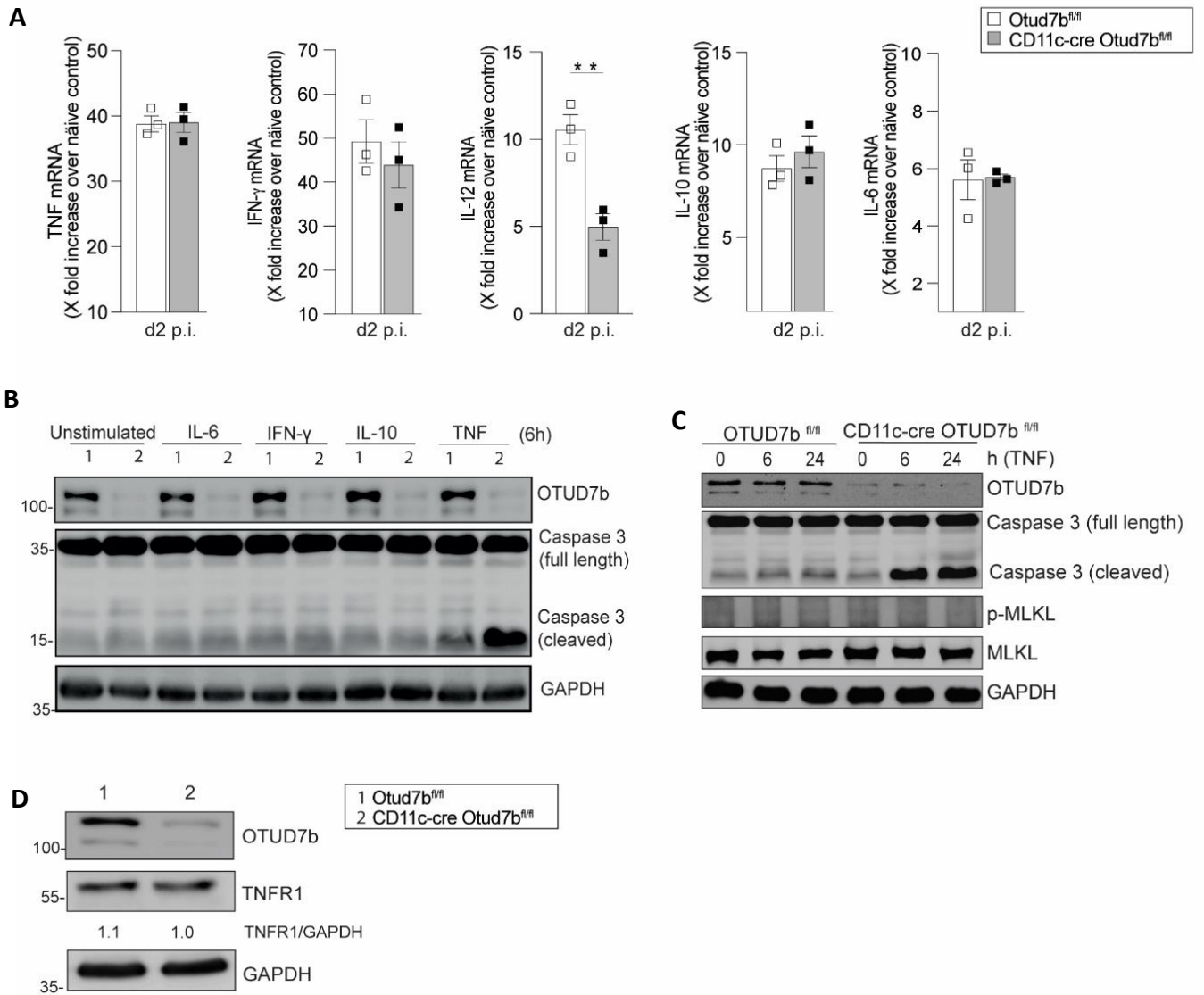


Figure 22: OTUD7b is a negative regulator of TNF induced apoptosis of DCs

(A) *Otud7b^{fl/fl}* and *CD11c-Cre Otud7b^{fl/fl}* mice were infected with 1×10^6 infected RBCs. Relative mRNA expression of mentioned cytokines in the spleen of mice was measured by qRT-PCR. Bar graphs represents one of three independent experiments ($n=3$ per experimental group). Mean values \pm SEM are shown. (B, C) BMDCs of OTUD7b-sufficient and -deficient mice were treated with IL-6, IFN- γ , IL-10 and TNF, respectively, for the indicated time points and proteins were immunoblotted with antibodies for OTUD7b, Caspase-3, p-MLKL, MLKL and the loading control GAPDH. (D) TNFR1 expression was determined in unstimulated BMDCs by immunoblotting. All blots are representative of one of three independent experiments. (A) Student's t-test, $**p < 0.01$

4.5 Inhibition of DC death induces ECM in CD11c-Cre Otud7b^{fl/fl} mice

To test whether enhanced cell death in CD11c-Cre Otud7b^{fl/fl} mice is protective against ECM, TNF-stimulated OTUD7b sufficient and deficient BMDCs were treated either with Z-VAD-FMK (pan caspase inhibitor), Necrostatin-1s (RIPK1 inhibitor) or a combination of Z-VAD-FMK and Necrostatin-1s. In line with previous findings, TNF-treatment resulted in enhanced activation of caspase-3, increased cell death and reduced cell viability of OTUD7b deficient cells (Fig. 23 A-C).

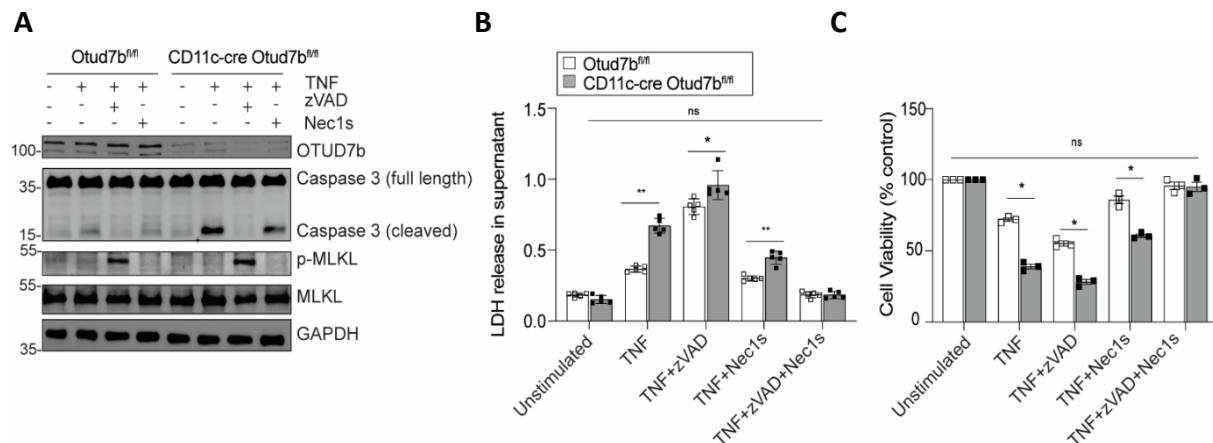


Figure 23: OTUD7b inhibits RIPK1-dependent and -independent apoptosis upon TNF stimulation

OTUD7b-sufficient and -deficient BMDCs were pre-treated with zVAD-FMK, Nec-1s or a combination of both for 90 mins followed by stimulation with TNF for 6h. (A) Total protein lysates were analyzed by western blotting with indicated antibodies. (B) Supernatant was collected and measured for LDH levels using LDH assay kit. (C) Cell viability was analyzed using MTT assay. For LDH assay values are represented as absorbance 490nm-680nm and for MTT assay values are calculated with percentage viability compared to untreated controls. Blots are representative for one of three independent experiments. (B, C) All bars represent mean value \pm SEM. Student's t-test, * $p < 0.05$, ** $p < 0.01$

Addition of Z-VAD-FMK inhibited apoptosis but activated necroptosis in TNF-stimulated cells as indicated by phosphorylation of MLKL (Figure 23A). Ablation of the kinase activity of RIPK1 by necrostatin-1s slightly reduced apoptosis in both genotypes. However the levels of cleaved caspase-3 were still higher in the OTUD7b-deficient BMDCs (Figure 23A). This indicates that OTUD7b regulates both RIPK1-dependent and independent apoptosis. In good agreement with this assumption, a combined treatment with Z-VAD-FMK and Necrostatin-1s completely blocked cell death and the cell viability was equivalent to untreated controls (Figure 23 B, C). To validate these findings *in vivo*, *PbA*-infected Otud7b^{fl/fl} and CD11c-Cre Otud7b^{fl/fl} mice were injected with a combination of zVAD-FMK and Necrostatin-1s and progression of disease was monitored daily. Effective inhibition of DC death in both genotypes by inhibitor treatment was validated by an equal reduction of Annexin-V/7AAD double positive DCs populations upon treatment. (Figure 24 A, B).

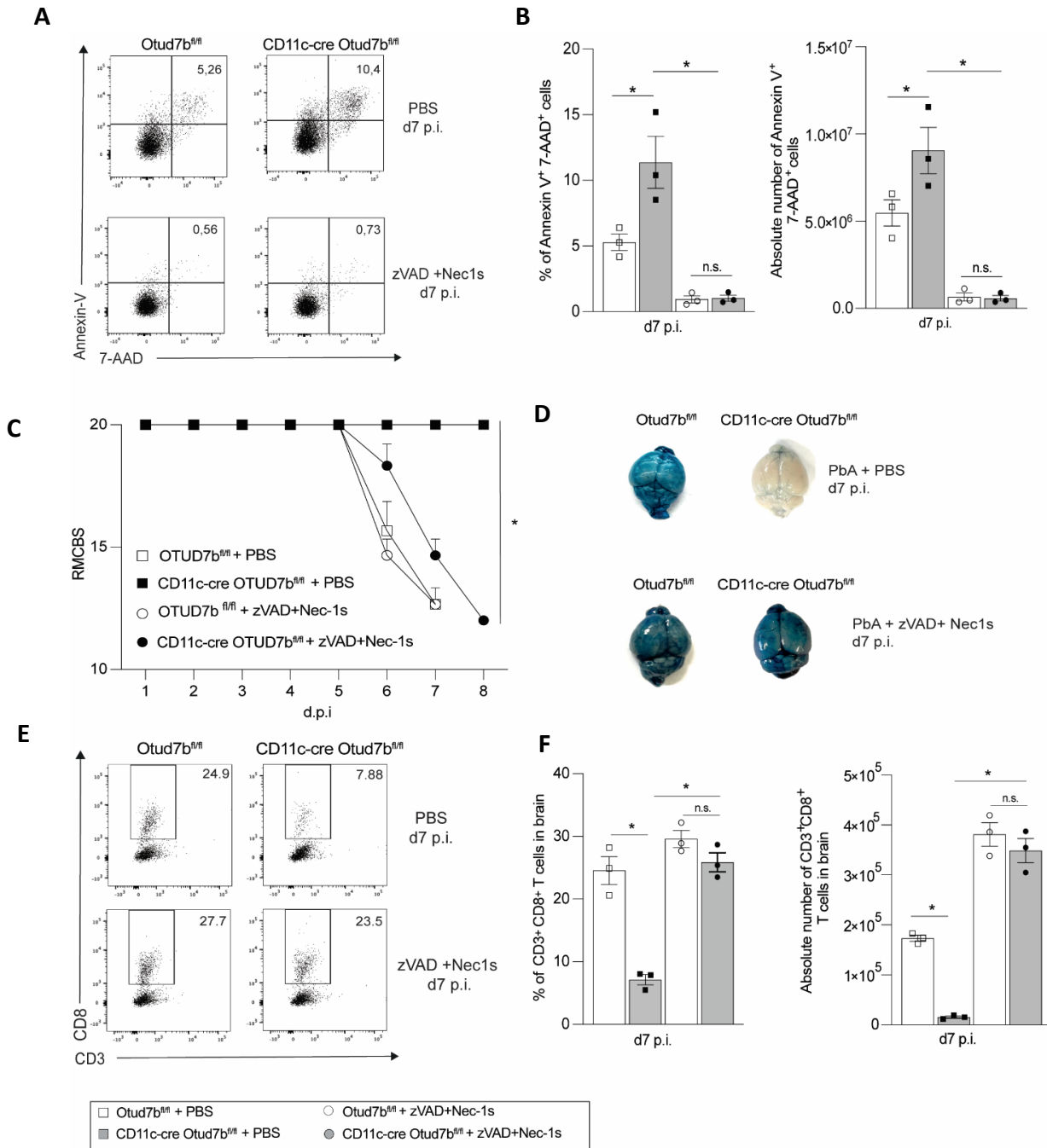


Figure 24: Inhibition of cell death renders CD11c-Cre Otud7b^{fl/fl} mice susceptible to ECM

Otud7b^{fl/fl} and CD11c-Cre Otud7b^{fl/fl} mice were injected i.v. with a combination of zVAD-FMK and Nec-1s or PBS/DMSO 90 mins prior to PbA infection. Inhibitor treatment was continued daily up to d7 p.i. At d7 p.i., mice were sacrificed and organs were collected for flow cytometric analysis. (A) Representative dot plots, (B) relative (left) and absolute (right) cell numbers of Annexin V⁺ 7AAD⁺ CD11c⁺ cells in spleen. (C) RMCBS score. (D) Representative images of Evans blue dye stained brains. (E) Representative dot plots, (F) relative (left) and absolute (right) cell numbers of CD3⁺CD8⁺ T cells in the brain. All bar graphs represent mean values \pm SEM. Student's t-test * $p < 0.05$ (B) Student's t-test * $p < 0.05$

In good agreement with untreated mice (Figure 12 A), all PBS-treated *PbA*-infected *Otud7b^{fl/fl}* mice showed clinical signs of disease and developed ECM around day 7 p.i., whereas all *CD11c-Cre Otud7b^{fl/fl}* were protected against the disease (Figure 24A). However, upon treatment with zVAD-FMK/Nec-1s the differences between both genotypes were abolished and also *CD11c-Cre Otud7b^{fl/fl}* developed identical clinical signs of ECM and were susceptible to *PbA* infection (Figure 24 C). Furthermore, the number of intracerebral CD8⁺ T cells and loss of BBB integrity were significantly increased to the same level as in *Otud7b^{fl/fl}* mice after zVAD-FMK/Nec-1s treatment of *CD11c-Cre Otud7b^{fl/fl}* mice (Figure 24 D - F). These results indicate that the increased sensitivity of OTUD7b- deficient DCs to apoptosis reduces priming and intracerebral accumulation of pathogenic CD8⁺ T cells and thereby protects mice from ECM.

4.6 OTUD7b prevents proteasomal degradation of TRAF2

Our data suggest that deletion of OTUD7b in DCs promotes TNFR1-mediated DC death. To uncover the mechanism leading to the increased TNF-induced apoptosis of OTUD7b-deficient DCs, *Otud7b^{fl/fl}* and *CD11c-Cre Otud7b^{fl/fl}* BMDCs were stimulated with TNF and the expression of proteins in the apoptosis-inducing cytoplasmic complex-II were analyzed by WB. TNF stimulation resulted in significant reduction of TRAF2, while an increase of active caspase 8 (p43/p18) was observed in OTUD7b-deficient as compared to OTUD7b-sufficient BMDCs. However, no difference was observed in the levels of other members of the complex-II including c-IAP, FADD and TRADD (Figure 25A).

To determine whether the reduced level of TRAF2 in the absence of OTUD7b was due to increased proteasomal degradation, proteasome activity was inhibited in TNF-stimulated BMDCs using the proteasome inhibitor MG132. MG132 treatment restored TRAF2 levels of OTUD7b-deficient BMDC demonstrating that OTUD7b prevented proteasomal degradation of TRAF2 (Figure 25 B, C).

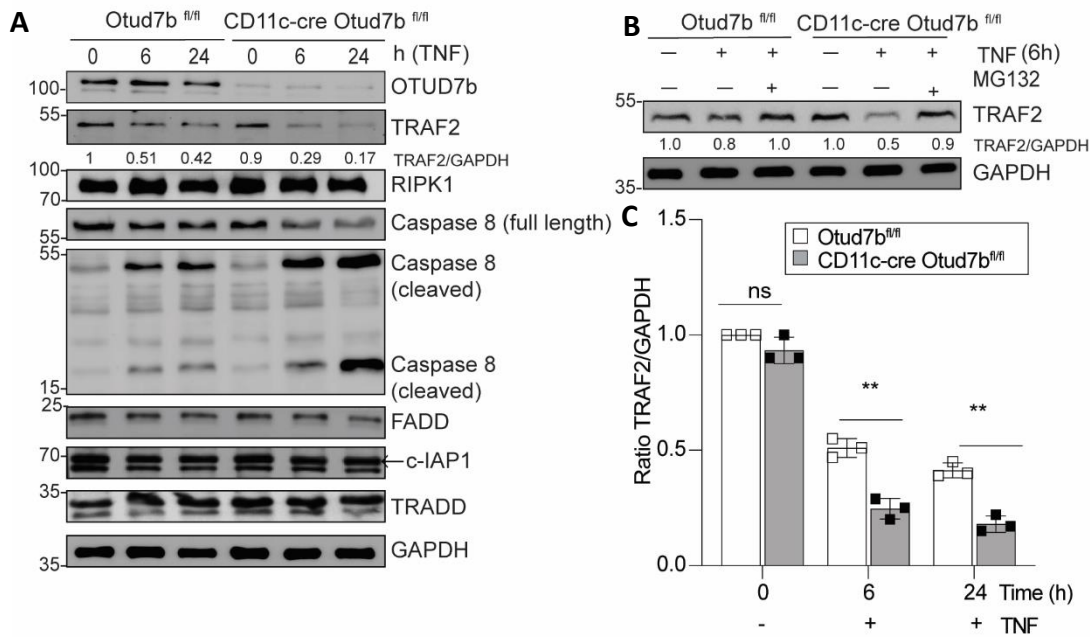


Figure 25: OTUD7b prevents the proteasomal degradation of TRAF2 upon TNF stimulation

(A, B) OTUD7b-sufficient and -deficient BMDCs were stimulated with TNF (A) or a combination of MG132 and TNF (B) for indicated time points. Proteins were isolated and analyzed by western blot. GAPDH was used as loading control. (C) Quantification of TRAF2 normalized to GAPDH. All blots are representative images of one of three independent experiments. All bars represent mean \pm SEM. (C) Student's t-test $**p < 0.01$

Since K48-linked polyubiquitin chains promote proteasomal degradation of target proteins, and OTUD7b can remove K48-linked polyubiquitin chains from target proteins, we next investigated whether OTUD7b interacts with TRAF2 and reduces K48-linked polyubiquitination of TRAF2 upon TNF stimulation. TNF treatment induced interaction of OTUD7b with TRAF2 as revealed by co-immunoprecipitation experiments (Figure 26A). Furthermore, immunoprecipitation of TRAF2 from TNF-stimulated OTUD7b-sufficient and -deficient BMDCs showed enhanced accumulation of K48-linked polyubiquitin chains on TRAF2 in OTUD7b- deficient BMDCs (Figure 26B).

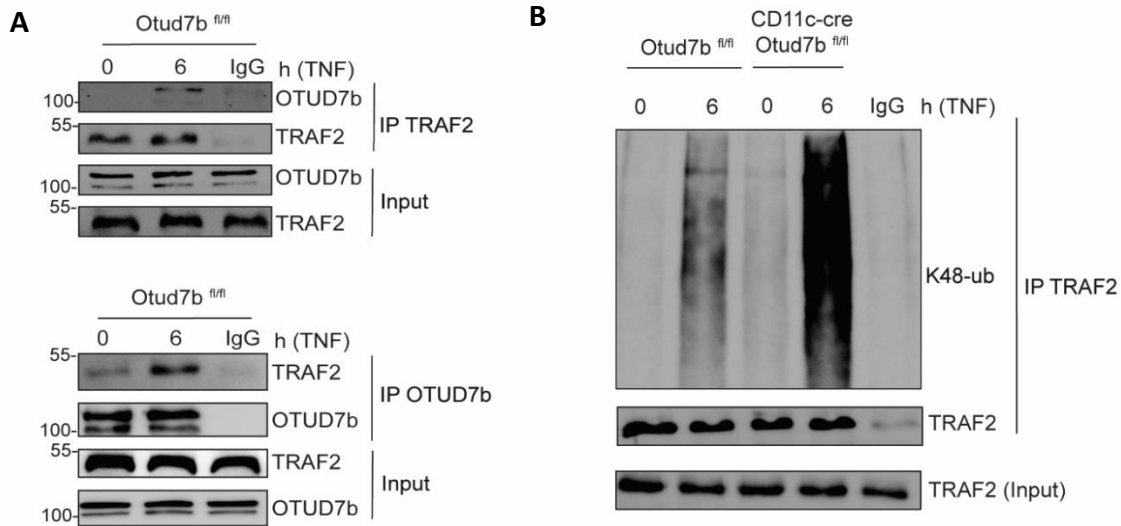


Figure 26: OTUD7b removes K48-linked polyubiquitin chains from TRAF2

(A, B) BMDCs from Otud7b^{fl/fl} and CD11c-Cre Otud7b^{fl/fl} mice were stimulated with TNF only (A) or with TNF in presence of MG132 (B). Immunoprecipitation of total cell lysate was performed using anti-TRAF2 (A upper panel, B) or anti-OTUD7b (A, lower panel) antibodies. Western blot was performed thereafter with indicated antibodies. All blots are representative of one out of three independent experiments.

4.7 OTUD7b regulates DC apoptosis by cleaving K48-linked ubiquitin chains from TRAF2

Upon TNF stimulation, the TRAF2/cIAP1 complex mediates K63-linked polyubiquitination of RIPK1, which prevents auto-phosphorylation of RIPK1 at S166, and, thereby, RIPK1 kinase activity. This cascade of events inhibits RIPK1-dependent cell death. In good agreement, our co-immunoprecipitation studies showed an interaction between TRAF2-RIPK1 and RIPK1-OTUD7b upon TNF treatment (Figure 27A). To further analyze whether reduction of TRAF2 levels fostered RIPK1 mediated apoptosis of OTUD7b-deficient BMDCs, RIPK1 was immunoprecipitated from OTUD7b-sufficient and -deficient BMDCs after TNF stimulation and the K63-linked polyubiquitination of RIPK1 was analyzed by WB. Interestingly, the K63-linked polyubiquitination of RIPK1 was reduced in OTUD7b-deficient BMDCs as compared to OTUD7b-sufficient BMDCs (Figure 27B). The reduction in K63-linked polyubiquitination was accompanied by increased phosphorylation of RIPK1 at S166 (Figure 27B). These data indicate that the prevention of TRAF2 K48-polyubiquitination and proteasomal degradation by OTUD7b prevents the pro-apoptotic function of RIPK1 by sustaining K63-polyubiquitination and reducing S166 phosphorylation of RIPK1. This is in line with enhanced activation of caspase 8 (Figure 25A) and caspase-3 (Figure 22B, C) observed.

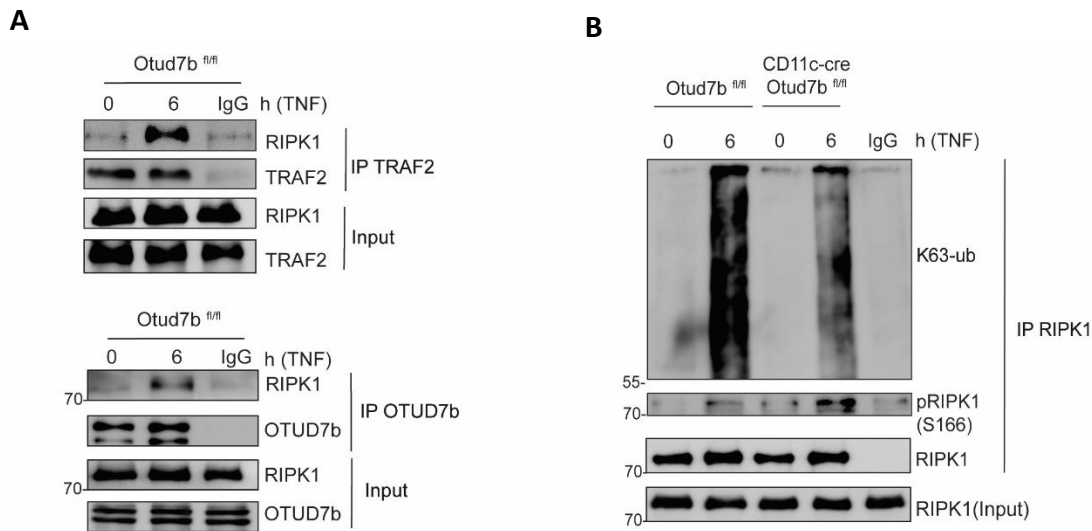


Figure 27: OTUD7b regulates K63-linked ubiquitination of RIPK1 via TRAF2

(A, B) Total cell lysates obtained from TNF-treated BMDCs were immunoprecipitated with anti-TRAF2 (A, upper panel), anti-OTUD7b (A, lower panel) and anti-RIPK1 (B) and analyzed with western blot. All blots are representative and experiments were repeated three times.

4.8 UBA domain of OTUD7b is required for TRAF2 binding

To identify the domain of OTUD7b that is essential for the interaction with TRAF2, we established OTUD7b mutants (i) lacking the N-terminal UBA domain, (ii) the C-terminal zinc finger domain and (iii) a catalytic inactive mutant with point mutation in catalytic active C194 residue where cysteine was replaced by a serine.

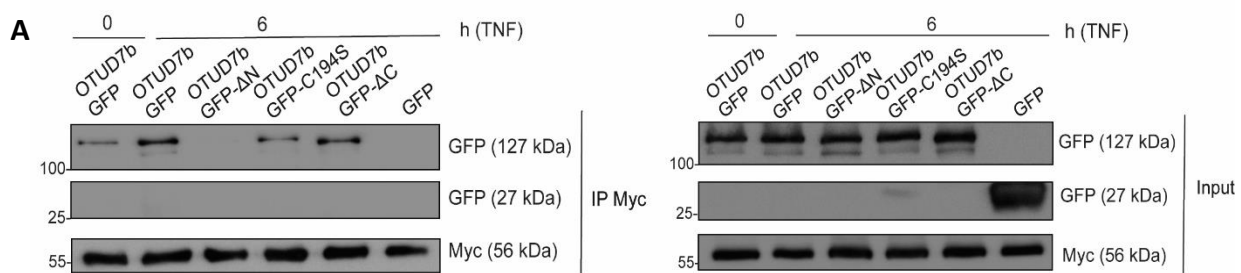


Figure 28: UBA domain of OTUD7b is indispensable for binding with TRAF2

HEK 293T cells were co-transfected with either OTUD7b-GFP, OTUD7b-GFP-ΔN, OTUD7b-GFP-ΔC, empty GFP plasmid and TRAF2-Myc plasmid. Transfected cells were treated with TNF for 6h and total cell lysates were prepared. Protein complex immunoprecipitation was performed using anti-Myc antibody and IP-western analysis was performed to confirm protein-protein interaction. Representative blots of three independent experiments.

Immunoprecipitation experiments showed that the interaction between TRAF2 and OTUD7b was completely abolished in the mutant lacking the N-terminal UBA domain which is required for protein-protein interactions. Interestingly, the catalytic inactive mutant OTUD7b mutant

also showed reduced binding to TRAF2, while no difference was observed with the C-terminal zinc finger mutant suggesting that both the UBA domain and the catalytic C194 site of OTUD7b contribute to interaction with TRAF2 (Figure 28A).

4.9 OTUD7b fosters the activation of NF- κ B, MAP kinase signaling pathways via stabilization of TRAF2

Since TRAF2 is also a part of the TNF-receptor associated signaling complex-I, which mediates activation of NF- κ B and MAP-kinase pathways, we further addressed the role of OTUD7b-TRAF2 interaction in TNF-mediated inflammation. BMDCs from *Otud7b^{fl/fl}* and *CD11c-Cre Otud7b^{fl/fl}* mice were stimulated with TNF and the activation of the NF- κ B and MAP kinase pathway was analyzed by western blot. In OTUD7b-deficient BMDCs, TNF stimulation resulted in impaired activation of NF- κ B and MAP kinase pathways as compared to OTUD7b-sufficient BMDCs as shown by reduced levels of p-p65, p-p38 and p-ERK (Figure 29A). Since the transcription factor NF- κ B regulates the expression of anti-apoptotic genes, and OTUD7b-deficient BMDCs are prone to apoptosis, we determined whether impaired activation of NF- κ B in OTUD7b-deficient BMDCs resulted in reduced transcription of anti-apoptotic molecules and thereby induction of RIPK1-independent apoptosis. qRT-PCR analysis showed reduced expression of the anti-apoptotic genes Bcl-xL (*Bcl2l1*) and cFLIP (*cflar*) (Figure 29B) in OTUD7b-deficient BMDCs.

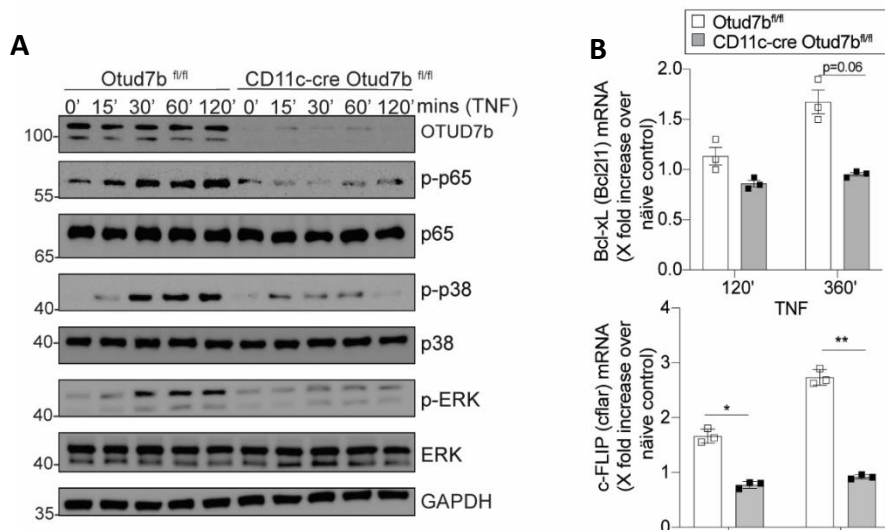


Figure 29: Impaired activation of NF- κ B, MAPK signaling pathways in OTUD7b-deficient BMDCs

(A, B) BMDCs from *Otud7b^{fl/fl}* and *CD11c-Cre Otud7b^{fl/fl}* mice were stimulated with TNF for the indicated time points. (A) Protein lysates were immunoblotted with indicated antibodies. Representative blots are shown for three independent experiments. (B) Relative gene expression of indicated genes was analyzed by qRT-PCR. Data represent mean value + SEM. n=3, Student's t test, *p<0.05, **p<0.01

These data indicate the enhanced apoptosis of OTUD7b-deficient BMDCs may be a result of both increased kinase function of RIPK1 and impaired production of anti-apoptotic Bcl-xL (Bcl2l1) and cFLIP (cflar) in the absence of TRAF2

Reduced TNFR1 complex-I signaling in absence of OTUD7b intrigued us to investigate whether reduced stability of TRAF2 during early TNFR1 activation was responsible for the observed differences. Therefore, we checked for TRAF2 levels under same stimulatory conditions and, indeed, a significantly higher degradation of TRAF2 was detectable in OTUD7b-deficient DCs which could be prevented upon proteasome inhibition (Figure 30 A, B).

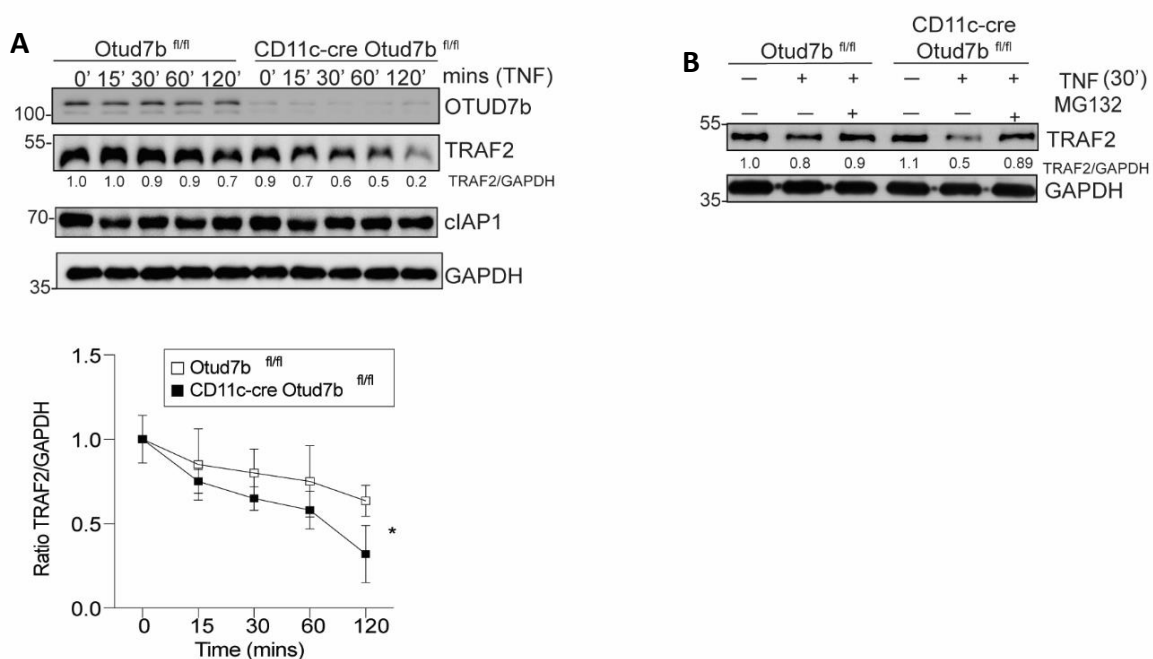


Figure 30: OTUD7b inhibits proteasomal degradation of TRAF2 upon TNF stimulation

(A, B) BMDCs were treated with TNF in absence (A) or presence of MG132 (B). Proteins were isolated at indicated time points and analyzed by WB. GAPDH was used as a loading control. (A, lower panel) TRAF2 expression level were quantified from WB and normalized to GAPDH. Blots are representative for three independent experiments. Data represents mean \pm SEM. n=3, Student's t test, *p<0.05.

In line with OTUD7b-dependent stabilization of TRAF2 in TNF-stimulated BMDCs, TNF induced TRAF2-OTUD7b interaction and OTUD7b reduced K48-linked polyubiquitination of TRAF2 (Figure 31 A, B).

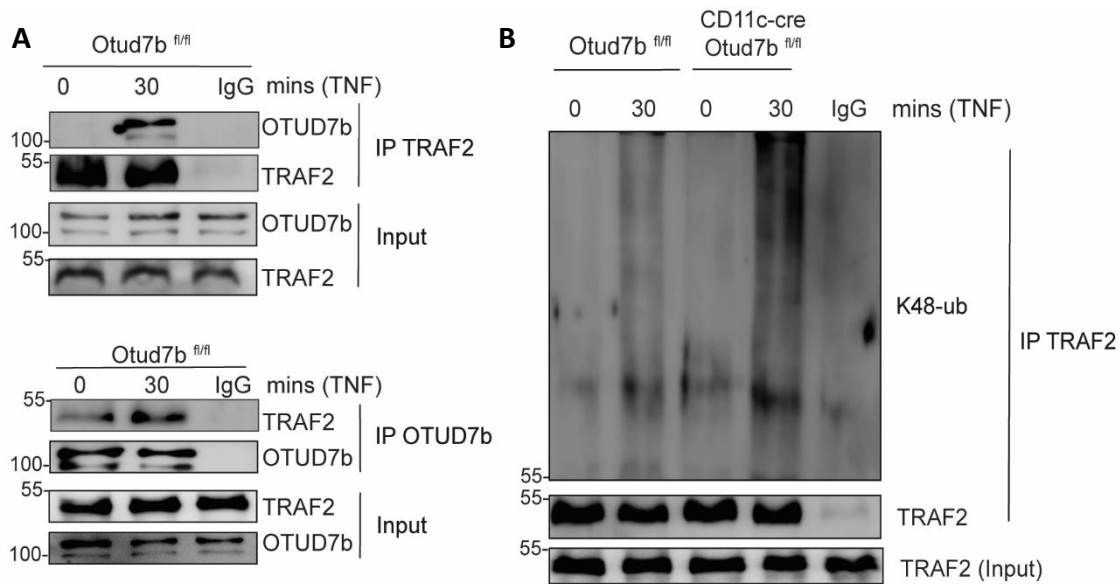


Figure 31: OTUD7b interacts with TRAF2 and prevents K48 polyubiquitin of TRAF2

(A, B) BMDCs were stimulated with TNF and proteins were harvested at indicated time points. Protein lysates were immunoprecipitated using anti-TRAF2 (A, upper panel, B) and anti-OTUD7b (A, lower panel). Immunoprecipitates and inputs were immunoblotted and analyzed. In (B) TRAF2 immunoprecipitates were immunoblotted for K48 ubiquitin. Representative western blots of one of three independent experiments are shown.

Furthermore, our results show that increased TRAF2 degradation and reduced interaction of TRAF2 with RIPK1 in OTUD7b-deficient conditions compromised K63-linked ubiquitination of RIPK1 which is required for stabilization of complex-I and recruitment of downstream molecules for activation of NF- κ B and MAP kinase signaling pathways (Figure 32 A,B).

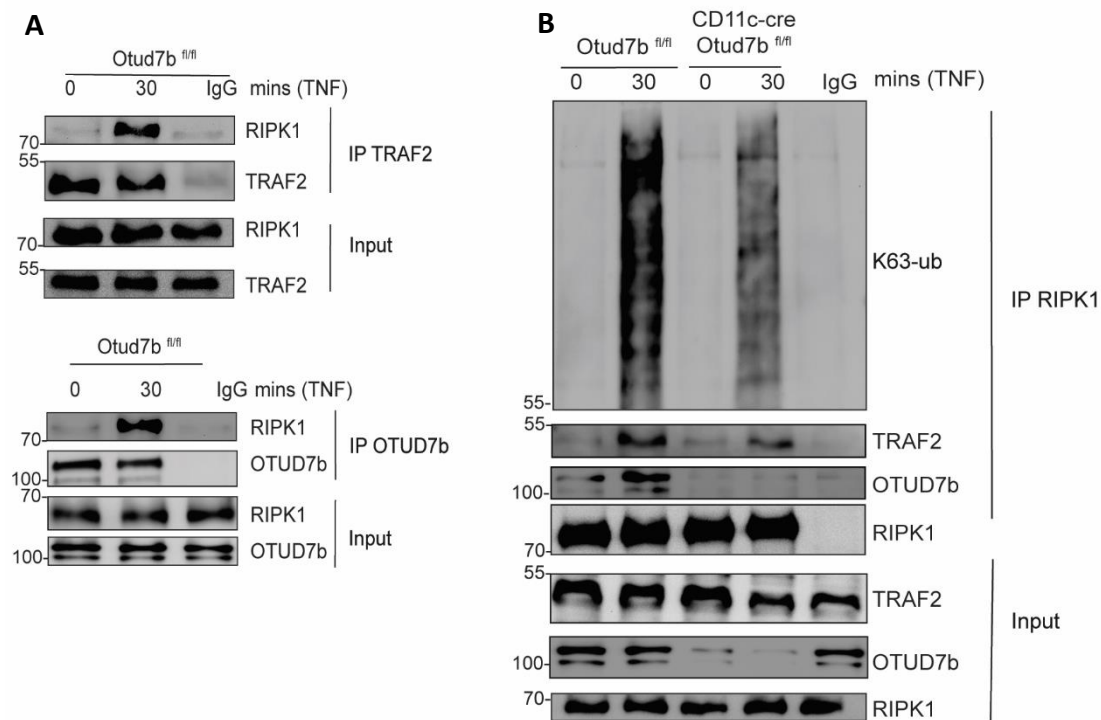


Figure 32: OTUD7b is part of the TRAF2/RIPK1 complex in TNF-stimulated BMDCs and enhances K63-linked ubiquitination of RIPK1

(A, B) Total cell lysates were immunoprecipitated with anti-TRAF2 (A, upper panel), anti-OTUD7b (A, lower panel) and anti-RIPK1 (B) antibodies from TNF-stimulated BMDCs of the indicated mouse strains and analyzed by western blot for the indicated proteins. Representative western blots of one of three biological replicates are shown.

In summary, our data suggest that OTUD7b fosters activation of inflammatory TNF signaling by stabilizing TRAF2 leading to increased K63-linked ubiquitination of RIPK1 (early checkpoint) and increased production of anti-apoptotic molecules (late checkpoint) thereby restricting formation of cytosolic complex-II and activation of RIPK1-dependent and -independent apoptosis.

4.10 TRAF2-deficiency sensitizes OTUD7b^{+/+} BMDCs to TNF-mediated apoptosis

Given the increased apoptosis of OTUD7b-deficient DCs due to enhanced TRAF2 degradation, we deleted TRAF2 in WT BMDCs using CRISPR-Cas9 system to confirm OTUD7b-TRAF2 mediated regulation of TNF-induced DC apoptosis. TRAF2-deficient BMDCs showed were more sensitive towards TNF-mediated apoptosis at 6h as indicated by enhanced caspase-3 cleavage (Figure 33A). Thus, TRAF2-deficient BMDCs phenocopied the enhanced sensitivity of OTUD7bdeficient BMDCs with respect to TNF-induced apoptosis. Next,

we aimed to validate that TRAF2-deficiency and DC apoptosis were responsible for protection against *PbA* infection. In these experiments, we performed an adoptive transfer of TRAF2^{+/+} and TRAF2^{-/-} BMDCs to CD11c-Cre Otud7b^{fl/fl} mice prior to infection with *PbA*-infected RBCs. While CD11c-Cre Otud7b^{fl/fl} mice reconstituted with TRAF2^{-/-} BMDCs showed no clinical signs of ECM and no breakage of BBB, CD11c-Cre Otud7b^{fl/fl} mice injected with TRAF2^{+/+} BMDCs behaved similar to control Otud7b^{fl/fl} mice and rapidly developed clinical ECM, BBB dysfunction and, succumbed to disease at d7 p.i (Figure 33B, D). Furthermore compared to their WT counterparts, CD11c-Cre Otud7b^{fl/fl} mice with TRAF2^{-/-} BMDCs harbored higher parasite load (Figure 33 C). Collectively, these data confirms that mechanistically TRAF2 deficiency increases sensitivity of DCs towards TNF mediated cell death and impairs activation and thus intracerebral accumulation of CD8⁺ T cells. Impaired CD8⁺ T cell accumulation in brain microvasculature prevents BBB damage and thus protects mice against ECM.

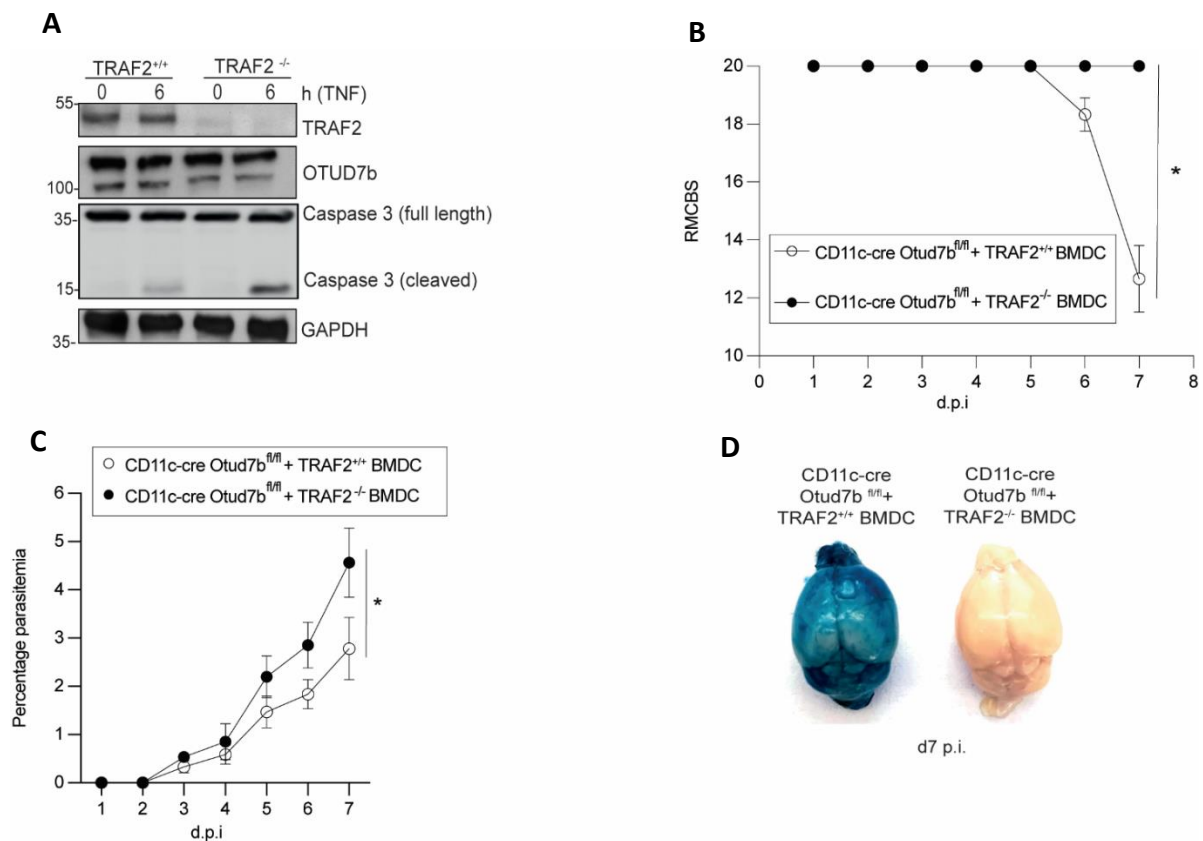


Figure 33: Adoptive transfer of WT BMDCs in CD11c-Cre Otud7b^{fl/fl} mice induces ECM

(A) CRISPR-Cas9 mediated gene editing was used to knockdown TRAF2 in BMDCs. TRAF2 sufficient and deficient BMDCs were stimulated with TNF. After 6h, cells were harvested for protein isolation and western blotting. (B-D) CD11c-Cre Otud7b^{fl/fl} mice were injected i.v. with 1x10⁶ with WT or TRAF2^{-/-} BMDCs prior to infection with 1x10⁶ *PbA*-infected RBCs. Disease progression was monitored daily up to d7 p.i. employing the RMCBS score (B) peripheral blood parasitemia (C). (D) Representative images of brains of Evans blue-treated infected mice at d7 p.i. All data represent the mean \pm SEM. (B, C) Student's t test *p<0.05

4.11 Increased TNF-mediated apoptosis of OTUD7b-deficient human moDCs

To translate our data regarding OTUD7b as an inhibitor of TNF-induced apoptosis to human DCs, we generated OTUD7b-deficient primary monocyte-derived DCs (mo-DC) by CRISPR/Cas9-mediated OTUD7b deletion. After 6h of TNF stimulation, an increased TRAF2 degradation was observed in OTUD7b^{-/-} moDC as compared to OTUD7b-competent mo-DC and TRAF2 degradation was associated with increased sensitivity towards TNF-mediated apoptosis (Figure 34A, B). These data reveal an identical function of OTUD7b with respect to TNF-induced apoptosis in murine and human DCs,

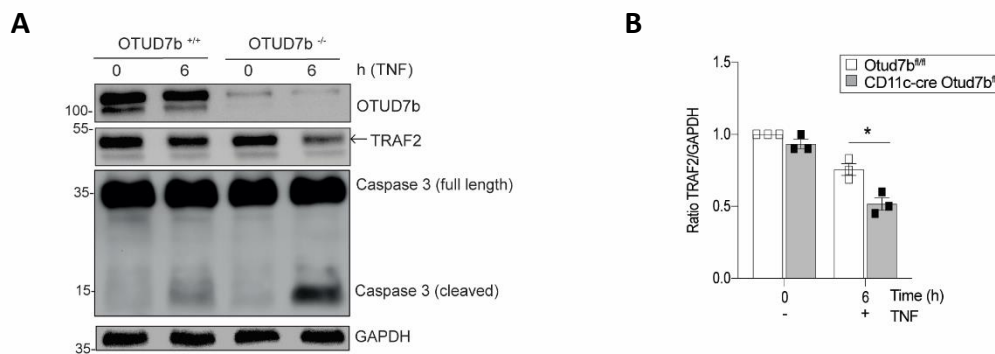


Figure 34: OTUD7b inhibits TNF-mediated apoptosis in human mo-DC by stabilizing TRAF2

(A) Primary human mo-DCs were nucleofected using OTUD7b gRNAs to generate stable OTUD7b knockdown. Non-targeting gRNAs were used as a control. OTUD7b-sufficient and -deficient mo-DCs were stimulated with TNF and harvested after 6h. Proteins were immunoblotted with indicated antibodies. (B) Relative change in TRAF2 expression was normalized to GAPDH and quantified. Blots are representative of three independent experiments. Data represent the mean \pm SEM. (B) Student's t test * $p < 0.05$

4.12 OTUD7b regulates TRAIL- and CD95L (FasL)-induced apoptosis of DCs

Since our data show that OTUD7b regulates TNFR1-mediated signaling, we further wanted to investigate the role of OTUD7b in cell death response to other members of the TNFR superfamily. Karl et al. reported inhibition of TRAIL- and CD95L-induced apoptosis by TRAF2 (104), therefore, we determined for role of OTUD7b in regulation of TRAF2 stability and apoptosis signaling upon stimulation of murine BMDCs with TRAIL and CD95L, respectively. To this end, we stimulated WT and OTUD7b^{-/-} BMDCs with TRAIL or FasL for 6h and 24h to activate their death domain containing receptors-DR4/5 and Fas/CD95 respectively (Fig. 35A, B). Western blot analysis revealed that increased TRAF2 degradation and apoptosis was observed in the absence of OTUD7b, indicating that OTUD7b is a master regulator TNF-, TRAIL- and CD95-mediated cell death signaling.

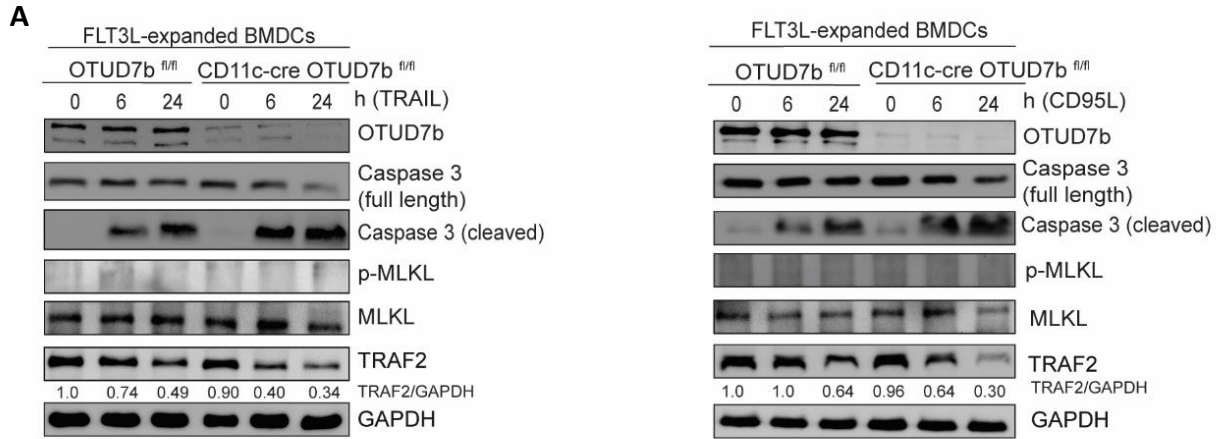


Figure 35: OTUD7b inhibits TRAF2 degradation and TRAIL- and CD95L-mediated DC apoptosis

(A, B) BMDCs from *Otud7b^{fl/fl}* and *CD11c-cre Otud7b^{fl/fl}* mice were stimulated with TRAIL (A) and CD95L (B), respectively, for 6h and 24h. Proteins were harvested and immunoblotted for the indicated proteins. TRAF2 levels were quantified by normalization to GAPDH. All western blots are representative for total of three independent experiments.

5. Discussion

DCs play a central role in the orchestration of adaptive and innate immune responses in infectious diseases. Already very early after infection and before the onset of a DC-induced T cell response, the DC intrinsic regulation of cell death and pro-inflammatory signaling pathways determines the outcome of infection. The infection-induced swift regulation of DC signaling is dependent on inflammatory milieu and critically regulated by dynamic ubiquitination and deubiquitination of signaling molecules. Here, we newly identify that the DUB OTUD7b critically regulates TNF-induced pro-inflammatory and cell death signaling in DCs and, thereby, determines the outcome of ECM.

5.1 DC-specific function of OTUD7b during ECM

During blood stage *PbA* infection, DCs phagocytose iRBCs resulting in the maturation of the DCs, characterized by upregulation of MHC-I/II surface molecules (signal 1) and costimulatory molecules CD80, CD86 (signal 2). Our study shows that OTUD7b is dispensable for the maturation of DCs as the expression of MHC and co-stimulatory molecules was not altered by OTUD7b-deficiency. In addition to TCR stimulation, IL-12 production by DCs is essential for the induction of a pathogen-specific CD8⁺ T cell response (signal 3) (105). Interestingly, IL-12 production by OTUD7b-deficient DCs was impaired. Consequently, CD11c-Cre *Otud7b*^{fl/fl} mice harbored reduced numbers of pathogen-specific CD8⁺ T cells in the spleen and brains upon *PbA* infection.

Cerebral malaria is an inflammatory disease and both human and murine cerebral malaria are characterized by high levels of circulating TNF (22, 27). In good agreement, we also observed a similar increase in the TNF levels in the spleens of both *Otud7b*^{fl/fl} and CD11c-Cre *Otud7b*^{fl/fl} mice upon *PbA* infection. Engagement of TNFR1 by TNF induces the activation of the transcription NF- κ B and the mitogen-activated protein kinases (MAPKs) resulting in the production of IL-12. Interestingly, the activation of both the NF- κ B and MAPK pathways was reduced in OTUD7b-deficient DCs upon TNF stimulation leading to impaired IL-12 production. This is in contrast to a previous study by Enesa et al. (106), which showed that siRNA-mediated knockdown of OTUD7b in human umbilical vein endothelial cells resulted in enhanced NF- κ B activation upon TNF stimulation (79). These data may indicate a cell-type specific function of OTUD7b.

During ECM, conventional CD8 α ⁺ DC are essential for the priming of pathogenic CD8⁺ T cells (40, 41), which then migrate to the brain to induce the disruption of the BBB and the disease pathology. *In vivo* depletion of CD11c⁺ DCs abrogates priming of pathogenic CD8⁺ T cells and protects mice from ECM (40, 103). In good agreement, in our study, the reduced number of

CD8 α ⁺ DCs and CD11b⁺ DCs in CD11c-Otud7b^{fl/fl} mice upon *PbA* infection along with reduced IL-12 production resulted in reduced priming of IFN- γ and Granzyme B producing CD8⁺ T cells. Consequently, parasite control was impaired and ECM was prevented in CD11c-Otud7b^{fl/fl} mice.

5.2 Mechanistic role of OTUD7b in TNFR1 signaling

The reduction in the number of DCs *in vivo* in CD11c-Otud7b^{fl/fl} mice upon *PbA* infection was due to increased apoptosis of DCs. Mechanistically, we identified that OTUD7b prevented proteasomal degradation of TRAF2 by removing K48-linked ubiquitin chains, and thereby protecting DCs from TNF-induced apoptosis. TRAF2 is an E3 ligase and a master regulator of TNF signaling. Upon stimulation of TNFR1 by soluble TNF, TRAF2 is recruited to the TNFR1 complex-I comprising of TRADD and RIPK1, where it further recruits cIAP1/2 to facilitate K63-linked polyubiquitination of RIPK1. Ubiquitination of RIPK1 is essential for recruitment and activation of TAK/TAB and IKK complexes, thereby leading to the activation of NF- κ B and MAP kinase pathways (54). On the other hand, in the absence of K63-linked polyubiquitination, RIPK1 undergoes autophosphorylation at S166, which induces cell death by caspase-mediated apoptosis or MLKL-mediated necroptosis (76). Our data shows that OTUD7b deubiquitinates TRAF2 and prevents RIPK1 kinase dependent and independent apoptosis by (i) fostering the expression of anti-apoptotic molecules-cFLIP and Bcl-xL via the NF- κ B pathway (ii) suppressing RIPK1 kinase activation by conjugating K63-linked ubiquitin chains on RIPK1 thereby inhibiting S166 phosphorylation of RIPK1 and apoptotic signaling.

Our co-immunoprecipitation experiments show interaction between OTUD7b, RIPK1 and TRAF2 upon TNF stimulation indicating that OTUD7b regulates ubiquitination and activation of RIPK1 by regulating the stability of TRAF2.

Formation of complex-IIa (RIPK1-independent apoptosis) and complex-IIb (RIPK1-dependent apoptosis) is inhibited by complex-I-dependent pro-survival signals (107). Impaired activation of NF- κ B/ MAP kinases (late checkpoint) and ubiquitin mediated phosphorylation of RIPK1 (early checkpoint) promote disengagement of RIPK1 from membrane bound complex-I and translocation to cytoplasm for formation of complex-IIa/IIb (55, 58). In good agreement to this, enhanced TNF-induced degradation of TRAF2 in the absence of OTUD7b led to reduced K63-linked polyubiquitination of RIPK1, impaired activation of NF- κ B and MAP kinase pathways and, finally, increased apoptosis as compared to OTUD7b-sufficient BMDCs. Apoptosis as the responsible cell death pathways was indicated by increased levels of cleaved caspase-8 and cleaved caspase-3 in OTUD7b-deficient DCs. Inhibition of RIPK1 kinase activity by Nec-1s slightly reduced levels of cleaved caspase-3 and partially prevented DC death. However,

combined pharmacological inhibition of RIPK1 activity (Nec1s) and apoptosis (zVAD-FMK) completely rescued survival of OTUD7b-deficient BMDC *in vitro* and *in vivo* illustrating that OTUD7b inhibits both RIPK1-dependent and -independent apoptosis via stabilization of TRAF2 (106).

The N-terminal UBA domain of OTUD7b is essential for interaction with K11-, K48- and K63-linked ubiquitin chains on target proteins and determines target specificity (90). Deletion of the UBA domain resulted in complete loss of interaction between OTUD7b and TRAF2. In addition, loss of the active catalytic site C194 reduced binding of OTUD7b to TRAF2 upon TNF stimulation. This could be due to the disruption of TRAF binding region, which spans the catalytic domain of OTUD7b. These data indicate that both N-terminal UBA domain and to a lesser extent the catalytic domain are critical for the interaction with TRAF2.

Interestingly we could show that in addition to TNF, OTUD7b also prevented CD95L- and TRAIL-mediated apoptosis by stabilizing TRAF2. The only other study reporting regulation of cell death by OTUD7b was by Bremm et al. (106) where the authors showed that OTUD7b stabilizes HIF1- α by removing K11-linked polyubiquitin chains and prevents hypoxia-induced cell death in human and murine cell lines (108). However, we did not observe a K11 deubiquitinating activity of OTUD7b on TRAF2.

Taken together our study newly uncovers OTUD7b in murine and human DCs as a promoter of DC survival and activation, thereby, identifying it as a potential therapeutic target to manipulate DC and DC-dependent T cell responses *in vivo*.

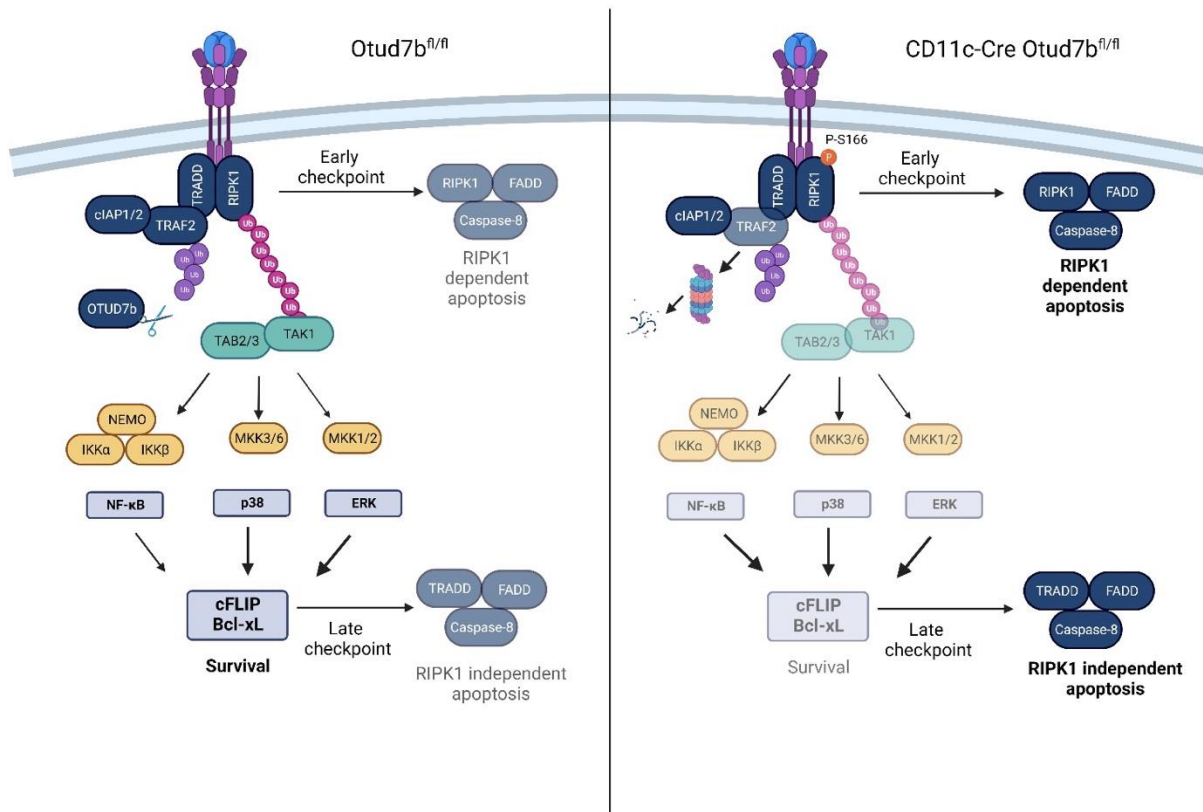


Figure 36: Schematic summary of OTUD7b-mediated regulation of TNF signaling in dendritic cells

Upon TNF stimulation, TRAF2 is recruited to TNFR-I and stabilized by OTUD7b, which facilitates K63-linked polyubiquitination of RIPK1. K63-linked polyubiquitination of RIPK1 prevents (i) RIPK1 autophosphorylation, (ii) activation of RIPK1 kinase function and (iii) RIPK1-dependent apoptosis by inhibiting the formation of complex IIb. Additionally, K63-linked polyubiquitination of RIPK1 activates NF-κB and MAP kinase signaling pathways inducing expression of anti-apoptotic molecules cFLIP and Bcl-xL and preventing formation of RIPK1-independent apoptotic complex IIa. However, in the absence of OTUD7b, TRAF2 undergoes proteasomal degradation resulting in reduced K63-linked polyubiquitination of RIPK1 and enhanced formation of RIPK1-dependent and -independent apoptotic complex IIa and IIb.

6. Conclusion

During ECM, DCs are the critical antigen presenting cell type and play a pivotal role in induction of the disease. Here we uncover a new mechanism how ubiquitination critically determines the immune response in ECM via modulation of DC function. We demonstrate an enhanced proteasomal degradation of TRAF2, an inhibitor of apoptotic cell death, in the absence of OTUD7b leading to increased DC apoptosis and diminished DC-dependent immune responses upon *PbA* infection. The impaired DC-dependent generation of effector CD8⁺ T cells and their reduced production of IFN- γ and GranzymeB in CD11c-Cre Otud7b^{fl/fl} mice protected these animals against ECM-associated pathology, a phenotype which was reversed upon *in vivo* inhibition of apoptosis of OTUD7b-deficient DCs. In addition, CD11c-Cre Otud7b^{fl/fl} mice developed disease and BBB breakage when supplemented with OTUD7b-sufficient DCs but not with TRAF2-deficient DCs. Human monocyte-derived DCs share several functionalities with conventional DCs and are also involved in antigen processing and presentation to CD8⁺T cells during *Plasmodium* infection. In a translational approach, we could recapitulate the key role of OTUD7b in the prevention of TNF-induced cell death in human OTUD7b-deficient TNF-treated mo-DCs demonstrating the clinical potential of OTUD7b inhibition for the potential treatment of DC-dependent diseases.

Our study emphasizes on role of DUBs in regulating the outcome of infection and as potential therapeutic targets. TNFR1 signaling is involved in various diseases and role of ubiquitination and DUBs has been widely studied in TNF signaling. Our study extends this knowledge and shows for the first time that OTUD7b regulates TNF-mediated apoptosis. It would also be interesting to determine how OTUD7b expressed in DCs and other cell types regulates the outcome of other infectious and inflammatory diseases.

7. References

1. WHO. World malaria report: WHO; 2022 [Available from: <https://www.who.int/teams/global-malaria-programme/reports/world-malaria-report-2022#:~:text=Malaria%20cases%20continued%20to%20rise,and%2032%20million%20in%202019.>
2. Meibalan E, Marti M. Biology of Malaria Transmission. *Cold Spring Harb Perspect Med.* 2017;7(3).
3. Ghazanfari N, Mueller SN, Heath WR. Cerebral Malaria in Mouse and Man. *Front Immunol.* 2018;9:2016.
4. Idro R, Marsh K, John CC, Newton CR. Cerebral malaria: mechanisms of brain injury and strategies for improved neurocognitive outcome. *Pediatr Res.* 2010;68(4):267-74.
5. Song X, Wei W, Cheng W, Zhu H, Wang W, Dong H, Li J. Cerebral malaria induced by plasmodium falciparum: clinical features, pathogenesis, diagnosis, and treatment. *Front Cell Infect Microbiol.* 2022;12:939532.
6. Laurens MB. RTS,S/AS01 vaccine (Mosquirix): an overview. *Hum Vaccin Immunother.* 2020;16(3):480-9.
7. Balikagala B, Fukuda N, Ikeda M, Katuro OT, Tachibana SI, Yamauchi M, et al. Evidence of Artemisinin-Resistant Malaria in Africa. *N Engl J Med.* 2021;385(13):1163-71.
8. Sinnis P, Zavala F. The skin: where malaria infection and the host immune response begin. *Semin Immunopathol.* 2012;34(6):787-92.
9. Haque A, Engwerda C. Hepatocytes break the silence during liver-stage malaria. *Nat Med.* 2014;20(1):17-9.
10. Paul AS, Egan ES, Duraisingh MT. Host-parasite interactions that guide red blood cell invasion by malaria parasites. *Curr Opin Hematol.* 2015;22(3):220-6.
11. Mohandas N, An X. Malaria and human red blood cells. *Med Microbiol Immunol.* 2012;201(4):593-8.
12. Chahine Z, Le Roch KG. Decrypting the complexity of the human malaria parasite biology through systems biology approaches. *Front Syst Biol.* 2022;2.
13. Josling GA, Llinas M. Sexual development in Plasmodium parasites: knowing when it's time to commit. *Nat Rev Microbiol.* 2015;13(9):573-87.
14. Cowman AF, Crabb BS. Invasion of red blood cells by malaria parasites. *Cell.* 2006;124(4):755-66.
15. John CC. Adults Are Not Big Children: What Brain Magnetic Resonance Imaging Findings Tell Us About Differences in Pediatric and Adult Cerebral Malaria. *Clin Infect Dis.* 2021;73(7):e2397-e8.
16. Idro R, Jenkins NE, Newton CR. Pathogenesis, clinical features, and neurological outcome of cerebral malaria. *Lancet Neurol.* 2005;4(12):827-40.
17. Hawkes M, Elphinstone RE, Conroy AL, Kain KC. Contrasting pediatric and adult cerebral malaria: the role of the endothelial barrier. *Virulence.* 2013;4(6):543-55.
18. Storm J, Craig AG. Pathogenesis of cerebral malaria--inflammation and cytoadherence. *Front Cell Infect Microbiol.* 2014;4:100.
19. Nishanth G, Schluter D. Blood-Brain Barrier in Cerebral Malaria: Pathogenesis and Therapeutic Intervention. *Trends Parasitol.* 2019;35(7):516-28.
20. Ramachandran A, Sharma A. Dissecting the mechanisms of pathogenesis in cerebral malaria. *PLoS Pathog.* 2022;18(11):e1010919.

21. Clark IA, Budd AC, Alleva LM, Cowden WB. Human malarial disease: a consequence of inflammatory cytokine release. *Malar J.* 2006;5:85.
22. Dunst J, Kamena F, Matuschewski K. Cytokines and Chemokines in Cerebral Malaria Pathogenesis. *Front Cell Infect Microbiol.* 2017;7:324.
23. Kwiatkowski D, Hill AV, Sambou I, Twumasi P, Castracane J, Manogue KR, et al. TNF concentration in fatal cerebral, non-fatal cerebral, and uncomplicated *Plasmodium falciparum* malaria. *Lancet.* 1990;336(8725):1201-4.
24. Kinra P, Dutta V. Serum TNF alpha levels: a prognostic marker for assessment of severity of malaria. *Trop Biomed.* 2013;30(4):645-53.
25. Agudelo O, Bueno J, Villa A, Maestre A. High IFN-gamma and TNF production by peripheral NK cells of Colombian patients with different clinical presentation of *Plasmodium falciparum*. *Malar J.* 2012;11:38.
26. Sato Y, Ries S, Stenzel W, Fillatreau S, Matuschewski K. The Liver-Stage *Plasmodium* Infection Is a Critical Checkpoint for Development of Experimental Cerebral Malaria. *Front Immunol.* 2019;10:2554.
27. Gimenez F, Barraud de Lagerie S, Fernandez C, Pino P, Mazier D. Tumor necrosis factor alpha in the pathogenesis of cerebral malaria. *Cell Mol Life Sci.* 2003;60(8):1623-35.
28. Mita-Mendoza NK, Magallon-Tejada A, Parmar P, Furtado R, Aldrich M, Saidi A, et al. Dimethyl fumarate reduces TNF and *Plasmodium falciparum* induced brain endothelium activation in vitro. *Malar J.* 2020;19(1):376.
29. King T, Lamb T. Interferon-gamma: The Jekyll and Hyde of Malaria. *PLoS Pathog.* 2015;11(10):e1005118.
30. Villegas-Mendez A, Strangward P, Shaw TN, Rajkovic I, Tosevski V, Forman R, et al. Gamma Interferon Mediates Experimental Cerebral Malaria by Signaling within Both the Hematopoietic and Nonhematopoietic Compartments. *Infect Immun.* 2017;85(11).
31. Hunt NH, Ball HJ, Hansen AM, Khaw LT, Guo J, Bakmiwewa S, et al. Cerebral malaria: gamma-interferon redux. *Front Cell Infect Microbiol.* 2014;4:113.
32. Renia L, Grau GE, Wassmer SC. CD8+ T cells and human cerebral malaria: a shifting episteme. *J Clin Invest.* 2020;130(3):1109-11.
33. Barrera V, Haley MJ, Strangward P, Attree E, Kamiza S, Seydel KB, et al. Comparison of CD8(+) T Cell Accumulation in the Brain During Human and Murine Cerebral Malaria. *Front Immunol.* 2019;10:1747.
34. Nacer A, Movila A, Baer K, Mikolajczak SA, Kappe SH, Frevort U. Neuroimmunological blood brain barrier opening in experimental cerebral malaria. *PLoS Pathog.* 2012;8(10):e1002982.
35. Ghosh D, Stumhofer JS. The spleen: "epicenter" in malaria infection and immunity. *J Leukoc Biol.* 2021;110(4):753-69.
36. Yap XZ, Lundie RJ, Beeson JG, O'Keeffe M. Dendritic Cell Responses and Function in Malaria. *Front Immunol.* 2019;10:357.
37. Amorim KN, Chagas DC, Sulczewski FB, Boscardin SB. Dendritic Cells and Their Multiple Roles during Malaria Infection. *J Immunol Res.* 2016;2016:2926436.
38. Grohmann U, Bianchi R, Belladonna ML, Vacca C, Silla S, Ayroldi E, et al. IL-12 acts selectively on CD8 alpha- dendritic cells to enhance presentation of a tumor peptide in vivo. *J Immunol.* 1999;163(6):3100-5.
39. Trinchieri G. Interleukin-12 and the regulation of innate resistance and adaptive immunity. *Nat Rev Immunol.* 2003;3(2):133-46.

40. Kuehlwein JM, Borsche M, Korir PJ, Risch F, Mueller AK, Hubner MP, et al. Protection of Batf3-deficient mice from experimental cerebral malaria correlates with impaired cytotoxic T-cell responses and immune regulation. *Immunology*. 2020;159(2):193-204.
41. Piva L, Tetlak P, Claser C, Karjalainen K, Renia L, Ruedl C. Cutting edge: Clec9A+ dendritic cells mediate the development of experimental cerebral malaria. *J Immunol*. 2012;189(3):1128-32.
42. Nitcheu J, Bonduelle O, Combadiere C, Tefit M, Seilhean D, Mazier D, Combadiere B. Perforin-dependent brain-infiltrating cytotoxic CD8+ T lymphocytes mediate experimental cerebral malaria pathogenesis. *J Immunol*. 2003;170(4):2221-8.
43. Haque A, Best SE, Unosson K, Amante FH, de Labastida F, Anstey NM, et al. Granzyme B expression by CD8+ T cells is required for the development of experimental cerebral malaria. *J Immunol*. 2011;186(11):6148-56.
44. Howland SW, Claser C, Poh CM, Gun SY, Renia L. Pathogenic CD8+ T cells in experimental cerebral malaria. *Semin Immunopathol*. 2015;37(3):221-31.
45. Lundie RJ, de Koning-Ward TF, Davey GM, Nie CQ, Hansen DS, Lau LS, et al. Blood-stage Plasmodium infection induces CD8+ T lymphocytes to parasite-expressed antigens, largely regulated by CD8alpha+ dendritic cells. *Proc Natl Acad Sci U S A*. 2008;105(38):14509-14.
46. Pai S, Qin J, Cavanagh L, Mitchell A, El-Assaad F, Jain R, et al. Real-time imaging reveals the dynamics of leukocyte behaviour during experimental cerebral malaria pathogenesis. *PLoS Pathog*. 2014;10(7):e1004236.
47. Belnoue E, Kayibanda M, Vigario AM, Deschemin JC, van Rooijen N, Viguier M, et al. On the pathogenic role of brain-sequestered alphabeta CD8+ T cells in experimental cerebral malaria. *J Immunol*. 2002;169(11):6369-75.
48. Hermsen C, van de Wiel T, Mommers E, Sauerwein R, Eling W. Depletion of CD4+ or CD8+ T-cells prevents Plasmodium berghei induced cerebral malaria in end-stage disease. *Parasitology*. 1997;114 (Pt 1):7-12.
49. Kurup SP, Butler NS, Harty JT. T cell-mediated immunity to malaria. *Nat Rev Immunol*. 2019;19(7):457-71.
50. Schmid U, Stenzel W, Koschel J, Raptaki M, Wang X, Naumann M, et al. The Deubiquitinating Enzyme Cylindromatosis Dampens CD8(+) T Cell Responses and Is a Critical Factor for Experimental Cerebral Malaria and Blood-Brain Barrier Damage. *Front Immunol*. 2017;8:27.
51. Renia L, Howland SW, Claser C, Charlotte Gruner A, Suwanarusk R, Hui Teo T, et al. Cerebral malaria: mysteries at the blood-brain barrier. *Virulence*. 2012;3(2):193-201.
52. Aggarwal BB. Signalling pathways of the TNF superfamily: a double-edged sword. *Nat Rev Immunol*. 2003;3(9):745-56.
53. Horiuchi T, Mitoma H, Harashima S, Tsukamoto H, Shimoda T. Transmembrane TNF-alpha: structure, function and interaction with anti-TNF agents. *Rheumatology (Oxford)*. 2010;49(7):1215-28.
54. Kondylis V, Pasparakis M. RIP Kinases in Liver Cell Death, Inflammation and Cancer. *Trends Mol Med*. 2019;25(1):47-63.
55. Ting AT, Bertrand MJM. More to Life than NF-kappaB in TNFR1 Signaling. *Trends Immunol*. 2016;37(8):535-45.

56. Schneider AT, Gautheron J, Feoktistova M, Roderburg C, Loosen SH, Roy S, et al. RIPK1 Suppresses a TRAF2-Dependent Pathway to Liver Cancer. *Cancer Cell*. 2017;31(1):94-109.
57. Bertrand MJ, Milutinovic S, Dickson KM, Ho WC, Boudreault A, Durkin J, et al. cIAP1 and cIAP2 facilitate cancer cell survival by functioning as E3 ligases that promote RIP1 ubiquitination. *Mol Cell*. 2008;30(6):689-700.
58. Annibaldi A, Meier P. Checkpoints in TNF-Induced Cell Death: Implications in Inflammation and Cancer. *Trends Mol Med*. 2018;24(1):49-65.
59. Pickart CM, Eddins MJ. Ubiquitin: structures, functions, mechanisms. *Biochim Biophys Acta*. 2004;1695(1-3):55-72.
60. Swatek KN, Komander D. Ubiquitin modifications. *Cell Res*. 2016;26(4):399-422.
61. Cockram PE, Kist M, Prakash S, Chen SH, Wertz IE, Vucic D. Ubiquitination in the regulation of inflammatory cell death and cancer. *Cell Death Differ*. 2021;28(2):591-605.
62. Ye Y, Rape M. Building ubiquitin chains: E2 enzymes at work. *Nat Rev Mol Cell Biol*. 2009;10(11):755-64.
63. Komander D. The emerging complexity of protein ubiquitination. *Biochem Soc Trans*. 2009;37(Pt 5):937-53.
64. Popovic D, Vucic D, Dikic I. Ubiquitination in disease pathogenesis and treatment. *Nat Med*. 2014;20(11):1242-53.
65. Tracz M, Bialek W. Beyond K48 and K63: non-canonical protein ubiquitination. *Cell Mol Biol Lett*. 2021;26(1):1.
66. Annibaldi A, Wicky John S, Vanden Berghe T, Swatek KN, Ruan J, Liccardi G, et al. Ubiquitin-Mediated Regulation of RIPK1 Kinase Activity Independent of IKK and MK2. *Mol Cell*. 2018;69(4):566-80 e5.
67. Shi JH, Sun SC. Tumor Necrosis Factor Receptor-Associated Factor Regulation of Nuclear Factor kappaB and Mitogen-Activated Protein Kinase Pathways. *Front Immunol*. 2018;9:1849.
68. Gerlach B, Cordier SM, Schmukle AC, Emmerich CH, Rieser E, Haas TL, et al. Linear ubiquitination prevents inflammation and regulates immune signalling. *Nature*. 2011;471(7340):591-6.
69. Haas TL, Emmerich CH, Gerlach B, Schmukle AC, Cordier SM, Rieser E, et al. Recruitment of the linear ubiquitin chain assembly complex stabilizes the TNF-R1 signaling complex and is required for TNF-mediated gene induction. *Mol Cell*. 2009;36(5):831-44.
70. Dynek JN, Goncharov T, Dueber EC, Fedorova AV, Izrael-Tomasevic A, Phu L, et al. c-IAP1 and UbcH5 promote K11-linked polyubiquitination of RIP1 in TNF signalling. *EMBO J*. 2010;29(24):4198-209.
71. Kanayama A, Seth RB, Sun L, Ea CK, Hong M, Shaito A, et al. TAB2 and TAB3 activate the NF-kappaB pathway through binding to polyubiquitin chains. *Mol Cell*. 2004;15(4):535-48.
72. Lin YC, Brown K, Siebenlist U. Activation of NF-kappa B requires proteolysis of the inhibitor I kappa B-alpha: signal-induced phosphorylation of I kappa B-alpha alone does not release active NF-kappa B. *Proc Natl Acad Sci U S A*. 1995;92(2):552-6.
73. Brown K, Gerstberger S, Carlson L, Franzoso G, Siebenlist U. Control of I kappa B-alpha proteolysis by site-specific, signal-induced phosphorylation. *Science*. 1995;267(5203):1485-8.

74. Chen ZJ. Ubiquitin signalling in the NF-kappaB pathway. *Nat Cell Biol.* 2005;7(8):758-65.
75. Xu YR, Lei CQ. TAK1-TABs Complex: A Central Signalosome in Inflammatory Responses. *Front Immunol.* 2020;11:608976.
76. Tang Y, Tu H, Zhang J, Zhao X, Wang Y, Qin J, Lin X. K63-linked ubiquitination regulates RIPK1 kinase activity to prevent cell death during embryogenesis and inflammation. *Nat Commun.* 2019;10(1):4157.
77. Gonzalez F, Lawrence D, Yang B, Yee S, Pitti R, Marsters S, et al. TRAF2 Sets a threshold for extrinsic apoptosis by tagging caspase-8 with a ubiquitin shutoff timer. *Mol Cell.* 2012;48(6):888-99.
78. Mevissen TET, Komander D. Mechanisms of Deubiquitinase Specificity and Regulation. *Annu Rev Biochem.* 2017;86:159-92.
79. Enesa K, Zakkar M, Chaudhury H, Luong le A, Rawlinson L, Mason JC, et al. NF-kappaB suppression by the deubiquitinating enzyme Cezanne: a novel negative feedback loop in pro-inflammatory signaling. *J Biol Chem.* 2008;283(11):7036-45.
80. Wertz IE, O'Rourke KM, Zhou H, Eby M, Aravind L, Seshagiri S, et al. De-ubiquitination and ubiquitin ligase domains of A20 downregulate NF-kappaB signalling. *Nature.* 2004;430(7000):694-9.
81. Brummelkamp TR, Nijman SM, Dirac AM, Bernards R. Loss of the cylindromatosis tumour suppressor inhibits apoptosis by activating NF-kappaB. *Nature.* 2003;424(6950):797-801.
82. Kovalenko A, Chable-Bessia C, Cantarella G, Israel A, Wallach D, Courtois G. The tumour suppressor CYLD negatively regulates NF-kappaB signalling by deubiquitination. *Nature.* 2003;424(6950):801-5.
83. Trompouki E, Hatzivassiliou E, Tschirritzis T, Farmer H, Ashworth A, Mosialos G. CYLD is a deubiquitinating enzyme that negatively regulates NF-kappaB activation by TNFR family members. *Nature.* 2003;424(6950):793-6.
84. Priem D, Devos M, Druwe S, Martens A, Slowicka K, Ting AT, et al. A20 protects cells from TNF-induced apoptosis through linear ubiquitin-dependent and -independent mechanisms. *Cell Death Dis.* 2019;10(10):692.
85. Keusekotten K, Elliott PR, Glockner L, Fiil BK, Damgaard RB, Kulathu Y, et al. OTULIN antagonizes LUBAC signaling by specifically hydrolyzing Met1-linked polyubiquitin. *Cell.* 2013;153(6):1312-26.
86. Hu H, Brittain GC, Chang JH, Puebla-Osorio N, Jin J, Zal A, et al. OTUD7B controls non-canonical NF-kappaB activation through deubiquitination of TRAF3. *Nature.* 2013;494(7437):371-4.
87. Peltzer N, Darding M, Walczak H. Holding RIPK1 on the Ubiquitin Leash in TNFR1 Signaling. *Trends Cell Biol.* 2016;26(6):445-61.
88. Abe J, Berk BC. Cezanne paints inflammation by regulating ubiquitination. *Circ Res.* 2013;112(12):1526-8.
89. Evans PC, Taylor ER, Coadwell J, Heyninck K, Beyaert R, Kilshaw PJ. Isolation and characterization of two novel A20-like proteins. *Biochem J.* 2001;357(Pt 3):617-23.
90. Mader J, Huber J, Bonn F, Dotsch V, Rogov VV, Bremm A. Oxygen-dependent asparagine hydroxylation of the ubiquitin-associated (UBA) domain in Cezanne regulates ubiquitin binding. *J Biol Chem.* 2020;295(8):2160-74.

91. Mevissen TET, Kulathu Y, Mulder MPC, Geurink PP, Maslen SL, Gersch M, et al. Molecular basis of Lys11-polyubiquitin specificity in the deubiquitinase Cezanne. *Nature*. 2016;538(7625):402-5.
92. Hu H, Wang H, Xiao Y, Jin J, Chang JH, Zou Q, et al. Otud7b facilitates T cell activation and inflammatory responses by regulating Zap70 ubiquitination. *J Exp Med*. 2016;213(3):399-414.
93. Pareja F, Ferraro DA, Rubin C, Cohen-Dvashi H, Zhang F, Aulmann S, et al. Deubiquitination of EGFR by Cezanne-1 contributes to cancer progression. *Oncogene*. 2012;31(43):4599-608.
94. Luong le A, Fragiadaki M, Smith J, Boyle J, Lutz J, Dean JL, et al. Cezanne regulates inflammatory responses to hypoxia in endothelial cells by targeting TRAF6 for deubiquitination. *Circ Res*. 2013;112(12):1583-91.
95. McNally RS, Davis BK, Clements CM, Accavitti-Loper MA, Mak TW, Ting JP. DJ-1 enhances cell survival through the binding of Cezanne, a negative regulator of NF-kappaB. *J Biol Chem*. 2011;286(6):4098-106.
96. Wang B, Jie Z, Joo D, Ordureau A, Liu P, Gan W, et al. TRAF2 and OTUD7B govern a ubiquitin-dependent switch that regulates mTORC2 signalling. *Nature*. 2017;545(7654):365-9.
97. Bonacci T, Suzuki A, Grant GD, Stanley N, Cook JG, Brown NG, Emanuele MJ. Cezanne/OTUD7B is a cell cycle-regulated deubiquitinase that antagonizes the degradation of APC/C substrates. *EMBO J*. 2018;37(16).
98. Gong Z, Li A, Ding J, Li Q, Zhang L, Li Y, et al. OTUD7B Deubiquitinates LSD1 to Govern Its Binding Partner Specificity, Homeostasis, and Breast Cancer Metastasis. *Adv Sci (Weinh)*. 2021;8(15):e2004504.
99. Xie W, Tian S, Yang J, Cai S, Jin S, Zhou T, et al. OTUD7B deubiquitinates SQSTM1/p62 and promotes IRF3 degradation to regulate antiviral immunity. *Autophagy*. 2022;18(10):2288-302.
100. Tian S, Jin S, Wu Y, Liu T, Luo M, Ou J, et al. High-throughput screening of functional deubiquitinating enzymes in autophagy. *Autophagy*. 2021;17(6):1367-78.
101. Carroll RW, Wainwright MS, Kim KY, Kidambi T, Gomez ND, Taylor T, Haldar K. A rapid murine coma and behavior scale for quantitative assessment of murine cerebral malaria. *PLoS One*. 2010;5(10).
102. Livak KJ, Schmittgen TD. Analysis of relative gene expression data using real-time quantitative PCR and the 2⁻(Delta Delta C(T)) Method. *Methods*. 2001;25(4):402-8.
103. deWalick S, Amante FH, McSweeney KA, Randall LM, Stanley AC, Haque A, et al. Cutting edge: conventional dendritic cells are the critical APC required for the induction of experimental cerebral malaria. *J Immunol*. 2007;178(10):6033-7.
104. Karl I, Jossberger-Werner M, Schmidt N, Horn S, Goebeler M, Leverkus M, et al. TRAF2 inhibits TRAIL- and CD95L-induced apoptosis and necroptosis. *Cell Death Dis*. 2014;5(10):e1444.
105. Osii RS, Otto TD, Garside P, Ndungu FM, Brewer JM. The Impact of Malaria Parasites on Dendritic Cell-T Cell Interaction. *Front Immunol*. 2020;11:1597.
106. Laurien L, Nagata M, Schunke H, Delanghe T, Wiederstein JL, Kumari S, et al. Autophosphorylation at serine 166 regulates RIP kinase 1-mediated cell death and inflammation. *Nat Commun*. 2020;11(1):1747.
107. Jaco I, Annibaldi A, Lalaoui N, Wilson R, Tenev T, Laurien L, et al. MK2 Phosphorylates RIPK1 to Prevent TNF-Induced Cell Death. *Mol Cell*. 2017;66(5):698-710 e5.

108. Bremm A, Moniz S, Mader J, Rocha S, Komander D. Cezanne (OTUD7B) regulates HIF-1alpha homeostasis in a proteasome-independent manner. *EMBO Rep.* 2014;15(12):1268-77.

DECLARATION OF HONOUR

“I hereby declare that I prepared this thesis without the impermissible help of third parties and that none other than the aids indicated have been used; all sources of information are clearly marked, including my own publications.

In particular I have not consciously:

- fabricated data or rejected undesirable results,
- misused statistical methods with the aim of drawing other conclusions than those warranted by the available data,
- plagiarized external data or publications,
- presented the results of other researchers in a distorted way.

I am aware that violations of copyright may lead to injunction and damage claims by the author and also to prosecution by the law enforcement authorities.

I hereby agree that the thesis may be electronically reviewed with the aim of identifying plagiarism.

This work has not yet been submitted as a doctoral thesis in the same or a similar form in Germany, nor in any other country.”

Hannover, 13.09.2023

Kunjan Harit

